Tackling complex models in Systems Biology

Mochamad Apri

Thesis Committee

Promotor
Prof. dr. J. Molenaar
Professor of Applied Mathematics
Wageningen University

Co-promotor
Dr. M. de Gee
Associate professor, Mathematical and Statistical Methods Group
Wageningen University

Other members
Prof. dr. ir. G. van Straten, Wageningen University
Prof. dr. B.M. Mulder, AMOLF, Amsterdam and Wageningen University
Dr. J.H.G.M. van Beek, VU University, Amsterdam
Dr. P.H.B. de Visser, Wageningen Universtity

This research was conducted under the auspices of the Graduate School of
Production Ecology & Resource Conservation (PE & RC)

Tackling complex models in Systems Biology

Mochamad Apri

Thesis
submitted in fulfilment of the requirement for the degree of doctor
at Wageningen University
by the authority of the Rector Magnificus
Prof. dr. M.J. Kropff,
in the presence of the
Thesis Committee apointed by the Academic Board
to be defended in public
on Tusday 5 March 2013
at 4 p.m. in the Aula.

Mochamad Apri
Tackling complex models in Systems Biology

Thesis, Wageningen University, Wageningen, NL (2013)
With references, with summaries in Dutch and English

ISBN 978-94-6173-524-9

Abstract

One of the main obstacles in systems biology is complexity, a feature that is inherent to living systems. This complexity stems both from the large number of components involved and from the intricate interactions between these components. When the system is described by a mathematical model, we frequently end up with a large nonlinear set of mathematical equation that contains many parameters. Such a large model usually has a number of undesirable properties, e.g., its dynamical behavior is hard to understand, its parameters are difficult to identify, and its simulation requires a very long computing time. In this thesis, we present several strategies that may help to overcome these problems. On the level of method development, we focus on two issues: a) method development to analyze robustness, and b) method development to reduce model complexity. On the level of practical systems biology, we develop and analyze a model for the cell cycle in tomato fruit pericarp.

Robustness, that is the ability of a system to preserve biological functionality in spite of internal and external perturbations, is an essential feature of a biological system. Any mathematical model that describes this system should reflect this property. This implies the needs of a mathematical method to evaluate the robustness of mathematical models for biological processes. However, assessing robustness of a complex non-linear model that contains many parameters is not straightforward. In this thesis, we present a novel method to evaluate the robustness of mathematical models efficiently. This method enables us to find which parameter combinations in a model are responsible for its robustness. In this way, we get more insight into the underlying mechanisms that govern the robustness of the biological system. The advantage of our method is that the effort to apply the method scales linearly with the number of parameters. It is therefore very efficient when it is applied on mathematical models that contain a large number of parameters.

The complexity in a model can be brought down by simplifying the model. In this thesis, we also present a novel reduction method to simplify mathematical representations of biological models. In this method, biological components and parameters that do not contribute to the observed dynamics are considered redundant and hence are removed from the model. This results in a simpler model with less components and parameters, without losing predictive capabilities for any testable experimental condition. Since the reduced model contains less parameters, parameter identification can be carried out more efficaciously.

In the last part of this thesis we show how modeling can help us in understanding the cell cycle in tomato fruit pericarp. The cell cycle in this system is quite unique since the classical cell cycle, in which the cell division takes place, after some periods turns into a partial cycle where the cell keeps replicating its DNA but skips the division. Several mechanisms that are putatively responsible for this transition have been proposed. With modeling, we show that although each of these putative mechanisms could lead on its own the cell cycle to this transition, also their combination could lead to the same result. We also show that the mechanisms that yield the transition are very robust.

Contents

Chapter 1

Introduction

1.1 Systems biology

Most biological processes are highly complex, involving many components with intricate interactions. An example is the cell cycle. A considerable part of this thesis has been devoted to this process in which the cell divides itself into two daughter cells. The cell cycle is governed by many key regulators that interact with each other in a sophisticated way and which may be strongly influenced by the environmental conditions of the cell [1]. The division process consists of an orderly sequence of events, during which the cell duplicates all its content and next divides into two parts. Before the decision to divide is taken, the cell checks whether the internal and the external environments are really favorable for division. If this is not the case, e.g., one of the key regulators does not work properly or the temperature is far from being optimal, the cell cycle process is delayed and the cell division postponed. In the worst scenario, e.g., in case of considerable DNA damage, the cell can even decide to commit suicide, i.e., applying the so-called "apoptosis" or "cell death programme" [2]. In short, the cell cycle, which is one of the most fundamental processes in life is the result of a highly complex interplay between many cell components and the environmental conditions.

In the past, however, biological systems were mostly studied by examining their constituent parts in an isolated way. As a consequence, one tended to apply a reductionist approach to unravel complex systems. The assumption underlying such an approach is that one could gain full understanding of biological systems by first investigating the behavior of the components and then combining these insights in a relatively simple way. In the course of time one came to the conclusion that this strategy is most of the time not sufficient to understand living systems, although it is not doubted that reduction may remain very useful and often is the only way one can initially follow when starting with studying a system from scratch [3]. Biological functions that appear to be fundamental in nature nearly always come into existence as emergent properties: they are only present when the components are in full interaction and disappear if one decouples the different modules. An impressive example of this is given in [4]: the so-called p53 protein that functions as a repressor of cancer in cells can only be effective if it is in interaction with several other cell components. This implies

that the study of biological systems will only be really successful if it is carried out at the system level. This insight has induced the introduction of the term systems biology [5, 6].

There are more reasons why the systems biology approach got a boost in the last decades. The advancement of experimental technology that allows for developments like genome sequencing and high-throughput measurements of proteins and metabolites has enabled us to obtain huge amounts of data. The interactions between the components in time and space turnout to be much too complex to be understood by intuition or common sense only. So, to gain information on the underlying biological processes from the many data, one needs to integrate them with a modeling approach.

Systems biology is an attitude rather than an independent discipline in the life sciences. It is way of thinking that encompasses several aspects. The first one is the intention to understand biological systems at the system level via a holistic approach, taking into account the interactions among the components and environments. The second one is the conviction that real progress can be made only by closely integrating experiments and modeling [7, 8]. This last idea is not new for the physical sciences, but in biology there was a tendency to consider the wet activities, related to lab work, and the dry activities, usually referred to as theoretical biology, as diverging paths. Kitano first emphasized the need for convergence of these both paths to unravel complex systems [8] and coined the ‘experiment-modeling cycle, depicted in Figure 1.1. The idea of the cycle is as follows. One usually starts with observations. They inspire a draft model based on some hypotheses. This initial model is used to make some prediction, which is tested in the lab. The outcome of the experiment usually deviates from the prediction. The new and old data are then combined to adjust and refine the model. This extended model leads to new predictions, which are again tested in the lab. The cycle is followed as long as the discrepancies between model outcomes and experimental data are unacceptable. A third aspect of systems biology is the conviction that for break-throughs we need multidisciplinary teams of researchers, in which biologists, mathematicians, chemists, and bioinformaticians tightly cooperate. For the work described in this thesis this was the case. For example, in developing the tomato cell cycle model in Chapter 5 we had many fruitful discussions with biologists, who are experts in tomato research and could, when faced with an enormous amount of literature on the phenomenon of endoreduplication, outline and explain the aspects that really matter for this topic.

1.2 Mathematical models in systems biology

One of the core activities in the systems biology approach is the development of a mathematical model to describe the dynamics of the system under consideration. In general two common approaches to model a biological system can be discerned [6, 9, 10]. Which one is preferred in practice heavily depends on the complexity of the system and the information about the system interactions that is already available. The first approach follows a top-down strategy that provides a broad overview of the system. In this type of modeling, one is usually faced with a quite complex system for which the detailed mechanistic knowledge is mainly lacking. Then, one starts from the experimental data and tries to deduce a model that describes the data, but this cannot be based on known physical or biological laws or principles

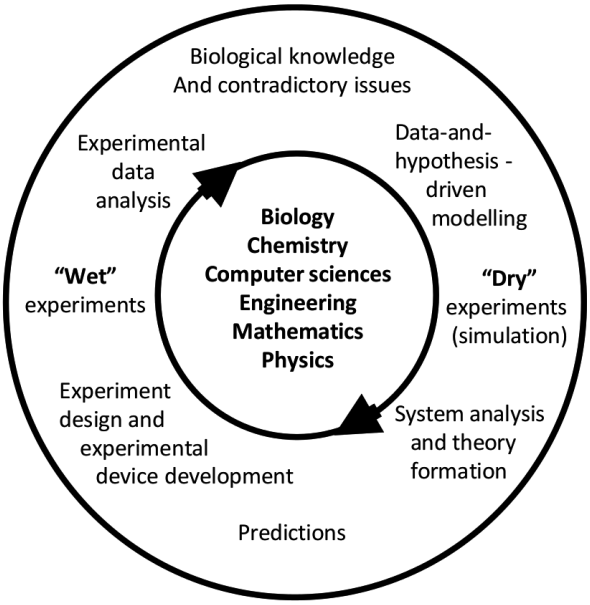

Figure 1.1: "The experiment modeling cycle in systems biology. A cycle of research begins with the selection of some issues of biological significance and the creation of a model representing the phenomenon. Models can be created either automatically or manually. The model represents a computable set of assumptions and hypotheses that need to be tested or supported experimentally. Computational 'dry' experiments, such as simulation, on models reveal computational adequacy of the assumptions and hypotheses embedded in each model. Inadequate models would expose inconsistencies with established experimental facts, and thus need to be rejected or modified. Models that pass this test become subjects of a thorough system analysis where a number of predictions may be made. A set of predictions that can distinguish a correct model among competing models is selected for 'wet' experiments. Successful experiments are those that eliminate inadequate models. Models that survive this cycle are deemed to be consistent with existing experimental evidence. While this is an idealized process of systems biology research, the hope is that advancement of research in computational science, analytical methods, technologies for measurements, and genomics will gradually transform biological research to fit this cycle for a more systematic and hypothesis-driven science" [8].

that are responsible for the interactions. One observes that there are correlations between measured variables in the system and one builds a regression model that represents these correlations. Such a more or less statistical model might allow to generate new hypotheses and to discover underlying molecular mechanisms and patterns of functional behaviour. Such a model is predictive and can be used in the experiment-modeling cycle, in which the model is refined by gradually putting more detailed information in each iteration of the cycle. The second approach is the bottom-up one. It utilizes pre-existing knowledge of the mechanisms

governing the dynamics of the system. One usually starts with a small subsystem, writing down rules or equations that describe the interactions between the components. The model is then gradually extended by incorporating other subsystems that interact with the first one and with each other, until all subcomponents are included and one eventually arrives at a full model that represents all aspects of the system simultaneously.

In this thesis, we restrict ourselves to the bottom-up approach and we focus on modeling in terms of ordinary differential equations (ODEs) framework. In these ODEs the interactions are mostly represented by standard expressions, e.g., Michaelis-Menten terms for interactions that saturate, linear terms for decay processes, and quadratic expressions for second order chemical reactions. However, it should be realized that there are more possibilities to arrive at predictive models. For example, if the nature of the biological systems changes at specific events, one might use a discrete modeling type such as a boolean network description, in which the dynamics is represented by decision rules. In most living systems the states change continuously in time and then a description in terms of ordinary differential equations (ODEs) might be more suitable. But, if spatial effects are important, since, e.g., diffusion processes take place, one has to invoke partial differential equations (PDEs) and if randomness plays a dominant role a stochastic approach is required [11, 12].

The bottom-up approach clearly has its limitations. This approach can hardly be applied to very complicated systems, since then one would arrive at a huge system of equations containing a lot of parameters. In practice the bottleneck does rather lie in the large number of parameters than in the number of equations. Integrating huge sets of differential equations is nowadays not a real problem, although it may lead to long computing times. The hard part is to find realistic values for the parameters. Since most of them cannot be measured directly, they have to be estimated from data. In most cases either the data do not contain enough information for this purpose or the estimation problem is technically speaking too hard. Whatever the obstruction may be, a model without reliable parameters values is often useless for predictive purposes.

The bottom up procedure usually starts with network topology reconstruction. In this stage one tries to develop a network that represents the system and can be used to calculate its dynamical behavior. The nodes in the network may represent concentrations of gene expressions, metabolites, proteins, or other biological entities. On the ecological level the nodes often stand for concentrations of predators and preys. The dynamics of the concentrations in the nodes are regulated through interactions with other nodes. Hierarchically, there are three levels of network reconstructions [13]. The first one is the strictly topological level. At this level, one is only interested in which nodes have some interaction with each other without bothering about the type of interaction. For example, the directionality of an interaction (who is influencing who?) is not yet taken into account. The second level is finding the topology including a description of the causality of the connections. The goal of this reconstruction is to develop a directionality network to indicate the causal relationships. The third level concerns specifying the interaction quantitatively via explicit expressions that can be included in the equations that constitute the network model.

In this thesis we are concerned with the third level, i.e., we assume that we have at hand or can develop a set equations to describe the dynamics of the node concentrations.

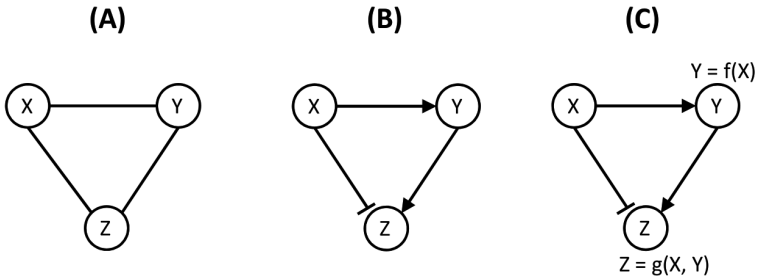

Figure 1.2: Three levels of network reconstructions. (A) Topology. Here one only concerns with the mapping interactions among the components in the system. No directionality is involved here. (B) Qualitative network topology. Here directionality is involved to indicate the causality, (C) Quantitative network topology. Here one tries to quantify, e.g., how the concentration of X affects the dynamics of Y.

1.3 Model complexity

The ultimate goal of systems biology is to gain understanding of the behaviour of biological systems at the system level and to develop models that have predictive power. Unfortunately, complexity is inherent to living systems and that may hinder us in achieving this goal. The cell cycle process that we will investigate in detail in Chapter 5, is a clear example how complex the interactions among the cell components and the environment may be. In most fleshly fruits like tomatoes, the cell cycle undergoes after some period a transition from the classical cell cycle, in which the standard cell division takes place, to a partial cell cycle, in which the cell keeps replicating its DNA but skips division [14]. Obviously, there are many components and factors needed to cause such an intricate transition and we will show how modeling can help us to elucidate this complex process.

One of the features of most biological systems that is very crucial for their functioning in a non-constant environment is robustness [15]. Robustness is defined as the ability of a system to preserve its functioning against internal and external perturbations. Phenomenologically, three types of robustness are observed in robust systems: (a) adaptation, i.e., the capability to survive under varying environmental conditions, (b) parameter insensitivity, i.e., the insensitivity of the systems to (limited) variations in the kinetic parameters, and (c) graceful degradation, which enables the systems to keep operating even if some of its components fail [8]. Since robustness is an essential feature of any biological system, a mathematical model describing a living system should also reflect this property. It is even proposed in [16] to use robustness as a means to check the plausibility of mathematical models. It is by no means simple to understand the robustness of complex models. For example, if there are many parameters in the model, it is very hard to find which parameter combinations are responsible for the robustness of the system.

A complication that is always faced when handling complex models is parameter identification. Parameters may either be estimated from observed data or derived from the literature. In the latter case, it is very important to assess the reliability of the parameter values with

respect to the system under consideration. If no parameter estimates are available in the literature one has to rely on fitting the model to the available data. In this procedure the aim is to find the parameter set that minimizes an object function that measures in some way the size of the residuals , i.e., the discrepancies between data and model output. This typically leads to a nonlinear optimization problem. In general, optimization algorithms can be categorized into local and global methods. Examples of local methods are Newton and steepest-descent methods, and examples of global methods are genetic algorithms and simulated annealing methods. Local optimization methods usually converge very fast, but using such a method one runs the risk to converge to a local minimum. In practice, this nearly always happens, since complex systems turn out to give rise to many local minima in the object function. On the other hand, for global optimization methods it is guaranteed that they converge to the global minimum, but computationally they are very expensive. The optimal strategy is using a hybrid approach that combines local and global methods. Such an optimization procedure starts with a global approach until some criteria are satisfied and then switches to a local method. At the moment, parameter estimation is one of the active fields of research in systems biology, and thus a lot of hybrid strategies have been proposed in the literature. In the present thesis we make use of procedures proposed in [17], implemented in MATLAB.

If one has solved the parameters estimation problem, the next step is to investigate the uncertainty in the estimated parameters. This is very important because uncertainty in parameter values usually propagates into uncertainty in model predictions. Thus, if the parameters of a model are not well determined, the model predictions are also not reliable [18]. In a deterministic approach parameter uncertainty analysis yields a confidence interval around the estimated parameter value. In a Bayesian analysis one even obtains probability distributions for the parameters. To decrease parameter uncertainty, one could add a new dataset obtained from different experiments to the parameter estimation procedure. To assure that the new data really lead to an improvement, the new experiment should be carefully designed. In this aspect, an optimal experimental design approach can help us to determine good experiments to be carried out [19].

In the ideal situation, parameter estimation and new experiments, based on optimal experimental design, can be carried out iteratively until all parameters are identified with high accuracy. However, in practice often only a limited number of experiments can be done and only a restricted number of biological components can be observed in experiments. Furthermore, obtained data are always noisy. Thus, identifying all parameters is often very difficult. This problem is especially urgent when the number of parameters is large. The reason is that, in developing a complex model, one could easily introduce interactions, and thus parameters, that in fact are redundant, since they are not necessary to secure the functioning of the system. Parameters related to redundant interactions can never be estimated. Because of these obstacles, parameter identification remains one of the big issues in systems biology. In this thesis we investigate in Chapters 3 and 4 how redundancy can be recognized and remedied.

A last complication that may arise when dealing with complex models is the computational time issue. Biological systems are driven by many processes that occur at largely different time scales. Gene expression, for example, occurs in the order of minutes to hours, whereas signal transduction occurs in the order of seconds [20]. When multiple time scales are present in a model, the computing time that is required to solve the differential equations

may be unacceptably long. However, in the present thesis project we were not faced with this problem.

1.4 Objective

As outlined above, the complexity of mathematical models for biological systems may give rise to difficulties in understanding its dynamical behaviour, to difficulties in parameter identification, and to very long computing time when integrating the model numerically. This calls for mathematical methods that may efficaciously handle these complexity issues. Therefore, the objective of this thesis is to develop methodologies to tackle complexity problems. Since this field is quite wide, we have to restrict ourselves and we therefore focus on three issues:

a) Robustness analysis. Here we aim at developing a method to estimate the robustness of biological functions with respect to variations in the parameters. Since this problem is relatively easy for small systems, we will develop a method that is especially suitable to deal with models that have a large number of parameters.

b) Complexity reduction. One way to overcome problems that arise from the complexity of a model is by simplifying it, also referred to as reduction. A suitable reduction method may lead to a reduced model that is still reliable for a given purpose, but much easier to manage.

c) Modeling of the cell cycle in tomato fruit pericarp. From such model, we want to gain understanding of the mechanisms underlying the transition from the classical cell cycle to endoreduplication, i.e., a partial cell cycle, and thus obtain better understanding of tomato fruit formation in general.

1.5 Outline of this thesis

The remainder of this thesis is organized as follows.

In Chapter 2, a novel method to assess the robustness region of biological models is presented. We focus on models that show oscillatory behaviour. Oscillations are ubiquitous in biological systems. It is found, for example, in the pulse of the heart, the circadian rhythm, and in the cell cycle. The models that describe such oscillatory phenomena are usually governed by many parameters. The presented method is especially designed to be efficient to handle such high dimensional situations.

In Chapter 3, a novel model reduction method is presented. The essence of this method is that components and/or reactions that do not contribute to the dynamics of the system are removed from the model. This yields a reduced model with less parameters that can still represent observed data.

A reduced model obtained with the method described in Chapter 3 will be a satisfactory representation of the system for the conditions under which the data used are obtained. However, if one requires more and wants the reduced system to represent the original model for any possible experimental condition, the reduction method in Chapter 3 is not suitable.

Therefore, in Chapter 4 the method of Chapter 3 is extended by combining this reduction method with a model discrimination method. The extended procedure leads to reduced models that can in the experimental practice not be discriminated from their original full models and thus form real substitutes. When applied to a biochemical model, our extended reduction procedure leads to the insight which parts of the original model are redundant and which parts belong to the core of the model.

In Chapter 5 we present research that is of a slightly different character compared to the methodological approaches in the preceding chapters. Here, we develop a mathematical model to describe the cell cycle in tomato fruit pericarp. Special attention is paid to the transition to a partial cycle. In the literature a number of putative mechanisms that might lead to this transition have been proposed. We show how modeling can help us to unravel and understand the complexity of this phenomenon. This is carried out by carefully including the putative mechanisms that might lead to the transition into the model and checking whether the resulting model can indeed describe the observed transition cell.

Eventually, in chapter 6, we reflect on how the methods that we developed can help us in tackling the complexity and understanding of biological systems. The discussion is concluded with some recommendations for future work.

Bibliography

[1] Alberts B, Johnson A, Lewis J, Raff M, Roberts K, et al. (2008) Molecular Biology of The Cell. Garland Science, 5th edition.

[2] Kerr J, Wyllie A, Currie A (1972) Apoptosis: a basic biological phenomenon with wide-ranging implications in tissue kinetics. Br J Cancer 26: 239-257.

[3] Regenmortel MHVV (2004) Reductionism and complexity in molecular biology. EMBO Rep 5: 1016–1020.

[4] Sionov RV, Haupt Y (1999) The cellular response to p53: the decision between life and death. Oncogene 18: 6145-6157.

[5] Kitano H (2002) Computational systems biology. Nature 420: 206–210.

[6] Keurentjes JJ, Angenent GC, Dicke M, Santos VAMD, Molenaar J, et al. (2011) Redefining plant systems biology: from cell to ecosystem. Trends Plant Sci 16: 183–190.

[7] Kitano H (2001) Foundations of Systems Biology. The MIT Press.

[8] Kitano H (2002) Systems biology: A brief overview. Science 295: 1662-1664.

[9] Bruggeman FJ, Hornberg JJ, Boogerd FC, Westerhoff HV (2007) Introduction to systems biology. In: Plant Systems Biology, Birkhäuser Verlag/Switzerland. pp. 1-19.

[10] Bruggeman FJ, Westerhoff HV (2007) The nature of systems biology. Trends Microbiol 15: 45–50.

[11] Klipp E, Liebermeister W, Wierling C, Kowald A, Lehrach H, et al. (2009) Systems Biology: A Textbook. Wiley-VCH.

[12] Periwal V, Szallasi Z, Stelling J (2010) System modeling: Why and why now? In: System Modeling in Cellular Biology, The MIT Press. pp. ix-xiv.

[13] Rice J, Stolovitzky G (2004) Making the most of it: pathway reconstruction and integrative simulation using the data at hand. Drug Discovery Today: BIOSILICO 2: 70–77.

[14] Bourdon M, Frangne N, Mathieu-Rivet E, Nafati M, Cheniclet C, et al. (2010) Endoreduplication and growth of fleshy fruits. In: Progress in Botany 71, Springer Berlin Heidelberg, volume 71. pp. 101-132.

[15] Kitano H (2004) Biological robustness. Nat Rev Genet 5: 826–837.

[16] Morohashi M, Winn AE, Borisuk MT, Boluri H, Doyle J, et al. (2002) Robustness as a measure of plausibility in models of biochemical networks. Journal of Theoretical Biology 216: 19-30.

[17] Balsa-Canto E, Peifer M, Banga J, Timmer J, Fleck C (2008) Hybrid optimization method with general switching strategy for parameter estimation. BMC Systems Biology 2: 26.

[18] Raue A, Kreutz C, Maiwald T, Bachmann J, Schilling M, et al. (2009) Structural and practical identifiability analysis of partially observed dynamical models by exploiting the profile likelihood. Bioinformatics 25: 1923–1929.

[19] Bandara S, Schlöder JP, Eils R, Bock HG, Meyer T (2009) Optimal experimental design for parameter estimation of a cell signaling model. PLoS Comput Biol 5: e1000558–.

[20] Alon U (2006) An introduction to systems biology: design principles of biological circuits. Chapman & Hall, 301 pp.

Chapter 2

Estimation of the robustness region of oscillating biological models [1]

Abstract

Robustness is an essential feature of biological systems, and any mathematical model that describes such a system should reflect this feature. Especially, persistence of oscillatory behavior is an important issue. A benchmark model for this phenomenon is the Laub-Loomis model, a nonlinear model for cAMP oscillations in Dictyostelium discoideum. This model captures the most important features of biomolecular networks oscillating at constant frequencies. Nevertheless, the robustness of its oscillatory behavior is not yet fully understood. Given a system that exhibits oscillating behavior for some set of parameters, the central question of robustness is how far the parameters may be changed, such that the qualitative behavior does not change. The determination of such a "robustness region" in parameter space is an intricate task. If the number of parameters is high, it may be also time consuming. In the literature, several methods are proposed that partially tackle this problem. For example, some methods only detect particular bifurcations, or only find a relatively small box-shaped estimate for an irregularly shaped robustness region.

Here, we present an approach that is much more general, and is especially designed to be efficient for systems with a large number of parameters. As an illustration, we apply the method first to a well understood low-dimensional system, the Rosenzweig-MacArthur model. This is a predator-prey model featuring satiation of the predator. It has only two parameters and its bifurcation diagram is available in the literature. We find a good agreement with the existing knowledge about this model. When we apply the new method to the high dimensional Laub-Loomis model, we obtain a much larger robustness region than reported earlier in the literature. This clearly demonstrates the power of our method. From this results, we conclude that the biological system underlying is much more robust than was realized until now.

[1] Based on: M. Apri, J. Molenaar, M. de Gee, and G. van Voorn – *"Efficient Estimation of the Robustness Region of Biological Models with Oscillatory Behavior,"* PLoS ONE 5(4): e9865

2.1 Introduction

It is remarkable but well-known that many biological systems are robust under vastly different conditions [1, 2]. Although these systems might experience strong internal or external perturbations, e.g., through environmental changes or noise, they still operate reliably. This is, for example, observed in chemotactic behavior and patterning development [2]. Robustness is an essential feature of biological systems [3, 4], and any mathematical model describing their behavior should also have this property [5]. This implies the need for an efficient tool to analyze the robustness of these models.

Here we focus on the parametric robustness of biological models that show oscillatory behavior. Oscillations are ubiquitous in biology. It is found, for example, in the pulse of the heart, the circadian rythm, and the signal transduction that involves adenosine 3',5'-cyclic monophospate (cAMP) in the chemotactic of *Dictyostelium discoideum* [6]. The robustness of a model is determined by answering the question how far the parameters of the model could be perturbed so that the qualitative behavior of the system does not change. An example of such a change is, e.g., the transition from oscillatory behavior to a steady state equilibrium. Such a drastic transition is called a *Hopf bifurcation*. There are many types of bifurcations possible in dynamical biological models.

Given a so-called *nominal point* in parameter space for which a system has a stable periodic solution, in general a region around this point exists within which the system oscillates. We call such a region a "robustness region" if no bifurcation of any kind occurs in its interior and if in each point of its boundary the system undergoes some bifurcation. The type of the latter bifurcations may be of any kind. An important consequence of this definition is that the period of the oscillations varies smoothly over the robustness region. If somewhere a period doubling bifurcation (also referred to as flip bifurcation) occurs, such a dramatic change in qualitative behavior indicates that the system is no longer robust. According to our definition we meet in such a point the boundary of the robustness region. (Note that in this paper, the words flip bifurcation and period doubling bifurcation are used interchangeably.)

In the literature, some methods have been proposed to analyze robustness of models with oscillatory behavior. Robustness with respect to perturbations of a single or at most two parameters simultaneously can be investigated using a bifurcation analysis package such as AUTO [7]. With this package, the boundary of the robustness region can be obtained. In most cases, however, more parameters are involved and AUTO is no longer applicable. In [8], the Structured Singular Value method (SSV) from control theory [9] was used to quantify the robustness of the Laub-Loomis model [6]. This model has an oscillatory solution for a specific set of parameter values, the so-called nominal values. It was investigated how much the nominal values might be changed before a bifurcation would occur. The authors initially claimed that the allowed maximum parameter variation is 8.3%. The work was then improved by applying a hybrid optimization method which yielded a much smaller variation of 0.6% [10]. Ghaemi et al. utilized a Routh-Hurwitz stability criterion that resulted in 0.51% variation for the Laub-Loomis model [11]. The percentage values of parameter variations that are presented in these papers suggest that all parameters have the same sensitivity. However, the model might be more sensitive to some parameters than to others [12]. Furthermore, the authors studied only the Hopf bifurcation that occurs when the stable periodic behavior turns

into an equilibrium.

Here we present an alternative method to analyze the parametric robustness of biological models with stable oscillatory behavior (also referred to as "periodic solution" or "limit cycle"). The method aims at finding an approximation for the whole robustness region, taking into account that the sensitivity of the system might be highly parameter dependent. The consequence is that in our approach it is not useful to report the resulting estimate in terms of a percentage of the nominal value. On the contrary, the robustness region often turns out to be far from symmetric around the nominal point. Furthermore, the present approach allows for the detection of any kind of bifurcations, and is not limited to Hopf bifurcations. Another aspect refers to dimensionality. In high-dimensional systems, an important feature of any numerical method is efficiency. Many methods suffer from the so-called "dimensional curse", i.e. the computing time scales exponentially with dimension. For example, if we would use a Monte-Carlo approach for estimating the shape of robustness regions, we would certainly be confronted with this limiting factor. However, the method presented here has the computational advantage that it scales linearly with the number of parameters. That is the reason that it is highly efficient for systems with a high-dimensional parameter space.

The present method is based on Floquet theory and continuation of the periodic solution. Starting from the nominal parameter set, we construct an estimate for the robustness region by scanning the parameter space in orthogonal directions. If necessary, the obtained estimate is refined by shifting the nominal point to a carefully chosen new position. We do not only focus on Hopf bifurcations, but take into account all types of bifurcation that might occur to periodic solutions, including period doubling and Neimark-Sacker bifurcations. So, also bifurcations that lead to chaotic behavior may be detected. In addition, the presented method yields extra information such as the period and the amplitude of the solution for free.

To demonstrate the ideas and power of the proposed method, we apply it to ecological and biological network models that admit stable periodic solutions: the Rosenzweig-MacArthur (RMA) model and the Laub-Loomis (LL) model. The RMA model is chosen for illustrational purposes. It is well known for its rich bifurcation pattern and serves as a test case here. It is a low dimensional system for which our method is not especially designed, but it serves as a useful check of performance. It consists of three state variables with six parameters where two of them are taken free. The LL model is a high dimensional system that consists of seven state variables with fourteen parameters. Its robustness has been already investigated in [8, 10, 11]. As an extra check on low dimensional systems we analyze the LL model with twelve fixed and only two parameters perturbed. Our results for two dimensional systems fully agree with those obtained with existing approaches. The results for the high dimensional LL model clearly demonstrate that the present method is a real extension of the existing approaches.

2.2 Methods

The stability of a periodic solution can be verified using Floquet theory (see [13] and [14]). In this theory, the Floquet multipliers, which are the eigenvalues of the so-called *monodromy*-matrix, are used to indicate stability. One of the Floquet multipliers is always real and equal to 1. A necessary and sufficient condition for a periodic solution to be stable is that the

modulus of the other Floquet multipliers is less than 1, i.e., they lie inside the unit circle in the complex plane. If the parameters are perturbed and one of the multipliers crosses the unit circle, the solution looses its stability and a bifurcation happens. This suggests that in order to analyze the robustness of oscillatory behavior of a model, we only need to observe its Floquet multipliers as functions of the parameters.

Here we describe the details to find in an efficient way an estimate for the robustness region. In short, starting in a so-called nominal point in parameter space for which a stable periodic solution exists, the parameter space is scanned along orthogonal directions to detect where along these lines bifurcations occur. This yields an initial estimate of the robustness region, that is gradually improved by shifting the nominal point and varying the directions.

2.2.1 Floquet Theory and Periodic Solutions

Consider an ordinary differential equation system

$$\frac{d\mathbf{x}}{dt} = F(\mathbf{x}, \mathbf{k}), \quad \mathbf{x} \in \mathbb{R}^n, \mathbf{k} \in \mathbb{R}^m, \tag{2.1}$$

where $\mathbf{x}$ denotes the vector of state variables and $\mathbf{k}$ the vector of parameters. Suppose that this system has a stable periodic solution at $\mathbf{k} = \mathbf{k}_0$ with periodic solution $\mathbf{x} = \mathbf{x}^*$ and period T.

In order to investigate the stability of the solution, we linearize around the periodic orbit $\mathbf{x}^*$ and obtain

$$\frac{d\boldsymbol{\delta}}{dt} = J(\mathbf{x}^*, \mathbf{k})\boldsymbol{\delta}(t), \tag{2.2}$$

where J is the Jacobian matrix of (2.1) with respect to its state variables $\mathbf{x}$. Since $\mathbf{x}^*$ is $T-$periodic, the Jacobian matrix J is also $T-$periodic. According to Floquet theory (see [13] and [14]), the fundamental solution of (2.2), which is a matrix that is composed of n independent solutions of (2.2), can be written as

$$\Phi(t) = P(t)e^{Bt}, \tag{2.3}$$

with $P(t)$ $T-$periodic and B a constant $n \times n$ matrix. Thus,

$$\Phi(t + T) = \Phi(t)e^{BT}. \tag{2.4}$$

Here, $C = e^{BT}$ is called the monodromy matrix of the system and the eigenvalues of C are called the Floquet multipliers of the system. One of them is always real and equal to 1. A necessary and sufficient condition for the periodic solution of (2.2) to be stable is that the other $n - 1$ multipliers have modulus less than 1, i.e. they lie inside the unit circle. The calculation of Φ is explained underneath.

Three cases may be discerned [15, 16, 17], as illustrated in Figure 2.1:

1. A multiplier leaves the unit circle at $(1, 0)$. In this case, the model experiences a fold bifurcation.

2. A multiplier leaves the unit circle at $(-1, 0)$. In this case, a flip bifurcation takes place and period doubling occurs.

3. Two conjugate multipliers cross the unit circle. In this case, a Neimark-Sacker bifurcation occurs.

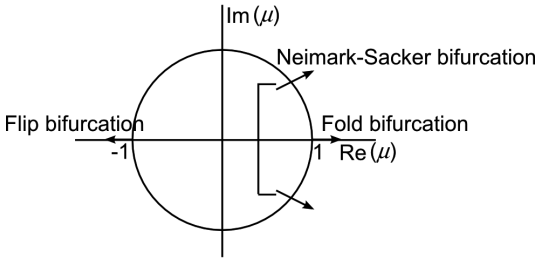

Figure 2.1: Limit cycle bifurcations according to the position of Floquet multipliers in the complex plane [15, 16, 17].

2.2.2 Calculation of Periodic Solutions

As has been indicated above, to calculate Floquet multipliers, first the periodic solution of (2.1) should be obtained. There are many methods discussed in the literature to approximate a periodic solution. To mention some of them: finite difference method, shooting method, and Poincare map method [17]. In this paper, we use the finite difference method because of its simplicity, and a short outline of the method is given below.

Consider again the ODE system (2.1). With the scaling

$$\tau = \frac{t}{T} \tag{2.5}$$

with T the period, the system reads as

$$\frac{d\mathbf{x}}{d\tau} = TF(\mathbf{x}, \mathbf{k}), \quad \mathbf{x} \in \mathbb{R}^n, \mathbf{k} \in \mathbb{R}^m. \tag{2.6}$$

Now, (2.6) has to be solved in the time interval $\tau \in (0, 1)$. This time interval is discretized into $N + 1$ points with a uniform time step h:

$$\tau_1 = 0, \tau_2 = h, \ldots, \tau_{N+1} = Nh = 1.$$

The solution of (2.6) at time steps $\tau = \tau_i$ and $\tau = \tau_{i+1}$ are related by

$$\mathbf{x}(\tau_{i+1}) = \mathbf{x}(\tau_i) + T \int_{\tau_i}^{\tau_{i+1}} \mathbf{F}\left(\mathbf{x}(\bar{\tau}), \mathbf{k}\right) d\bar{\tau}. \tag{2.7}$$

Using the trapezoidal rule to represent the integral, we obtain

$$\mathbf{x}^{i+1} - \mathbf{x}^i = \frac{1}{2} hT \left[\mathbf{F}(\mathbf{x}^{i+1}, \mathbf{k}) + \mathbf{F}(\mathbf{x}^i, \mathbf{k}) \right], \tag{2.8}$$

where $\mathbf{x}^i = \mathbf{x}(\tau_i)$. Since the system is periodic, $\mathbf{x}(\tau_{N+1}) = \mathbf{x}(\tau_1)$, or

$$\mathbf{x}^{N+1} = \mathbf{x}^1. \tag{2.9}$$

Therefore, we have nN algebraic equations from (2.8) with $nN + 1$ unknowns:

$$\mathbf{x}^1, \mathbf{x}^2, \ldots, \mathbf{x}^N, T.$$

Finally, since the system that we consider is autonomous, the system is invariant to a linear shift in the time origin. To remove the arbitrariness of the phase, we specify the value of one component at $\tau = 0$, for example

$$x_1^1(0) = \eta, \tag{2.10}$$

where the value η should be within the periodic solution of $x_1(t)$. Thus, at time $\tau = \tau_1$ we have $\mathbf{x}^1 = (\eta, \tilde{\mathbf{x}}^1)$ with $\tilde{\mathbf{x}}^1 \in \mathbb{R}^{n-1}$. By imposing this condition, we have nN unknowns

$$\tilde{\mathbf{x}}^1, \mathbf{x}^2, \ldots, \mathbf{x}^N, T \tag{2.11}$$

and nN algebraic equations. Its solution can be found using, e.g., Newton's scheme, provided (2.10) is in the orbit of $x_1(t)$. The details of this method can be found in [17].

So, we obtain the periodic solution in N discretized points and the value of the period T becomes known. The full periodic solution $\mathbf{x}^*(t)$ can then be obtained by integrating

$$\begin{aligned} \frac{d\mathbf{x}}{dt} &= \mathbf{F}(\mathbf{x}, \mathbf{k}) \\ \mathbf{x}(0) &= \begin{pmatrix} \eta \\ \tilde{\mathbf{x}}^1 \end{pmatrix} \end{aligned} \tag{2.12}$$

numerically from time $t = 0$ to $t = T$.

Computing Floquet Multipliers

Let us consider the principal fundamental problem, i.e. problem (2.2) with now $\boldsymbol{\delta}(t)$ taken to be a matrix

$$\dot{\boldsymbol{\delta}} = J(\mathbf{x}^*, \mathbf{k})\boldsymbol{\delta}(t) \tag{2.13}$$

with initial values

$$\boldsymbol{\delta}(0) = I_n \tag{2.14}$$

where I_n is the $n \times n$ identity matrix. The Floquet multipliers of the system can then be obtained by integrating the above equation for one period, that is from $t = 0$ to $t = T$. Then, the Floquet multipliers, denoted by μ_i, $i = 1, 2, \ldots, n$, are the eigenvalues of the matrix $\boldsymbol{\delta}(T)$.

Note that if we employ the same numerical technique to integrate (2.12) and (2.13), both systems can be solved simultaneously. We denote the $i-$th column of the matrix $\boldsymbol{\delta}$ by $\boldsymbol{\delta}_i$ and solve

$$\begin{cases} \dot{\mathbf{x}} = \mathbf{F}(\mathbf{x}, \mathbf{k}, T) \\ \dot{\boldsymbol{\delta}}_1 = J(\mathbf{x}, \mathbf{k}, T)\boldsymbol{\delta}_1(t) \\ \vdots \\ \dot{\boldsymbol{\delta}}_n = J(\mathbf{x}, \mathbf{k}, T)\boldsymbol{\delta}_n(t) \end{cases} \tag{2.15}$$

with initial conditions

$$\begin{cases} \mathbf{x}(0) = \left(\eta, \tilde{\mathbf{x}}^1\right)^T \\ \boldsymbol{\delta}_1(0) = (1, 0, \ldots, 0)^T \\ \vdots \\ \boldsymbol{\delta}_n(0) = (0, 0, \ldots, 1)^T \end{cases} \tag{2.16}$$

Since one of the multipliers should be real and equal to 1, the approximation of the periodic solution and the Floquet multipliers are carried out iteratively. If no multipliers are close to 1, we increase the number N and solve again (2.8) and (2.15) until one of the multipliers is close to 1 within a prespecified accuracy.

2.2.3 Continuation Method

In this section, we describe how a robustness region estimate can be constructed. The idea is to scan the parameter space along orthogonal directions to detect where along these lines bifurcations occur. We start at a nominal point $\mathbf{k}_0$ in parameter space, where the model has a stable limit cycle, so that the Floquet multipliers lie within the unit circle (except for one). The approach outlined here is also applicable if $\mathbf{k}_0$ lies on the boundary of the robustness region. The first direction $\mathbf{v}_1$, the construction of which is described below, will then point into the robustness region. It suffices to follow that direction until the boundary at the other side is met in a point $\mathbf{k}_1$, say, and to choose as new nominal point the midpoint of $\mathbf{k}_0$ and $\mathbf{k}_1$. The next step is to perturb the nominal point $\mathbf{k}_0$ along n orthogonal directions $\mathbf{v}_1, \mathbf{v}_2, \ldots, \mathbf{v}_m$.

To construct $\mathbf{v}_1$, we introduce the function

$$g(\mathbf{k}) = g(k_1, k_2, \ldots, k_m) = \max_{i=2,\ldots,n} \|\mu_i\| < 1 \tag{2.17}$$

which is nothing else but the largest modulus multiplier in $\mathbf{k}$ that is less than 1. The gradient

$$\nabla g = \left(\frac{\partial g}{\partial k_1}, \ldots, \frac{\partial g}{\partial k_m}\right) \tag{2.18}$$

is calculated numerically by

$$\frac{\partial g}{\partial k_j} \approx \frac{g(k_1, \ldots, k_j + \varepsilon, \ldots, k_m) - g(k_1, \ldots, k_m)}{\varepsilon}, j = 1, \ldots, m, \tag{2.19}$$

taking ε smaller and smaller until convergence is reached.

For the first direction $\mathbf{v}_1$, we now take $\mathbf{v}_1 = \nabla g(\mathbf{k}_0)$. For the other perturbation directions we choose vectors that are orthogonal to $\mathbf{v}_1$ and to each other. They are calculated by the Gram-Schmidt method. The set of perturbation directions is thus

$$\{\mathbf{v}_1 = \nabla g(\mathbf{k}_0), \mathbf{v}_2, \ldots, \mathbf{v}_m\} \tag{2.20}$$

Note that the choice of $\mathbf{v}_1$ is unique, but the choice of $\mathbf{v}_2, \ldots, \mathbf{v}_m$ is not. However, the resulting approximate for the robustness region does not much depend on this choice, unless this region is highly irregularly shaped. To check the outcome it is recommendable to apply the method with a number of different nominal points and compare the outcomes. This will give a very good impression of the situation in parameter space.

The idea is now to perturb the nominal parameters $\mathbf{k}_0$ along these directions, so for direction $\mathbf{v}_i$, we walk along the line

$$\mathbf{k}_0 + \gamma \mathbf{v}_j, \tag{2.21}$$

with γ both positive and negative and check for which γ we approach a bifurcation. This yields the principal axes of the estimated robustness region. An improvement of this concept is obtained by repeating this procedure but with $\mathbf{k}_0$ replaced by, e.g., the center of the longest axis. This leads to a refined approximation of the full robustness region.

2.2.4 Algorithm

The algorithm to construct a robustness region is given in Figure 2.2. In this diagram we point out in a concise way that the algorithm contains the following steps:

1) Calculate the perturbation directions $\mathbf{v}_j$ at the nominal parameter $\mathbf{k}_0$. For $\mathbf{v}_1$, take $\mathbf{v}_1 = \nabla g(\mathbf{k}_0)$ using (2.19) and construct the other perturbation directions using the Gram-Schmidt method.

2) Calculate the periodic solution and its multipliers along the lines (2.21) starting from $\mathbf{k}_0$. If one or more multipliers pass the unit circle, a bifurcation has been detected.

3) If refinement is required, move the nominal point to the center of the longest axis and repeat the procedure. Also, extra directions could be chosen.

2.3 Results

In the next sections, we apply our method to two biological models: the low-dimensional RMA model and the high-dimensional LL model.

2.3.1 Application to the Rosenzweig-MacArthur Model

The Rosenzweig-MacArthur (RMA) model is an ecological model that describes the time evolution of a predator-prey system [18]. In dimensionless form, this 3-dimensional model

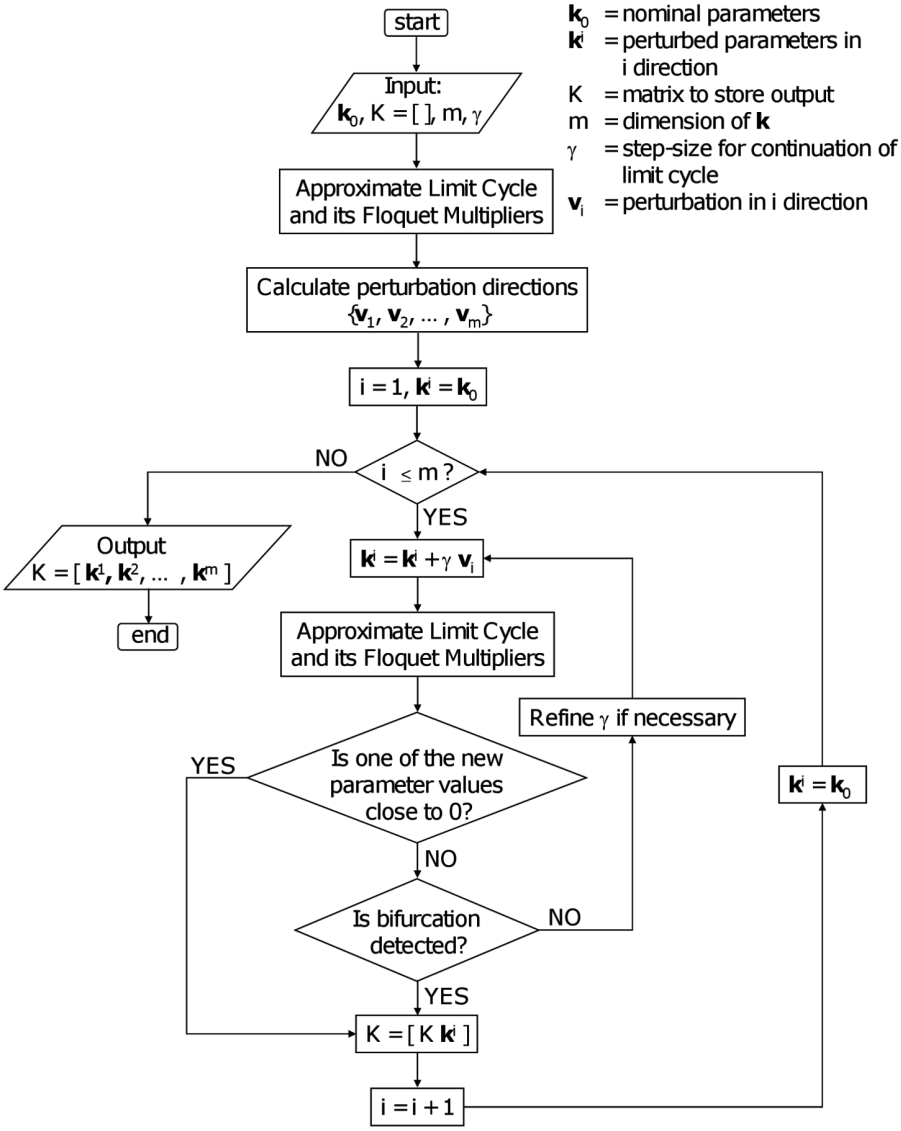

Figure 2.2: Flow chart of the method to approximate the robustness region around a nominal point $\mathbf{k}_0$. The approximated region is obtained by scanning the parameter space along orthogonal directions starting at $\mathbf{k}_0$.

reads as

$$\begin{aligned} \dot{x}_1 &= x_1(1-x_1) - f_1(x_1)x_2 \\ \dot{x}_2 &= f_1(x_1)x_2 - k_1 x_2 - f_2(x_2)x_3 \\ \dot{x}_3 &= f_2(x_2)x_3 - k_2 x_3, \end{aligned} \tag{2.22}$$

where

$$\begin{aligned} f_1(x_1) &= \frac{a_1 x_1}{1 + b_1 x_1} \\ f_2(x_2) &= \frac{a_2 x_2}{1 + b_2 x_2}. \end{aligned} \tag{2.23}$$

Here, x_1, x_2, x_3 denote the prey, predator, and top predator populations, respectively, a_1, a_2, b_1, b_2 are the parameters in the Michaelis-Menten functions f_1 and f_2, and k_1, k_2 are death rate parameters.

The dynamical behavior of this model for the fixed coefficient values

$$a_1 = 5, a_2 = 0.1, b_1 = 3, b_2 = 2, \tag{2.24}$$

has been extensively investigated in [19, 20, 21] as a function of k_1 and k_2. The resulting bifurcation diagram is depicted in Figure 2.3A. From this figure, we see that the limit cycle behavior of the model may experience a Hopf bifurcation, a transcritical bifurcation, or may transform into a flip bifurcation. Since there are infinitely many flip bifurcations in this bifurcation diagram, it is not possible to indicate all their positions in Figure 2.3A. Therefore, as a warning, we shade some areas in Figure 2.3C to indicate that flip bifurcations may occur somewhere in these areas. Due to infinitely many flip bifurcations, we restrict ourselves to the positions of the first period doubling bifurcations, which lie on the red curved line.

We apply our method to show how an estimate is obtained for the region in Figure 2.3A where a stable limit cycle exists. As nominal starting point we take $\mathbf{k}_0 = (k_1 = 0.6, k_2 = 0.008)$. In $\mathbf{k}_0$, the solution converges to a periodic solution with period $T = 120.04$ as shown in Figure 2.4A. The corresponding Floquet multipliers are

$$\boldsymbol{\mu} = \{\mu_1, \mu_2, \mu_3\} = \{0.9991, -4.5654\text{e-}016, -0.2319\}.$$

We notice that the largest multiplier μ_1 is indeed equal to 1 within the numerical accuracy. μ_2 and μ_3 lie inside the unit circle, so the limit cycle in $\mathbf{k}_0$ is stable. Following the method described above and summarized in equations (2.17) - (2.21), we construct two orthogonal directions, $\mathbf{v}_1$ and $\mathbf{v}_2$, and perturb the nominal parameter set $\mathbf{k}_0$ in these directions. The direction $\mathbf{v}_1$ is chosen such that the Floquet multipliers will change mostly when moving along $\mathbf{v}_1$ in the (k_1, k_2) plane and $\mathbf{v}_2$ is orthogonal to $\mathbf{v}_1$.

Continuation is applied along perturbation direction $\mathbf{v}_1$ until points B, denoted by a green star, and F, denoted by a red star, in Figure 2.3B are reached. Continuation is stopped at point B because the multipliers at that point are

$$\boldsymbol{\mu} = \{1.0000, 0.9991, -1.1102\text{e-}016\}.$$

So, $\mu_2 = 0.9991 \approx 1$ and this indicates that the method has successfully found a fold bifurcation. Using only Floquet multipliers, one cannot discriminate between a tangent, for which the cycle collides with a saddle limit cycle, and a Hopf bifurcation, for which the limit cycle disappears into an equilibrium. However, since in both cases the boundary of the robustness region is reached, this is not a problem at all. Just for curiosity we used AUTO

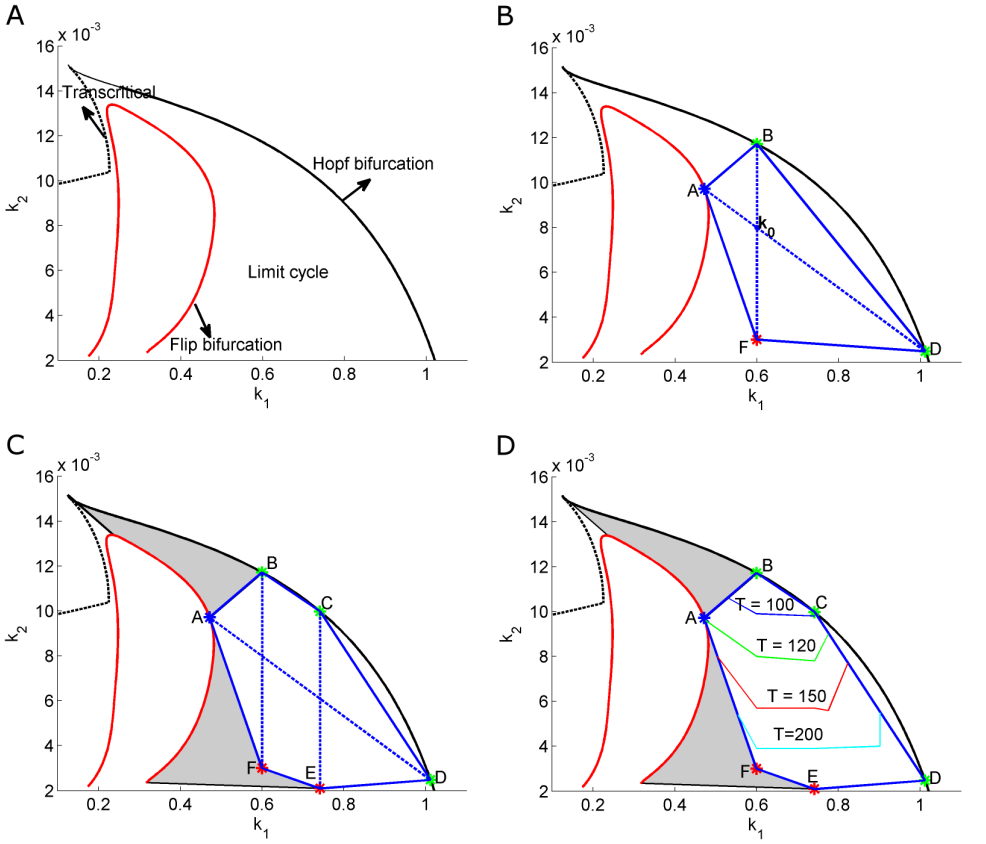

Figure 2.3: Bifurcation diagram and successive approximations of the robustness region of the RMA model. (A) Bifurcation diagram as a function of the death rate parameters k_1 and k_2 [20]. (B) Initial approximation. (C) Second approximation. (D) Estimated level lines of the period of the periodic solution. Note that the scale for k_1 and k_2 is not the same, which is the reason the orthogonality of the lines AD and BF is not directly clear from the picture. The shaded areas in C and D indicate regions where an infinitely number of period doubling bifurcations are located.

to confirm that it is the latter option. Continuation is stopped at point F. It does not make sense to continue beyond this point, since the value of parameter k_2 is so small there, that it is already hardly acceptable from a biological point of view. This also manifests itself in a very long period and a highly irregular shape of the limit cycle, that gives rise to a very long computational time. An example is given in Figure 2.4B, where we show the time behavior of the components at point F.

When the continuation procedure is applied along direction $\mathbf{v}_2$, the method hits two bi-

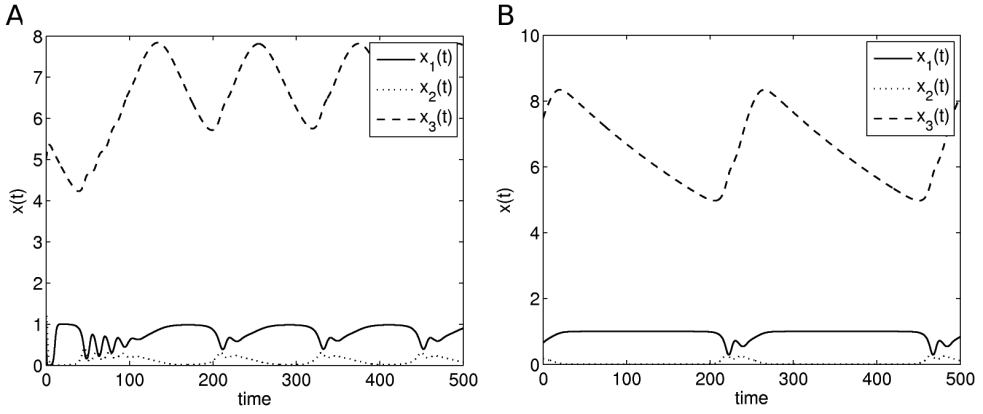

Figure 2.4: Behavior of the limit cycle solution of the RMA model. (A) In nominal point $\mathbf{k}_0$. (B) in point F.

furcation points, A and D. At point A, the mutlipliers are

$$\boldsymbol{\mu} = \{1.0006, -1.2583\text{e-}015, -1.0003\}.$$

We notice that $\mu_3 = -1.0003 \approx -1$, and we conclude that the method has successfully found a flip bifurcation, which is denoted by a blue-star. Since a flip indicates a possible route to chaos and it means the end of the limit cycle, as meant in the definition of robustness, this is also a boundary of robustness. On the other hand, we detect point D as a Hopf bifurcation. Thus, we obtain region ABDF as our first, crude approximation of the robustness region of the model. Note that the orthogonality of $\mathbf{v}_1$ and $\mathbf{v}_2$ that leads to the axes AD and BF is not directly clear from Figure 2.3B, because the axes have different scales.

Next, an improvement on this initial approximation is obtained by shifting the nominal point $\mathbf{k}_0$ to the midpoint of the longest axis, in this case the midpoint of AD which is denoted by $\mathbf{k}_0^*$ in Figure 2.3C. Applying the continuation procedure to the shifted nominal point $\mathbf{k}_0^*$ along the direction $\mathbf{v}_1$, we obtain a new axis CE. Here, point C is a Hopf bifurcation point. Just as for point F, we stop continuation in E since the value of k_2 becomes too small. Together with the previous findings, we now obtain the bigger estimating region ABCDEF, as shown in Figure 2.3C.

During the calculations, we simultaneously obtain a lot of information on the period and the shape of the limit cycle. In fact, this information is available along all the lines through $\mathbf{k}_0$ and $\mathbf{k}_0^*$. In Figure 2.3D, this info is used to draw level lines for the period. It provides a nice indication how the period behaves as a function of the parameters. Since the RMA model only serves as a low-dimensional illustration of the ideas behind the proposal estimation algorithm, we will not refine the approximation further, but rather turn to a high-dimensional example.

2.3.2 Application to the Laub-Loomis Model

The Laub-Loomis (LL) model [6] describes the dynamical behavior of the molecular network underlying cAMP (adenosine 3',5'-cyclic monophospate) oscillation observed in population of *Dyctiostelium discoideum* cells. The molecular network is depicted in Figure 2.5.

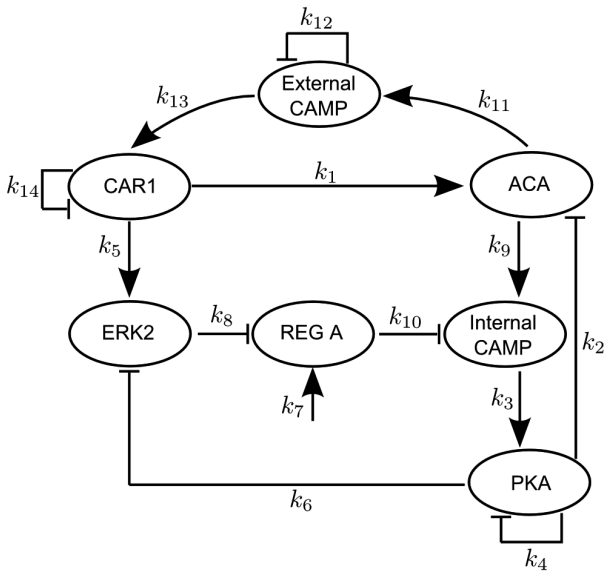

Figure 2.5: The network underlying the Laub-Loomis model

Here, after the binding of extracellular cAMP to the surface receptor CAR1, adenylate cyclase (ACA) activates internal cAMP. When internal cAMP is accumulated, it activates protein kinase PKA. In addition, ligand-bound CAR1 also activates the MAP kinase ERK2, which is then inactivated by PKA. Therefore, ERK2 no longer inhibits the cAMP phosphodiesterase REG A. A protein phosphatase activates REG A such that REG A can hydrolyze internal cAMP, hence the concentration of internal cAMP is reduced. When the internal cAMP is hydrolyzed by REG A, PKA activity is inhibited by its regulatory subunit, so that both ACA and ERK2 activities go up.

Based on the network above, the spontaneous oscillation in cAMP is a solution of the following model

$$\dot{\mathbf{x}} = \begin{bmatrix} k_1 x_7 - k_2 x_1 x_2 \\ k_3 x_5 - k_4 x_2 \\ k_5 x_7 - k_6 x_2 x_3 \\ k_7 - k_8 x_3 x_4 \\ k_9 x_1 - k_{10} x_4 x_5 \\ k_{11} x_1 - k_{12} x_6 \\ k_{13} x_6 - k_{14} x_7 \end{bmatrix}. \tag{2.25}$$

Here, the state variable $\mathbf{x} = (x_1, x_2, \ldots, x_7)$ represents the concentrations of seven proteins: x_1 = [ACA], x_2 = [PKA], x_3 = [ERK2] , x_4 = [REG A], x_5 = [Internal cAMP], x_6 = [External cAMP], and x_7 = [CAR1]. The model has 14 parameters, incorporated in the parameter vector $\mathbf{k} = (k_1, k_2, \ldots, k_{14})$.

At the nominal parameter set in Table 2.1, which is denoted by $\mathbf{k}_0$, this system has a stable periodic solution. Thus, if we choose the initial concentrations within the basin of attraction, the solution will converge to this periodic solution, as shown in Figure 2.6.

Table 2.1: Parameter values for the Laub-Loomis model. The nominal values $\mathbf{k}_0$ are obtained from [8, 10, 11]. The perturbed parameter values are obtained from $\mathbf{k}_p = \mathbf{k}_0 + 12.6\mathbf{v}_{12}$

Parameter	Units	Nominal value $\mathbf{k}_0$	Perturbed value $\mathbf{k}_0 + \gamma\mathbf{v}_{12}$
k_1	min^{-1}	2.0	2.6982
k_2	$\mu\text{M}^{-1}.\text{min}^{-1}$	0.9	0.9330
k_3	min^{-1}	2.5	2.4641
k_4	min^{-1}	1.5	1.3871
k_5	min^{-1}	0.6	0.7495
k_6	$\mu\text{M}^{-1}.\text{min}^{-1}$	0.8	0.6507
k_7	$\mu\text{M}.\text{min}^{-1}$	1.0	0.9006
k_8	$\mu\text{M}^{-1}.\text{min}^{-1}$	1.3	1.3690
k_9	$\mu\text{M}^{-1}.\text{min}^{-1}$	0.3	0.0009
k_{10}	$\mu\text{M}^{-1}.\text{min}^{-1}$	0.8	0.6758
k_{11}	min^{-1}	0.7	1.1100
k_{12}	min^{-1}	4.9	17.4668
k_{13}	min^{-1}	23	23.0125
k_{14}	min^{-1}	4.5	4.4666

We found that the periodic solution at the nominal parameters $\mathbf{k}_0$ has period $T = 7.3782$ and the multipliers are given by

$$\begin{aligned}\boldsymbol{\mu} =&\{1.0006, 0.9391, 6.6590\text{e-}006, 4.0012\text{e-}018 \pm 9.9791\text{e-}018i,\\ &-1.5203\text{e-}005 \pm 5.3021\text{e-}006i\}.\end{aligned}$$

We notice that the largest multiplier, $\mu_1 = 1.0006$, is equal to 1 within the numerical accuracy. Since the second largest multiplier μ_2 is also quite close to 1, we expect that the nominal point $\mathbf{k}_0$ is close to a bifurcation point.

Restriction to a 2-dimensional cross-section of parameter space

For illustrational purposes, we first fix 12 parameters setting them at the values in Table 2.1 and only vary k_2 and k_{14}. In this way we deal with a two dimensional cross-section in the high-dimensional parameter space. The advantage is that the results can be compared to

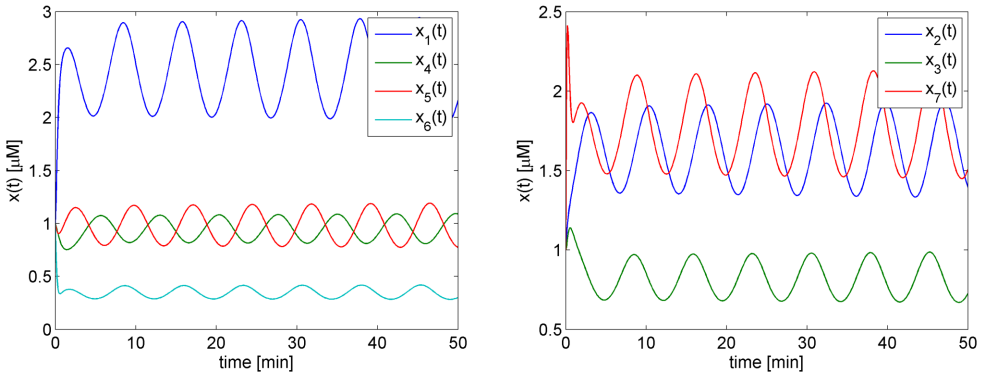

Figure 2.6: Periodic solution of the Laub-Loomis model (2.25) at the nominal parameter values in Table 2.1.

results obtained with AUTO and in [11]. AUTO yields the robustness region given in Figure 2.7A. This region perfectly agrees with the region reported in [11]. However, it should be noted that the method in [11] yields a very good estimate only in the two-dimensional case. For higher dimensions, their approach leads to a much more restricted estimated region. If we would apply the more-than-two-dimensions approach in [11] or in [8, 10] to the present two-dimensional case, we would only find the small square shaped estimate indicated in Figure 2.8.

Applying the algorithm in (2.17)-(2.21), we obtain two directions: $\mathbf{v}_1$, which is the most sensitive direction; and $\mathbf{v}_2$, which is orthogonal to $\mathbf{v}_1$. Along these directions, we perform the continuation procedure. This leads to our first approximation of the robustness region ABDF as shown in Figure 2.7B.

As denoted in the figure, our method successfully detected the four fold bifurcation points, A, B, D, and F which are indicated with black stars. According to the results obtained by AUTO, these points are Hopf bifurcations points where the second largest modulus of multipliers is very close to 1. For instance, at point A

$$\begin{aligned}\boldsymbol{\mu} =&\{0.9996, 0.9990, 4.1520\text{e-}005, -1.7673\text{e-}018, -1.6024\text{e-}016,\\ &-4.7223\text{e-}006 \pm 1.9026\text{e-}006i\}.\end{aligned}$$

We notice that the initial approximation is much smaller than the real robustness region found by AUTO. We improve our approximation by shifting the nominal parameter $\mathbf{k}_0$ to $\mathbf{k}_0^*$, the midpoint of AD. When the continuation procedure is applied to the new nominal parameter $\mathbf{k}_0^*$ along direction $\mathbf{v}_2$, we find the Hopf bifurcation points C and E. Together with the first approximation, we now have obtained the larger approximation region ABCDEF, as shown in Figure 2.7C. As extra information, we get for free the level lines for the period as indicated in Figure 2.7D. The approximation could be further improved by taking more perturbation directions, but this is hardly necessary to get a very good impression of the robustness region.

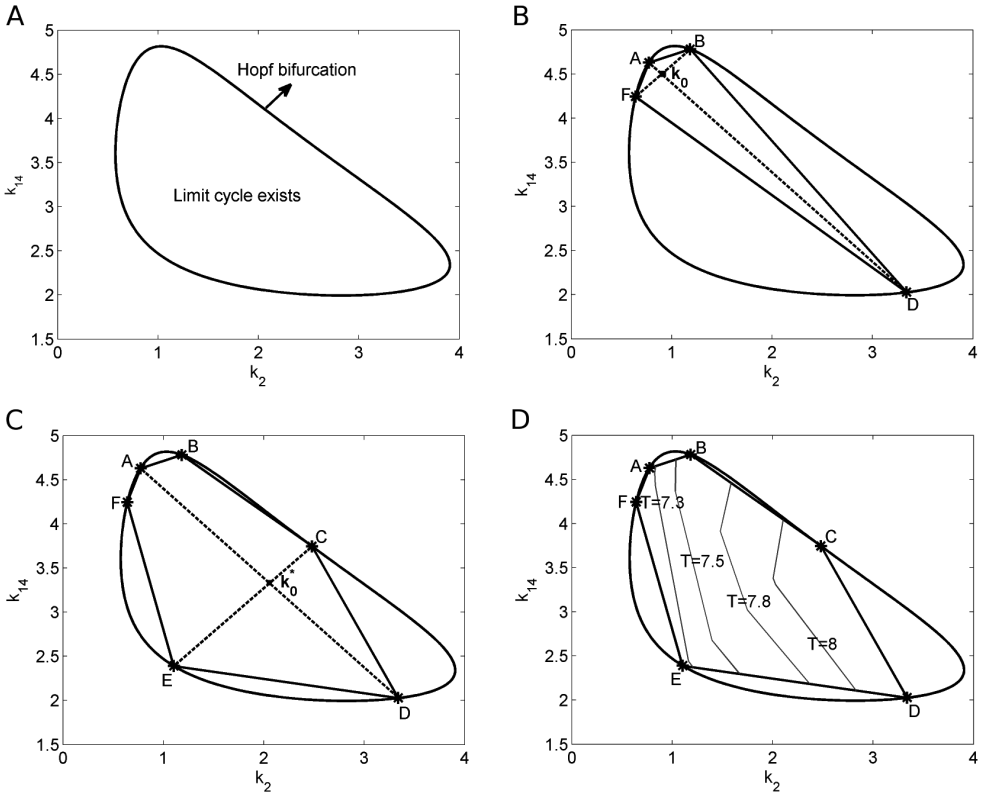

Figure 2.7: Cross-section of the robustness region of the Laub-Loomis model in the (k_2, k_{14}) plane. (A) Result by AUTO. (B) First approximation based on 4 boundary points. (C) Second approximation based on 6 boundary points. (D) Level lines of the period of the periodic solution.

Application in full-dimensional parameter space

Let us now investigate the robustness region of the Laub-Loomis model in the 14-dimensional parameter space. It will be clear that in this high-dimensional case the results are hard to present visually. According to algorithm (2.17)-(2.21), we find 14 orthogonal directions $\{\mathbf{v}_1, \mathbf{v}_2, \ldots, \mathbf{v}_{14}\}$ which, for convenience, are normalized to have unit length.

By applying continuation and observing the multipliers during the continuation, we easily obtain an estimate of the 14-dimensional robustness region. This estimate is shown in Figure 2.9A in a dedicated form. In this figure, the range of perturbations that is allowed to maintain the stability of the limit cycle is shown by horizontal lines for each perturbation direction. There are three possibilities that we stop the continuation: one of the perturbed parameters becomes close to 0 (in the LL model, all parameters should be positive), a bifurcation is detected, or the limit cycle gets an extremely long period. In the latter case, we need too

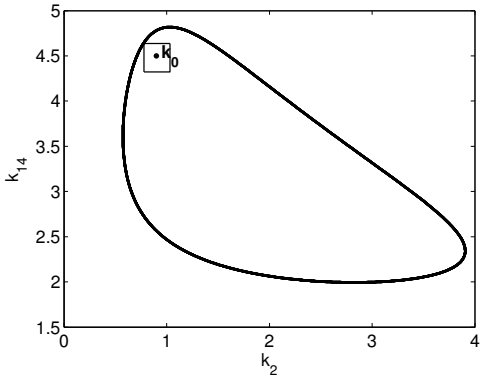

Figure 2.8: Robustness region of the Laub-Loomis model in parameter space. Black-line from AUTO, the black box indicates the estimate that would be obtained if the methods published earlier and developed for high-dimensional system [8, 10, 11] would be applied to the two dimensional case, in which only k_2 and k_{14} are varied.

much computational time to approximate the limit cycle. If one of the parameters becomes close to 0, we denote in Figure 2.9 the point by ('|'); if a bifurcation is detected, we do not put any marker on the point; and if the continuation is stopped because of computing time, we denote the point by (*). For example, in the $\mathbf{v}_{12}$ direction the nominal parameter $\mathbf{k}_0$ can be perturbed in the range

$$\mathbf{k} = \mathbf{k}_0 + \gamma \mathbf{v}_{12}, \quad \gamma \in [-1.332, 12.6]. \tag{2.26}$$

The continuation is stopped at $\gamma = -1.332$ because then a fold bifurcation is detected, which follows from the Floquet multipliers

$$\begin{aligned}\boldsymbol{\mu} =\{&1.0002, 0.9991, -1.3091\text{e-}005 \pm 1.3186\text{e-}006i, 2.7715\text{e-}006,\\ &2.2113\text{e-}016 \pm 5.501\text{e-}016i\}.\end{aligned}$$

At $\gamma = 12.6$, the system still admits a stable limit cycle behavior as shown in Figure 2.10, but we stop the continuation because one of the perturbed parameters becomes very close to 0, see Table 2.1.

In the $\mathbf{v}_7$ direction, the nominal parameter can be perturbed in the range

$$\mathbf{k} = \mathbf{k}_0 + \gamma \mathbf{v}_7, \quad \gamma \in [-1.0228, 4.22]. \tag{2.27}$$

Continuation is stopped at $\gamma = -1.0228$ because the period of the limit cycle becomes extremely long and requires too much computational time. The behavior of the period along this direction is shown in Figure 2.11. At $\gamma = 4.22$, the continuation is stopped because one of the perturbed parameters becomes very close to 0.

To get still a better impression of the robustness region, we shift the nominal parameter. From the result in Figure 2.9A, we find that the system can be mostly perturbed in the direction of $\mathbf{v}_{12}$. Therefore, we shift the nominal point $\mathbf{k}_0$ to the midpoint of this axis, and we

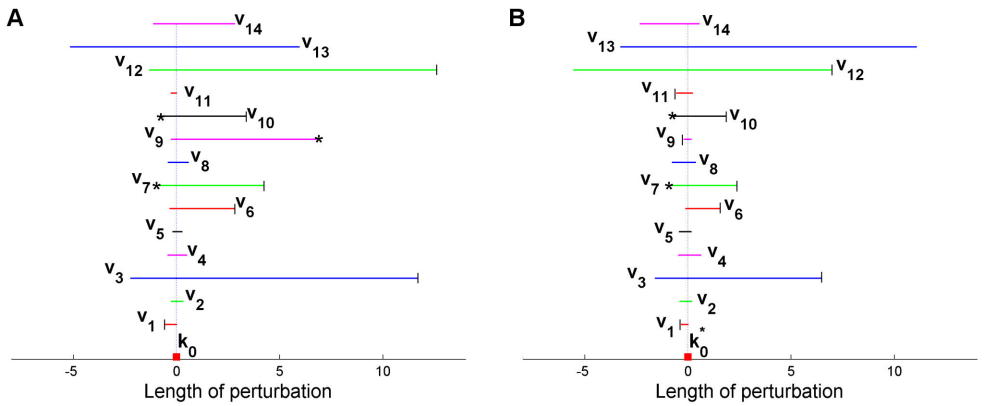

Figure 2.9: Representation of the "width" of the robustness region of the LL model. This region is measured along the 14 orthogonal directions $\mathbf{v}_1, \mathbf{v}_2, \ldots, \mathbf{v}_{14}$ used to scan the parameter space. In A, these directions start in nominal point $\mathbf{k}_0$ (see Table 2.1). In B, the directions start in $\mathbf{k}_0^* = \mathbf{k}_0 + 5.634\mathbf{v}_{12}$. If an end point is marked with "|", one of the parameters has become close to zero. If an end point marked with "*", the period of the limit cycle becomes extremely long. If an end point does not have mark, a fold bifurcation is detected. The lengths of the horizontal lines indicate how far this direction can be followed in negative and positive directions so that a stable limit cycle is found. All directions are normalized to have unit length. A step of, e.g., length 6 in $\mathbf{v}_{13}$ direction in A means that the unit vector in this direction can be made 6 times longer before a bifurcation is detected.

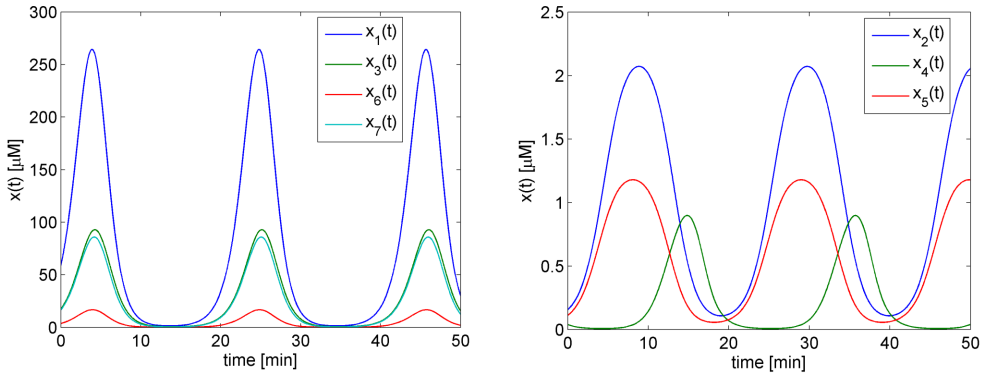

Figure 2.10: Limit cycle behavior of the Laub-Loomis model for parameter vector $\mathbf{k}_0 + 12.6\mathbf{v}_{12}$. These parameter values are given in Table 2.1.

denote the new nominal point by $\mathbf{k}_0^* = \mathbf{k}_0 + 5.634\mathbf{v}_{12}$. When the method is applied to $\mathbf{k}_0^*$, we obtain the results shown in Figure 2.9B.

Combining the information in Figures 2.9A and 2.9B, we obtain a good impression of the

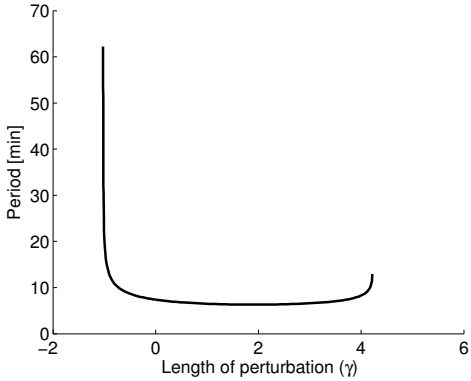

Figure 2.11: Behavior of the limit cycle period in the LL model along the $\mathbf{v}_7$ direction. Note that the period dramatically increases in the vicinity of $\gamma = -1$.

robustness region of the system. Contrary to the findings in [8, 10, 11], we conclude that the LL model has a large robustness region with a quite irregular shape.

2.4 Discussion

An important question in the modeling of biological systems is for which parameter values the model has a stable limit cycle, since this is often the parameter range in which the model describes reality. In the literature [8, 10, 11], one mostly studies this topic by analyzing the eigenvalues of the Jacobian matrix of the equilibrium points of the model. For example, if some of these eigenvalues become purely imaginary, a so-called Hopf bifurcation takes place and a limit cycle comes into existence. However, analysis of eigenvalues of a Jacobian matrix is not the most appropriate way to study this problem, since these eigenvalues yield only local information. In the present paper we have presented a method to construct an estimate for the so-called robustness region in parameter space. The approach that we follow has a global, rather than a local character. Within a robustness region the system possesses a stable limit cycle and on its boundaries the system undergoes a bifurcation. A bifurcation is a dramatic change in the system dynamics indicating that the system is no longer robust if the parameters are perturbed further. For the present method, these bifurcations may be of any type and different parts of the boundary may be connected to different bifurcations.

The present method has especially been designed to scan robustness regions of systems with a high-dimensional parameter space. Its power stems from the fact that it scales linearly with the number of parameters. This implies that it is highly efficient from a numerical point of view. The present approach is based on observing the behavior of the Floquet multipliers of the periodic solution if the systems parameters are changed. In this way, one easily detects all bifurcations that may occur to the periodic solution, such as Hopf, fold, flip, and Neimark-Sacker bifurcations, which lead to disappearance or period doubling of the periodic solution.

The method has first been tested for low-dimensional systems. It is shown that for a 2-dimensional parameter space, the results are in full agreement with those obtained by the package AUTO. Thereafter the method has been applied to a high-dimensional system, the Laub-Loomis model which has 14 parameters. In this case, the method appears to be highly efficient, indeed. Contrary to the results reported in the literature [8, 10, 11], the method yields an estimate that is very big and irregularly shaped. The latter means that the Laub-Loomis model is much more robust with respect to changes in one parameter than in another. The present approach yields this information and is as such an extension of the methods available in literature. In the present method, a first direction is chosen such that the Floquet multipliers will change mostly if the continuation is applied along this direction. The approach finds axes that together span the estimated region.

Since all information about the limit cycle along the used axes becomes available, it requires no extra work to present, e.g., level line plots of the period of the limit cycle. Together with the general types of bifurcation that are detected, this provides a reliable and insightful impression of the dynamical behavior of a model in a wide range of values around a nominal point.

Acknowledgements

This work was carried out within the research programme of the Netherlands Consortium for Systems Biology (NCSB), which is part of the Netherlands Genomics Initiative/Netherlands Organization for Scientific Research.

Bibliography

[1] Kaneko K (2006) Life: an introduction to complex systems biology. Springer, 369 pp.

[2] Alon U (2006) An introduction to systems biology: design principles of biological circuits. Chapman & Hall, 301 pp.

[3] Kitano H (2004) Biological robustness. Nature Reviews Genetics 5: 826–837.

[4] Klipp E, Herwig R, Kowald A, Wierling C, Lehrach H (2005) Systems biology in practice: concepts, implementation and application. Wiley-VCH, 465 pp.

[5] Morohashi M, Winn AE, Borisuk MT, Boluri H, Doyle J, et al. (2002) Robustness as a measure of plausibility in models of biochemical networks. Journal of Theoretical Biology 216: 19-30.

[6] Laub MT, Loomis WF (1998) A molecular network that produces spontaneous oscillations in excitable cells of *Dictyostelium*. Molecular biology of the cell 9: 3521-3532.

[7] Doedel E, Paffenroth R, Champneys A, Fairgrieve T, Kusnetsov Y, et al. (2007) Auto 07p: Continuation and bifurcation software for ordinary differential equations. Department of Computer Science, Concordia University, Montreal, Canada .

[8] Ma L, Iglesias PA (2002) Quantifying robustness of biochemical network models. BMC Bioinformatics 3: 38.

[9] Zhou K, Doyle J, Glover K (1996) Robust and optimal control. Prentice Hall, 596 pp.

[10] Kim J, Bates DG, Postlethwaite I, Ma L, Iglesias PA (2006) Robustness analysis of biochemical network models. IEE Proceedings - Systems Biology 153: 96-104.

[11] Ghaemi R, Sun J, Iglesias PA, Del Vecchio D (2009) A method for determining the robustness of bio-molecular oscillator models. BMC Systems Biology 3: 95.

[12] Barabási AL, Oltvai ZN (2004) Network biology: understanding the cell's functional organization. Nature Reviews Genetics 5: 101-113.

[13] Verhulst F (1996) Nonlinear differential equations and dynamical systems. Springer, 303 pp.

[14] Mattheij R, Molenaar J (2002) Ordinary differential equations in theory and practice. Society for Industrial Mathematics, 405 pp.

[15] Kuznetsov YA (2004) Elements of applied bifurcation theory. Springer, 631 pp.

[16] Torrini G, Genesio R, Tesi A (1998) On the computation of characteristic multipliers for predicting limit cycle bifurcations. Chaos, Solitons & Fractals 9: 121-133.

[17] Nayfeh A, Balachandran B, Rand R (2004) Applied nonlinear dynamics: analytical, computational, and experimental methods. Wiley-VCH, 685 pp.

[18] Rosenzweig ML, MacArthur RH (1963) Graphical representation and stability conditions of predator-prey interactions. The American Naturalist 97: 209-223.

[19] Klebanoff A, Hastings A (1994) Chaos in three species food chains. Journal of Mathematical Biology 32: 427-451.

[20] Kuznetsov YA, Rinaldi S (1996) Remarks on food chain dynamics. Mathematical Biosciences 134: 1-33.

[21] Boer MP, Kooi BW, Kooijman SALM (2001) Multiple attractors and boundary crises in a tri-trophic food chain. Mathematical Biosciences 169: 109-128.

Chapter 3

Complexity reduction of biochemical networks[1]

Abstract

The complexity of biochemical systems, stemming from both the large number of components and the intricate interactions between these components, may hinder us in understanding the behavior of these systems. Therefore, effective methods are required to capture their key components and interactions. Here, we present a novel and efficient reduction method to simplify mathematical models of biochemical systems. Our method is based on the exploration of the so-called admissible region, that is the set of parameters for which the mathematical model yields some required output. From the shape of the admissible region, parameters that are really required in generating the output of the system can be identified and hence retained in the model, whereas the rest is removed.

To describe the idea, first the admissible region of a very small artificial network with only three nodes and three parameters is determined. Despite its simplicity, this network reveals all the basic ingredients of our reduction method. The method is then applied to an epidermal growth factor receptor (EGFR) network model. It turns out that only about 34% of the network components are required to yield the correct response to the epidermal growth factor (EGF) that was measured in the experiments, whereas the rest could be considered as redundant for this purpose. Furthermore, it is shown that parameter sensitivity on its own is not a reliable tool for model reduction, because highly sensitive parameters are not always retained, whereas slightly sensitive parameters are not always removable.

[1] Based on: M. Apri, M. de Gee, and J. Molenaar – *"Complexity reduction preserving dynamical behavior of biochemical networks,"* Journal of Theoretical Biology, vol. 304, pp. 16–26, July 2012.

3.1 Introduction

Biochemical systems are usually very complex [1], consisting of hundreds to thousands components with intricate interactions. A quantitative description of the dynamics of such systems is canonically formulated in terms of ordinary differential equations (ODEs). However, the usage of such large systems of ODEs is often problematic, since one is faced with the challenge to numerically solve a very large nonlinear set of differential equations. The complexity of this task is often a serious obstacle to get required information about the system. For example, the possible presence of multiple time scales in huge systems may result in unacceptably long computing times. Furthermore, often the question arises how to interpret the behavior of huge networks biologically.

At the level of the modeler, the problems are even more serious, because a large number of interactions gives rise to a large number of parameters. Of course, one may try to find values for these parameters in the literature, but even if they can be found, their reliability and applicability to the specific purpose is often unknown. Furthermore, after all available information from the literature is used to the limit, still a number of parameters may remain that have to be fitted to data. Fitting procedures require the system of ODEs to be solved iteratively, so it has to be evaluated many times which is quite time consuming. Other problems may involve the questions of identifiability, sensitivity, and robustness. Therefore, there is a need for reduction methods that deliver simplified models that still capture the essential dynamical behavior of the original system [2, 3].

Complexity reduction can be carried out in several ways, and the choice for the most appropriate approach depends on the purpose one has in mind. For example, one may try to decompose a large biochemical network into smaller submodules that have relatively little interaction with each other [4, 5, 6, 7, 8]. In this way, the network becomes more manageable, easier to analyze, and it could make sense to study and interpret the modules separately. A large network can also be replaced by a functional module that has lower dimension (less ODEs) but still mimics the input-output behavior. This could be done, e.g., by replacing the network by a black box model [9] or by lumping together components and/or reactions based on their characteristics [6, 10, 11, 12, 13]. A disadvantage of both black box modeling and lumping is that the new reduced model may be structurally different from the original one, e.g., a component in the new reduced model may be a linear combination of several components in the original model, or a component in the original model could be contained in several new components in the reduced model. In practice, this may obstruct us in interpreting the new reduced model.

Alternatively, complexity reduction can be carried out by selecting only those components and/ or reactions of the network that determine the required dynamics of the system. This could be done, e.g., by exploiting possible time-scale differences that are often present in biological and chemical systems [14]. However, the classical time-scale separation such as in [15, 16, 17] for example, raises the question how to obtain the prior knowledge that some reactions are fast and others are slow. On the other hand, the automatic time-scale separation in [18, 19, 20] requires that the original system of equations is mathematically transformed into another system before it can be reduced. This transformation impedes the biological interpretation of the reduced model.

One could also omit components and/or reactions that seem to contribute little to the behavior of the network. These components or reactions are usually selected via an optimization approach [21, 22, 23] or a sensitivity analysis [24, 25, 26, 27, 28]. In the first approach, given a nominal parameter values, it is investigated whether some parameters can be set to zero without adjusting the other ones. In the example given in Section 3.2.2 below, we show that this approach may not always be successful, even if the system is extremely simple. In the latter approach, the importance of a particular parameter is measured by evaluating the effect of variations in this parameter on the dynamics of all concentrations. If the effect is large, the system is said to be highly sensitive to this parameter. If, on the other hand, the sensitivity is low, this parameter is considered unimportant and removable. However, one should be careful with this kind of conclusions, since, e.g., the omission of a low-sensitivity parameter may lead to useless results. An example of this phenomenon is found in [29] from a model of the central carbon metabolism of E. coli, for which the authors show that the sensitivity of flux concentrations to some enzymes, e.g., aldolase, is nearly zero. However, the removal of this reaction would result in the shut-down of the whole network, which is of course undesirable. For completeness' sake, we also mention the somewhat different way of reduction in which complicated mathematical expressions in the ODE equations are replaced with simplified ones [30, 31].

We present a novel reduction method that yields a biochemical model with less equations and parameters and still generates some required output. In this context, this output is interpreted as the dynamical behavior of the concentrations of a number of selected network components that are considered important for biological questions at hand and are responsible for its functional behavior. So, as data we take measured time series of some constituents and we look for a reduced model that generates these data. The reduction method proposed in this paper is based on the exploration of the so-called "admissible region", that is the region in the parameter space where the model outcomes match the output data within some given tolerance. From the shape of this admissible region important conclusions can be drawn. For example, if this region includes a part of one of the parameter axes, this parameter can apparently be set to zero. If, on the other hand, this region extends to infinity in some direction, this indicates that lumping of nodes might be allowed. These insights form our starting point to obtain reduced networks. The proposed method does not need to transform the original equations. It can be applied to any system of equations, linear or nonlinear. Contrary to the classical time-scale separation technique, this method does not rely on prior biological knowledge; therefore, it can be automated appropriately. On the other hand, the method can be tuned easily to incorporate any available prior knowledge. Our method also conserves the network structure and maintains the dynamics of the system's output and shows in this sense similarities with the method from [17]. Once a reduced biologically plausible model has been obtained, parameter identification can be carried out more efficaciously.

This paper is organized as follows. In section 3.2, we first introduce the concept of an admissible region which forms the basic concept in our reduction method. For illustrational purposes, we use a very simple artificial metabolic network with only three metabolites and three parameters. In spite of its simplicity, this system appears to be rich enough to show all the basic ingredients involved in the reduction process. Next we discuss how the reduction can be carried out effectively, and we conclude this section by formulating our algorithm. In

section 3.3, the reduction method is applied to a signaling network model taken from [32]. We show that this network can be considerably reduced with regard to reproducing the time-series of the key proteins. Furthermore, we demonstrate the surprising fact that parameters with high sensitivity are not always necessary and may be removed without any consequence for the purposes we have in mind.

3.2 Methods

A mathematical model is considered good if it is able to describe and predict the phenomena for which it has been designed. Here, we assume that the dynamical behavior of some components are essential for the predictive power of a model and that their dynamics has been measured. This dynamics should be preserved by any reduction method. In the following, we refer to system components that are measured as "target species". These target species play a pivotal role in the concept of admissible region, which is the basis idea of our reduction method.

3.2.1 The concept of admissible region

Consider a collection of n chemical species that form a biochemical network, the dynamics of which is modeled by a system of ordinary differential equations (ODEs)

$$\begin{aligned} \frac{d\mathbf{x}}{dt} &= \mathbf{f}(\mathbf{x}, \mathbf{k}_0), \\ \mathbf{y}(t, \mathbf{k}_0) &= \mathbf{B}\,\mathbf{x}(t, \mathbf{k}_0) \end{aligned} \tag{3.1}$$

with initial values

$$\mathbf{x}(0) = \mathbf{x}_0. \tag{3.2}$$

Here $\mathbf{x}(t) \in \mathbb{R}^n$ denotes the vector of biochemical concentrations, $\mathbf{f}$ is the vector valued function representing the interactions, and $\mathbf{k}_0 \in \mathbb{R}^m$ is the vector of kinetic parameters. The output of the system is the vector $\mathbf{y}(t) \in \mathbb{R}^q, 0 \leq t < \infty$, containing the dynamical behavior of the target species. The vector $\mathbf{y}$ is obtained from the state space vector $\mathbf{x}$ by the matrix multiplication $\mathbf{B}\,\mathbf{x}$, with $\mathbf{B}$ a constant $q \times n$ matrix. So, a target species $y_i(t)$ can be a linear combination of several biochemical concentrations. We call the specific parameter vector $\mathbf{k}_0$ in (3.1) - (3.2) the nominal parameter set and the corresponding system the nominal system. Here, the nominal parameter set $\mathbf{k}_0$ can be obtained from a parameter fitting procedure and/or derived from literature.

Suppose that M different data time-series of $\mathbf{y}(t)$ are available, denoted as $\hat{\mathbf{y}}^l(t_i), l = 1, \ldots, M,\ i = 1, \ldots, N$. If we substitute in (3.1) a parameter vector $\mathbf{k}_p$, that is different from $\mathbf{k}_0$, and integrate it, we obtain solution for all components of $\mathbf{x}$, thus also for the target species. We denote the latter by $\mathbf{y}(t, \mathbf{k}_p)$. The distance of the target species of the perturbed system to the reference time-series $\hat{\mathbf{y}}$ is quantified by the following distance function

$$S(\mathbf{y}(t, \mathbf{k}_p), \hat{\mathbf{y}}(t)) = \frac{1}{M \cdot q \cdot N} \sum_{l=1}^{M} \sum_{j=1}^{q} \sum_{i=1}^{N} \left(\frac{y_j^l(t_i, \mathbf{k}_p) - \hat{y}_j^l(t_i)}{\hat{y}_j^l(t_i)} \right)^2 \tag{3.3}$$

where N is the number of time discretization points. S can be interpreted as the average squared deviation between the model prediction and the data. Around the nominal parameter vector $\mathbf{k}_0$, there exists a region in the parameter space $\mathbb{R}^m$ such that any parameter vector $\mathbf{k}_p$ in this region gives model output that is close to the data.

To formalize this idea, we choose a small positive number ε^2 and say that all $\mathbf{k}_p$ for which the condition

$$S(\mathbf{y}(t, \mathbf{k}_p), \hat{\mathbf{y}}(t)) < \varepsilon^2 \tag{3.4}$$

holds, belong to the so-called "admissible region". The inaccuracy in the data could be used as a guideline to choose a value for ε, but also other considerations, such as an expert guess of the reliability of the model itself, could play that role. The shape of the admissible region contains important information. For example, if it includes (a part of) a parameter axis, then this parameter could be removed. Or, if the region extends to infinity in a certain parameter direction, some state-variables in the ODE model might be lumped. In the following example we make these ideas explicit.

3.2.2 Example

To illustrate the concepts above, we consider the extremely simple metabolic network sketched in Figure 3.1A, which represents a system with three metabolites and five interactions. Its dynamics is described by the linear ODE model

$$\begin{aligned} \frac{dx_1}{dt} &= v_1 - (k_1 + k_3)x_1(t) \\ \frac{dx_2}{dt} &= k_1 x_1(t) - k_2 x_2(t) \\ \frac{dx_3}{dt} &= k_2 x_2(t) + k_3 x_1(t) - v_2 x_3(t) \end{aligned} \tag{3.5}$$

with initial conditions

$$x_1(0) = x_2(0) = x_3(0) = 0. \tag{3.6}$$

The parameter v_1 denotes the input flux. It is fixed to $v_1 = 1$. The parameter v_2 that governs the output flux of the network is also fixed to $v_2 = 1$. In this example, we focus on the network behavior as a function of the parameters k_1, k_2 and k_3.

Let us suppose that metabolite x_3 is the target species and the nominal parameter values are $\mathbf{k}_0 = (k_1, k_2, k_3) = (1, 1, 0.2)$. As data we take $\hat{y} = x_3(t_i), i = 1, 2, \ldots, 10$. For simplicity, here the data $\hat{y}$ is obtained by integrating the nominal model in (3.5) - (3.6). This is plotted in Figure 3.2. If we choose $\varepsilon = 0.05$ as the tolerance and search for all parameter vectors $\mathbf{k}_p$ that satisfy condition (3.4), we obtain the 'admissible region' depicted in Figure 3.3. In this figure, the admissible region consists of all parameter vectors that lie between the two depicted surfaces. These surfaces were obtained by sampling the k_1-k_2 plane and searching in the k_3 direction for admissible values. Obviously, the admissible region includes the nominal parameter vector. The cross sections of the admissible region through the nominal point and parallel to the axes are given in Figure 3.4.

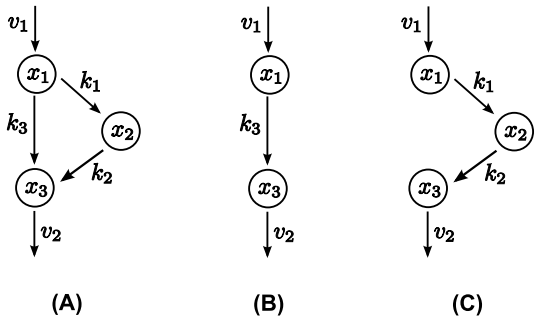

Figure 3.1: Example networks. **(A)** Full model. **(B)** Reduced model obtained by removing k_1, k_2, and adjusting the k_3 value. **(C)** Reduced model obtained by removing k_3 and adjusting k_1 and k_2.

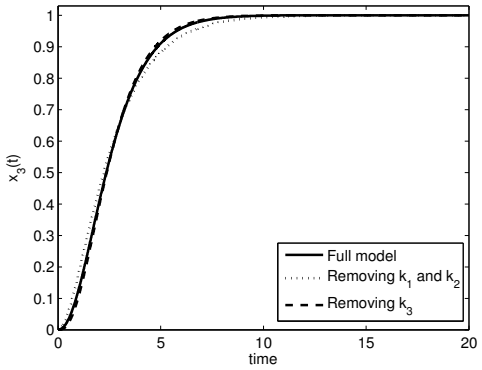

Figure 3.2: Comparison of x_3-output of the full with x_3-output of two reduced models. Parameters in the full model (solid line) are $(k_1, k_2, k_3) = (1, 1, 0.2)$. In the reduced models we have (dotted line) $(k_1, k_2, k_3) = (0, 0, 0.59)$, and (dashed line) $(k_1, k_2, k_3) = (1.2, 1.2, 0)$.

We observe from Figure 3.3 that, although the chosen tolerance value $\varepsilon = 0.05$ is rather small, the admissible region is quite large. Therefore, one would clearly run into identification problems when trying to estimate the parameter values (k_1, k_2, k_3) only from x_3 data with 5% inaccuracy. We notice that the admissible region in Figure 3.3 intersects the planes $k_1 = 0$ and $k_2 = 0$. This indicates that one might set either k_1 or k_2 at zero. Even more than this, the admissible region contains a part of the k_3-axis, where both k_1 and k_2 are zero; for example, the parameter vector $(k_1, k_2, k_3) = (0, 0, 0.59)$ leads to x_3-output that satisfies (3.4). Furthermore, we see that the admissible region also intersects the plane $k_3 = 0$; indeed, also the parameter vector $(k_1, k_2, k_3) = (1.2, 1.2, 0)$ is consistent with (3.4), as is shown in Figure 3.2. Therefore, we might remove either (k_1, k_2) or k_3 from the network. Doing so, we obtain the reduced models in Figures 3.1B and 3.1C.

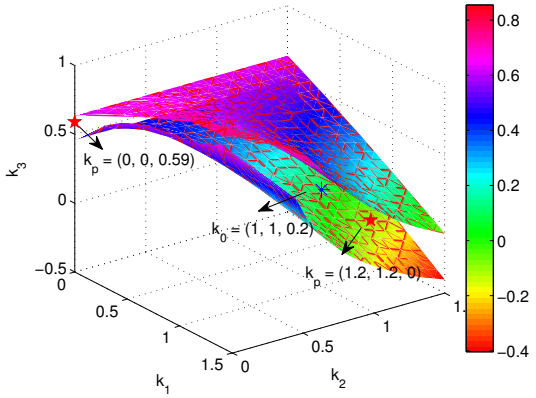

Figure 3.3: Admissible region of the network in Figure 3.1A. The layer between the two surfaces consists of parameter vectors (k_1, k_2, k_3) that satisfy (3.4) with $\varepsilon = 0.05$. The region extends for $k_1 > 1.5$ and $k_2 > 1.5$, but this extension is not shown. At the front, the region is closed but for clarity it has been sketched as open. The color bar represents the level value of k_3.

In Figure 3.3 only a part of the admissible region is shown, since k_2 is limited to $0 < k_2 < 1.5$. In reality the admissible region extends to infinity and k_2 may be increased unboundedly, provided that the k_1 and k_3 values are adapted appropriately. This observation reveals an intriguing aspect. If k_2 may be given a very large value, this implies that the flux between nodes x_2 and x_3 in the network of Figure 3.1A may be taken very large. Thus, as soon as metabolite x_1 is converted into x_2, metabolite x_2 will be converted immediately into x_3. This effectively implies that nodes x_2 and x_3 could be lumped without affecting the $x_3(t)$ dynamics, which topologically leads to the reduced network in Figure 3.1B. This approach thus also yields information on possible reduction via lumping of nodes.

Another important observation concerns the application of the so-called optimization approach proposed in [21]. In this approach, all parameters are initially set at nominal values. Next, it is checked whether some parameters can be set equal to zero without adjusting the other ones. From the cross-sections in Figure 3.4 we see that it is not possible to set some parameters equal to zero without adjusting the other parameters. The present example thus shows that this optimization approach may not always be successful, even if the system is extremely simple.

3.2.3 Complexity reduction method

From the example above, we learn that any parameter set that lies in the admissible region yields an acceptable dynamical behavior of the target species. This admissible region reflects the concept of parameter sloppiness, i.e., the property that different parameter sets may yield the same model prediction [33]. Furthermore, the broad admissible region also implies that

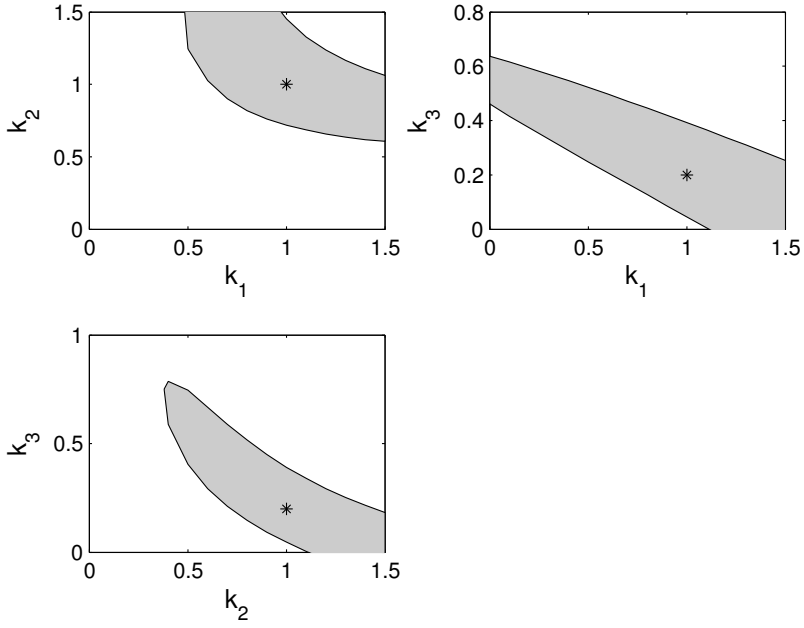

Figure 3.4: Cross sections of the admissible region. The grey areas are the cross-sections of the admissible region of (3.5)-(3.6) with $\varepsilon = 0.05$ in condition (3.4). All three cross sections go through the nominal point, indicated with (*), and lie in the planes $k_3 = 0.2, k_2 = 1$, and $k_1 = 1$, respectively.

the model encounters a practical identifiability problem [34]. When non-identifiability and sloppiness are explored thoroughly, the gained insight can be used to simplify the model significantly. Here we found three possible ways to reduce the model: (a) by removing k_1 and k_2 which leads to the removal of metabolite x_2, (b) by lumping node x_2 with x_3; both (a) and (b) lead to the reduced network in Figure 3.1B, (c) by removing parameter k_3 which leads the reduced network in Figure 3.1C. On account of parsimony, we may prefer to have the strongest reduction, such as in Figure 3.1B, although we must realize that all reduced networks produce similar behavior.

However, the system in the example is an extremely simple model: only three nodes with three parameters. Thus, it is easy to draw the admissible region and find possible reductions. In real systems biology applications, the models frequently contain a high number of parameters, and therefore, it might be very difficult to calculate their admissible regions. Fortunately, in practice it is not necessary to determine the admissible region completely. We learn from the example above that a reduced model can be obtained when parameters can either be set at 0 or extended to infinity. The remaining parameters are then adjusted such that the behavior of the target species in the perturbed system still mimics the reference time-series. In

what follows, we discuss several possibilities how complexity reduction can be carried out efficaciously.

Parameter reduction

A simple heuristic strategy is to try to remove parameters, one at a time. So, we start with setting $k_1 = 0$, and check, by re-estimating the other parameters, whether (3.4) can still be satisfied. If this is the case, k_1 can indeed be removed, otherwise it stays in the network. This procedure is repeated for $k_2, \ldots, k_m$. If in this way, one or more parameters have been removed, we cycle through the remaining parameters again, until we find that no more parameters can be removed.

From a theoretical point of view, removing one parameter at a time is not the optimal strategy to reduce the network; setting sets of parameter equal to zero simultaneously would be better. However, when the original system contains m parameters, finding the reduced systems with l parameters ($l < m$) would call for $\begin{pmatrix} m \\ l \end{pmatrix}$ optimization problems, which may be a huge number.

Since in our approach the parameters are removed successively, we have to face the question whether the result depends on the ordering of the parameters. In general, this will indeed be the case, so the reduction method does not lead to a unique outcome. This phenomenon is very similar to what is found in the traveling salesman problem, in which given a list of cities and their pairwise traveling cost, one should find the cheapest route to visit all the cities (each city should only be visited once) and return to the starting point [35]. As all algorithms for this problem are based on iterative, heuristic procedures, the resulting solutions are also non-unique.

We recommend to utilize the concept of 'sensitivity' as a guideline for ordering the parameters. To that end, we measure the influence of relative variations in parameter k_j on the distance function $S(\mathbf{y}, \hat{\mathbf{y}})$ in (3.3) in the following way

$$C_j = \frac{k_j}{S} \frac{\partial S}{\partial k_j}. \tag{3.7}$$

and order the parameters from low to high sensitivity. In section 3.3 we come back to this point, showing that this ordering indeed leads to very good reduction rates. The algorithm for parameter reduction is described in the flowchart in Figure 3.5.

Node reduction

To investigate whether node x_1 could be removed, one simply sets $x_1 = 0$ in all equations and omits the ODE for x_1 from the system. The next step is to check, by re-estimating the parameters in the reduced system, whether (3.4) can still be satisfied. If this is the case, node x_1 is removed, otherwise it stays in the network. This procedure is repeated for $x_2, \ldots, x_n$. If in this way one ore more nodes have been removed, the procedure is repeated and we cycle through the remaining nodes again, until we find that no more nodes can be removed.

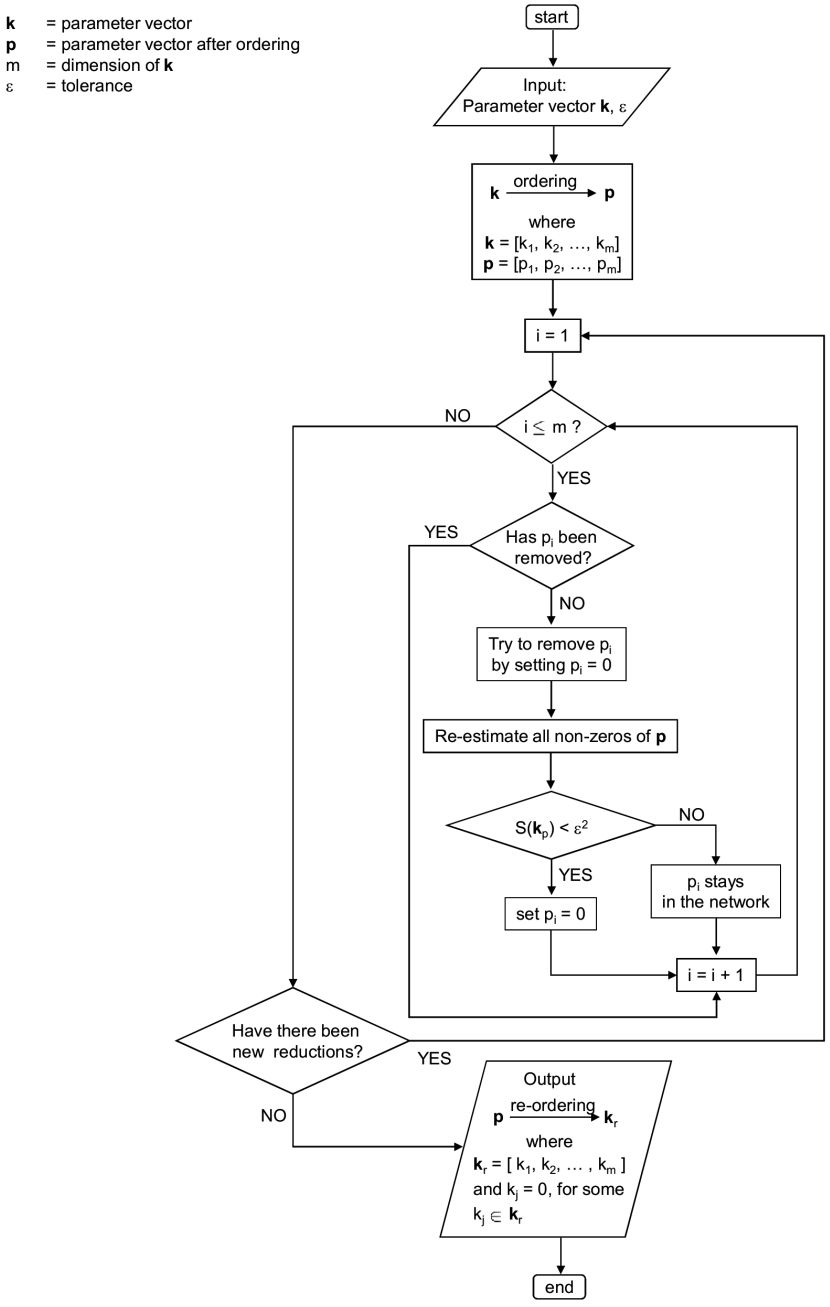

Figure 3.5: Flow chart of algorithm for parameter reduction. At the start, the entries of parameter vector $\mathbf{k}$ are ordered according to their sensitivities yielding new parameter vector $\mathbf{p}$, and reduction is conducted successively to the entries of $\mathbf{p}$. At the end, the entries of parameter vector $\mathbf{p}$ are ordered back, now containing some zeros if the reduction was successful.

Lumping of nodes

To investigate whether two nodes could be lumped, we set the parameter that measures their interaction strength at a very large value and adjust the other parameter values to satisfy (3.4). If this turns out to be possible, these nodes are lumped, i.e., replaced by one node.

Algorithm

In summary, we use the following reduction scheme:

1. Apply node reduction.
2. Calculate the sensitivity of the non-zero parameters and order the parameters accordingly.
3. Apply parameter reduction.
4. Apply a lumping procedure.

3.3 Results

We apply our reduction algorithm to a signaling network for the epidermal growth factor receptor (EGFR), as developed by [32]. This network consists of 25 proteins with 22 reversible mass action reactions and 3 Michaelis-Menten reactions. It is depicted in Figure 3.6A. The dynamics of the network is described by an ODE system consisting of 23 state variables (the concentrations of ATP and ADP are assumed to be constant) and 50 parameters. The kinetic parameters are taken from the literature and presented in the first column of Table 3.1. Furthermore, since the kinetic scheme contains several cycles, the kinetic parameters involved in the cycles satisfy so-called "detailed balance" relationships given by

$$\frac{k_9 \cdot k_{10} \cdot k_{11} \cdot k_{12}}{k_{-9} \cdot k_{-10} \cdot k_{-11} \cdot k_{-12}} = 1 \tag{3.8}$$

$$\frac{k_{15} \cdot k_{21} \cdot k_{-17} \cdot k_{-18}}{k_{-15} \cdot k_{-21} \cdot k_{17} \cdot k_{18}} = 1 \tag{3.9}$$

$$\frac{k_{18} \cdot k_{22} \cdot k_{-19} \cdot k_{-20}}{k_{-18} \cdot k_{-22} \cdot k_{19} \cdot k_{20}} = 1 \tag{3.10}$$

$$\frac{k_{12} \cdot k_{22} \cdot k_{21} \cdot k_{23}}{k_{-12} \cdot k_{-22} \cdot k_{-21} \cdot k_{-23}} = 1 \tag{3.11}$$

$$\frac{k_{15} \cdot k_{-20} \cdot k_{-23} \cdot k_{-24}}{k_{-15} \cdot k_{20} \cdot k_{23} \cdot k_{24}} = 1. \tag{3.12}$$

To validate the model, the authors measured the transient response of several proteins to EGF stimulations. The measured data consist of concentration time-series of total phosphorylated

EGFR, total phosphorylated PLCγ, total phosphorylated Shc, Grb2 bound to EGFR forms, and Grb2 bound to Shc isoforms. They are composed of several species in the model:

$$\begin{aligned}\text{Total phosphorylated EGFR} &= 2([\text{RP}] + [\text{R-PL}] + [\text{R-PLP}] + [\text{R-G}] + [\text{R-G-S}] + \\ &\quad [\text{R-Sh}] + [\text{R-ShP}] + [\text{R-Sh-G}] + [\text{R-Sh-G-S}]) \qquad (3.13)\\ \text{Total phosphorylated PLC}\gamma &= [\text{R-PLP}] + [\text{R-PLC}\gamma\text{P}] \qquad (3.14)\\ \text{Total phosphorylated Shc} &= [\text{R-ShP}] + [\text{R-Sh-G}] + [\text{R-Sh-G-S}] + \\ &\quad [\text{ShP}] + [\text{Sh-G}] + [\text{Sh-G-S}] \qquad (3.15)\\ \text{Total Grb2 bound to EGFR} &= [\text{R-G}] + [\text{R-G-S}] + [\text{R-Sh-G}] + [\text{R-Sh-G-S}] \qquad (3.16)\\ \text{Total Grb2 bound to Shc} &= [\text{R-Sh-G}] + [\text{Sh-G}] + [\text{R-Sh-G-S}] + [\text{Sh-G-S}]. \qquad (3.17)\end{aligned}$$

In this paper, we use this model to show how the reduction method that was outlined above can be applied. Therefore, it is not our intention to judge at the end whether the model as a whole is redundant. Thus, instead of using the above measured time-series for validation, here we consider them as our target species of which the dynamics should be preserved under model reduction. The parameters specified by the authors are considered as nominal parameter set $\mathbf{k}_0$. We choose the time-series corresponding to EGF stimulation levels of 20 nM and 2 nM as our reference data. The 5 nM data are used later to test the predictive power of the reduced network. Thus, in total we have 10 reference time-series, namely five target species time-series for two different conditions. Each time series contains data at 10 time points.

For the present analysis we took the EGFR model in SBML-format from the database "JWS Online" [36] and translated it into Matlab-format using the SBML Toolbox for Matlab [37]. As tolerance we take $\varepsilon = 0.03$, i.e., we allow an averaged relative distance between the reduced system and the reference data of at most 3%. So, equations (3.3) and (3.4) read for this specific case as

$$\frac{1}{100}\sum_{l=1}^{2}\sum_{j=1}^{5}\sum_{i=1}^{10}\left(\frac{y_j^l(t_i,\mathbf{k}_p)-\hat{y}_j^l(t_i)}{\hat{y}_j^l(t_i)}\right)^2 < 0.03^2. \qquad (3.18)$$

In addition to the dynamics of the target species that have to be preserved, the detailed balance relationships in (3.8)-(3.12) should also hold whenever the reduced model contains a cycle.

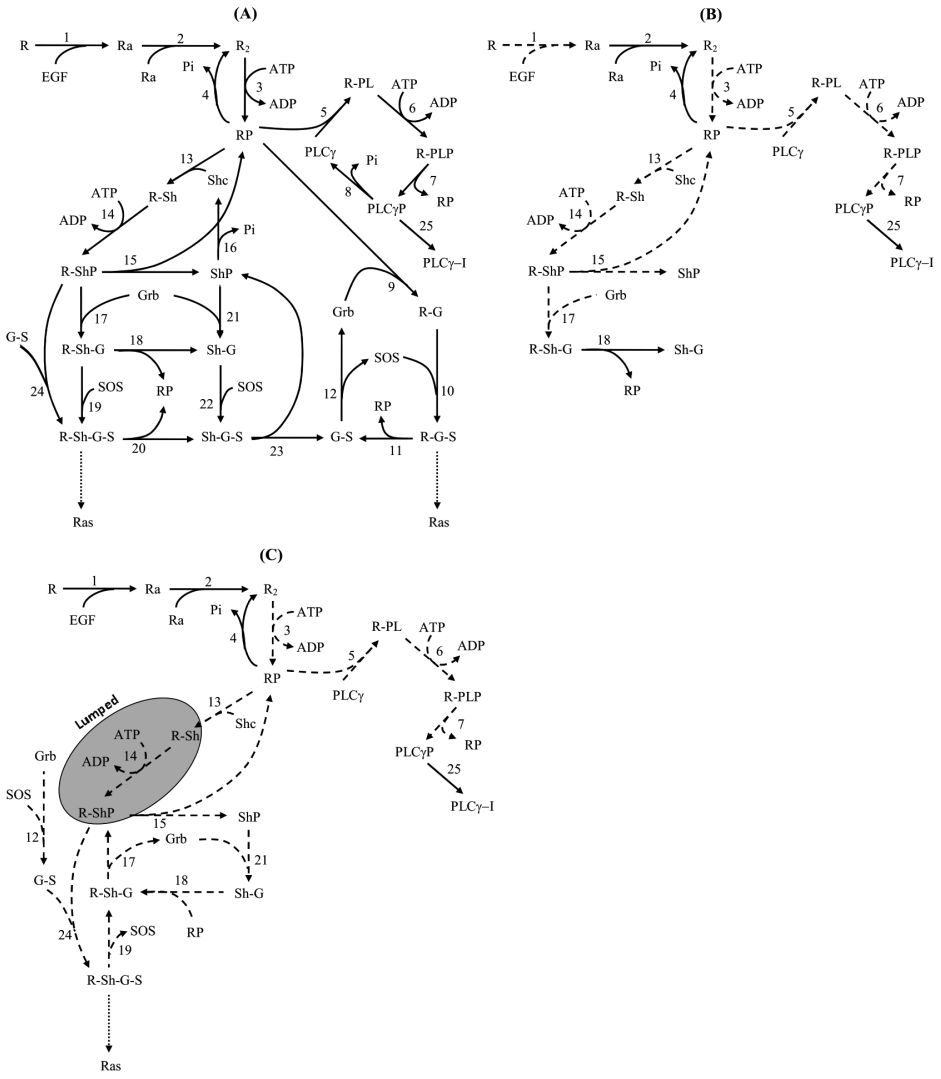

Figure 3.6: The EGFR biochemical network. **(A)** The full network from [32]. Note that all reactions in this network have two kinetic parameters. **(B)** Reduced network obtained by considering total phosphorylated EGFR, phosphorylated PLCγ, phosphorylated Shc, Grb2 bound to EGFR forms, and Grb2 bound to Shc isoforms as target species. The reduction is applied in two steps: node reduction followed by parameter reduction. **(C)** Reduced network obtained by considering total SOS bound to EGFR as additional target species. In this reduced network, R-Sh has been lumped with R-ShP. A solid arrow represents a reaction with two kinetic parameters, and a dashed arrow represents a reaction with one kinetic parameter.

Table 3.1: Parameter values of the original and the reduced models of the EGFR Network. The parameters equal to zero are removed from the original model. In addition, parameters K_8 and K_{16} are automatically removed since they figure in the denominator of the Michaelis-Menten reaction terms of which the enumerator becomes zero in the reduction. In reduced model 1, the target species are the total of phosphorylated EGFR, phosphorylated PLCγ, phosphorylated Shc, Grb2 bound to EGFR forms, and Grb2 bound to Shc isoforms. In reduced model 2, total SOS bound to EGFR is used as extra target species.

Parameter	Original model	Reduced model 1	Reduced model 2
k_1	$3 \cdot 10^{-3}$	$2 \cdot 10^{-3}$	$2.6 \cdot 10^{-3}$
k_{-1}	$6 \cdot 10^{-2}$	0	$6.5 \cdot 10^{-2}$
k_2	$1 \cdot 10^{-2}$	$2.68 \cdot 10^{-2}$	$3.1 \cdot 10^{-2}$
k_{-2}	0.1	0.6997	0.2
k_3	1	2.2804	0.5359
k_{-3}	$1 \cdot 10^{-2}$	0	0
V_4	450	422.7363	481.8840
K_4	50	36.6275	60.1878
k_5	$6 \cdot 10^{-2}$	$3.2 \cdot 10^{-2}$	$7.39 \cdot 10^{-2}$
k_{-5}	0.2	0	0
k_6	1	0.5364	0.6107
k_{-6}	$5 \cdot 10^{-2}$	0	0
k_7	0.3	0.2887	0.2839
k_{-7}	$6 \cdot 10^{-3}$	0	0
V_8	1	0	0
K_8	100	56.9514	63.5105
k_9	$3 \cdot 10^{-3}$	0	0
k_{-9}	$5 \cdot 10^{-2}$	0	0
k_{10}	$1 \cdot 10^{-2}$	0	0
k_{-10}	$6 \cdot 10^{-2}$	0	0
k_{11}	$3 \cdot 10^{-2}$	0	0
k_{-11}	$4.5 \cdot 10^{-3}$	0	0
k_{12}	$1.5 \cdot 10^{-3}$	0	0
k_{-12}	$1 \cdot 10^{-4}$	0	$1.62 \cdot 10^{-2}$
k_{13}	$9 \cdot 10^{-2}$	$5.01 \cdot 10^{-2}$	0.114
k_{-13}	0.6	0	0
k_{14}	6	4.6139	$1 \cdot 10^4$
k_{-14}	$6 \cdot 10^{-2}$	0	0
k_{15}	0.3	0.2965	0.4970
k_{-15}	$9 \cdot 10^{-4}$	0	0
V_{16}	1.7	0	0
K_{16}	340	336.7173	368.5164
k_{17}	$3 \cdot 10^{-3}$	$5.6 \cdot 10^{-3}$	0
k_{-17}	0.1	0	0.9347

Continued on next page

Table 3.1 – *Continued from previous page*

Parameter	Original model	Reduced model 1	Reduced model 2
k_{18}	0.3	0.2953	0
k_{-18}	$9 \cdot 10^{-4}$	$3.4 \cdot 10^{-3}$	$1.49 \cdot 10^{-2}$
k_{19}	$1 \cdot 10^{-2}$	0	0
k_{-19}	$2.14 \cdot 10^{-2}$	0	0.8527
k_{20}	0.12	0	0
k_{-20}	$2.4 \cdot 10^{-4}$	0	0
k_{21}	$3 \cdot 10^{-3}$	0	$5.7 \cdot 10^{-3}$
k_{-21}	0.1	0	0
k_{22}	$3 \cdot 10^{-2}$	0	0
k_{-22}	$6.4 \cdot 10^{-2}$	0	0
k_{23}	0.1	0	0
k_{-23}	$2.1 \cdot 10^{-2}$	0	0
k_{24}	$9 \cdot 10^{-3}$	0	$1.52 \cdot 10^{-2}$
k_{-24}	$4.29 \cdot 10^{-2}$	0	0
k_{25}	1	1.2152	1.2897
k_{-25}	$3 \cdot 10^{-2}$	$4.02 \cdot 10^{-2}$	$4.22 \cdot 10^{-2}$

3.3.1 Node reduction for the EGFR network

We order the nodes (proteins) in the network in a manner that is inspired by the internal structure of the pathway. Applying our node reduction algorithm, we find that six nodes out of 23 are redundant, namely [R-G], [R-G-S], [G-S], [SOS], [Sh-G-S], and [R-Sh-G-S]. The question could be raised whether this result depends on the specific ordering used. To answer this question, we apply again the node reduction but now with 30 randomly chosen node orderings. The result is shown in Figure 3.7. From Figure 3.7A, we observe that for all these random orderings, at most only six nodes can be removed. Furthermore, we conclude from Figure 3.7B that 16 nodes have 100% survival frequency throughout all 30 experiments. This implies that these 16 nodes are at least necessary to govern the dynamics of the output, whereas some of the other seven nodes can apparently be removed. Among these seven nodes are the six nodes that were removed using our original ordering, as indicated in Figure 3.7B by the grey bar.

As a last check, we order the nodes according to their survival frequency in Figure 3.7B and once again apply node reduction. Then we again find that the six nodes that we arrived at before are removable. These observations make us confident that this result is indeed the optimal one. So, we conclude that about 26% reduction in network nodes is allowed. By removing these 6 nodes, also their reactions disappear, so that we are now left with a system that contains 17 nodes and 32 parameters.

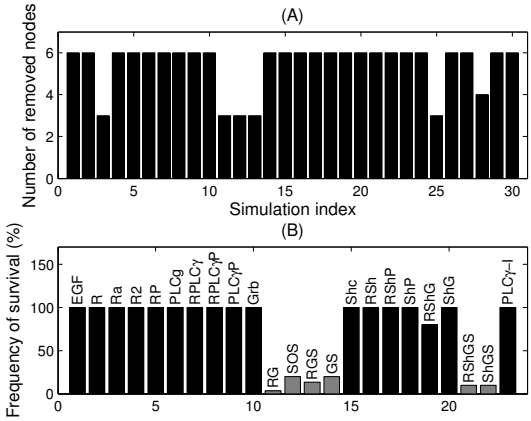

Figure 3.7: Node reduction with 30 different random orderings. (A) Number of nodes that can be removed for 30 randomly chosen orderings of the network nodes. (B) Spread of the nodes that survive across 30 randomly ordered node reductions. A node with 100% frequency of survival survives in all cases, a node with 0% frequency is always removed. The nodes that survive when we use sequential node ordering are indicated by the black bar and those that are removed are indicated by the grey bar.

3.3.2 Sensitivity analysis

Next, we perform a sensitivity analysis to the reduced network by calculating the sensitivity parameters

$$C_j = \frac{k_j}{S}\frac{\partial S}{\partial k_j}. \tag{3.19}$$

The result is shown in Figure 3.8. The parameters are then reordered based on their sensitivities from low to high. In this figure, the sensitivity of parameters that were already removed due to node removal in the previous step is irrelevant and therefore, omitted.

From Figure 3.8, we observe that the system is very sensitive to, e.g., k_{-4}, k_4, k_{18} and less sensitive to, e.g., k_{-8}, k_{-14}, k_{16}. A natural strategy seems to first remove the parameters that have the lowest sensitivities. However, we show below that sometimes a parameter with low sensitivity cannot be removed, whereas parameter with a high sensitivity still drops out.

3.3.3 Parameter reduction for the EGFR network

After the parameters have been ordered based on their sensitivities, parameter reduction is applied, as sketched in the flowchart in Figure 3.5. This leads to the removal of another 15 parameters. So, in combination with the result from node reduction, 33 out of 50 parameters are redundant. This means, that about 66% of the parameters are not necessary to produce the dynamics of the five target species. Eventually, we are now left with the biochemical

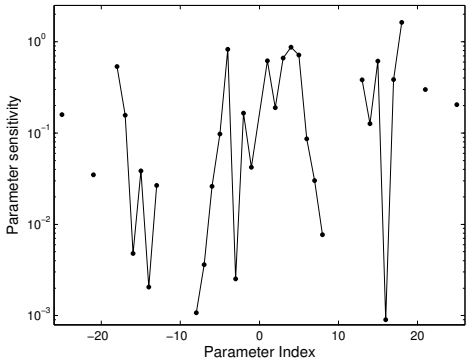

Figure 3.8: Sensitivity of parameters $k_{-25}, k_{-24}, \ldots, k_{24}, k_{25}$ of the EGFR network from [32] with respect to the squared deviation function in (3.7). The sensitivity of parameters that were already removed due to node removal is irrelevant and therefore not given.

network depicted in Figure 3.6B. The parameter values of the reduced system are presented in the second column of Table 3.1. Note that in this column, only 31 parameters are zero. However, two additional parameters, K_8 and K_{16}, are half-life parameters in a Michaelis-Menten reaction, and they are, of course, redundant if this reaction itself is removed. For example, the rate of the eighth reaction is

$$\text{Reaction}_8 = \frac{V_8[\text{PLC}\gamma\text{P}]}{K_8 + [\text{PLC}\gamma\text{P}]}. \tag{3.20}$$

Since in the parameter reduction V_8 is set to zero, K_8 becomes automatically redundant.

To check the effectiveness of the parameter ordering for the reduction, we run the parameter reduction again, but now with 30 different random parameter orderings. These parameter reductions are always applied to the same reduced network, obtained via node reduction. The result is shown in Figure 3.9. From Figure 3.9A we see that the number of parameters that can be removed ranges from 31 to 34 parameters, including the 6 nodes that were removed via node reduction. Here the number of reducible parameters are 31 in 10 runs, 32 in 15 runs, 33 in 4 runs, and 34 in only one run (note that the removed parameters are not always the same). The maximum reduction is attained in the 25th simulation. Therefore, the ordering according to sensitivity is not optimal, but it yields a reduction rate that is close to optimal.

In addition, the spread of the parameter survival across 30 random simulations is shown in Figure 3.9B. Together with the result from node reduction, 12 parameters have 100% survival frequency, 23 parameters have 0% survival frequency, and the rest are in between. This means that 12 parameters are non-removable and 23 parameters are completely redundant. Parameters that are removed via node reduction are indicated by grey text, whereas those that are removed via parameter reduction are indicated by black text. Parameters that are present in Figure 3.6B are indicated by the black text “s” in Figure 3.9B.

The dynamics produced by the full and the reduced systems are compared in Figure 3.10.

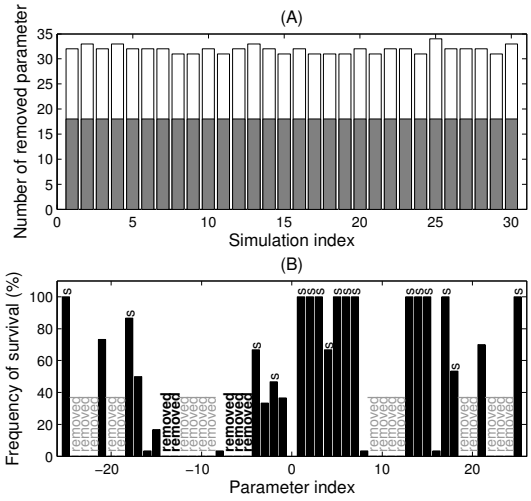

Figure 3.9: Parameter reduction (applied after node reduction) with 30 different random parameter orderings. (A) Number of parameters that can be removed at each simulation, grey bar from node reduction, white bar from parameter reduction. (B) Spread of the parameters that survive across 30 randomly ordered parameter reductions. A parameter with 100% frequency survival always survives in all random reductions, a parameters with 0% frequency is always removed. The parameters that are removed via node reduction are indicated by grey text, and those that are always removed via parameter reduction are indicated by black text. The parameters that are still present in the reduced network in Figure 3.6B are indicated by the black-text "s".

From this figure, we see that both systems lead to very similar dynamics of the target species from both 20 nM and 2 nM EGF stimulations. As an extra check, we also compare the prediction of the reduced system when the EGF stimulation is 5 nM with the outcomes of the full model in Figure 3.10. Note that these data were not used in the reduction procedure. The results of the reduced system also show a good agreement with that of the nominal system. We conclude that the reduced model reproduces the output of the full system fairly well. The reduced network in Figure 3.6B clearly indicates which parts of the network are responsible for the measured data.

An interesting observation is that some parameters that have low sensitivities, e.g., k_7, cannot be removed. On the other hand, some other parameters that have high sensitivities, e.g., k_{-17} and k_{21}, turn out to be removable. This implies that parameter sensitivity on its own is not a reliable tool for model reduction. However, we found that parameter sensitivity is still a useful tool to order the parameters before starting parameter reduction.

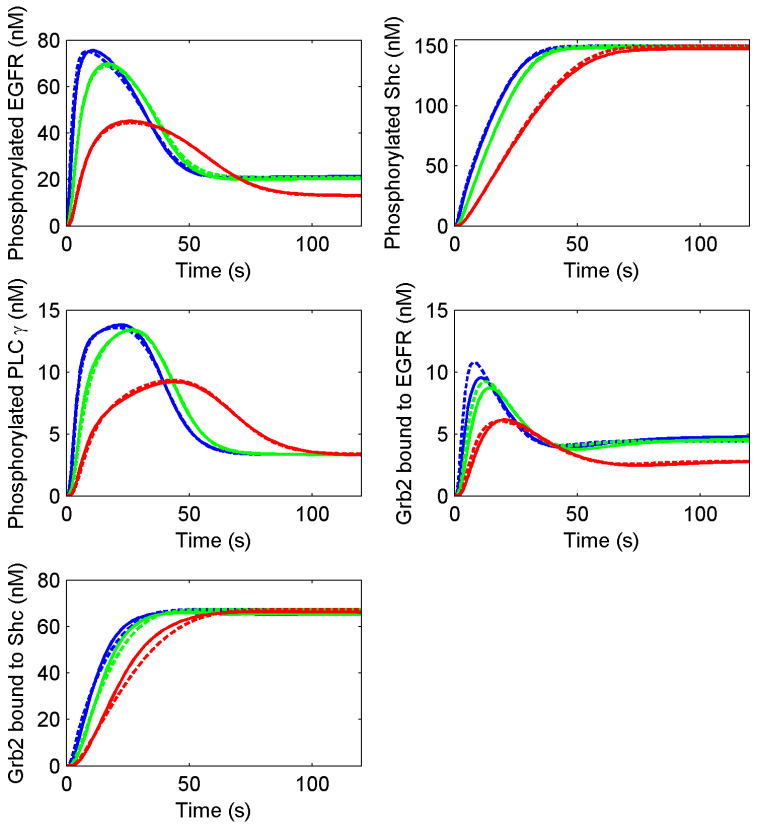

Figure 3.10: The dynamics of EGFR biochemical network. The solid lines represent the reference data for the target components; the dashed lines represent the output of the reduced system in Figure 3.6B. The blue line, green line, and red line are dynamics with EGF stimulation of 20, 5, and 2 nM, respectively. Note that only the reference data for 20 nM and 2 nM EGF are used in the reduction. The 5 nM EGF curves are plotted to show the predictive power of the reduced network.

3.3.4 Lumping of nodes

After applying parameter reduction, we try to lump nodes in the reduced network. This is carried out by iteratively setting one parameter at a time to a very large value and re-estimate the rest such that the dynamics of the target species fits the measured data. It appears that no node in the reduced network in Figure 3.6 can be lumped, and we conclude that the reduced model cannot be simplified further.

3.3.5 SOS complex protein as extra target species

From the results above, we end up with a reduced network in which the SOS protein has been removed. Yet, we know that in most cell types the activation of EGFR leads to the activation of the Ras $\rightarrow$ Raf $\rightarrow$ Mek $\rightarrow$ ERK cascade [38]. This activation can only be attained through SOS and hence, the reduced network that we obtained above is in some sense biologically non-sensical. Still, our procedure allows for an important conclusion with respect to experimental design. If one would like to address the question which data would be needed to estimate the parameter that are SOS related, our results clearly indicate that the measured data mentioned in [32] do not contain enough information for this purpose.

To assure that the nodes related to SOS remain in the network either we have to add extra data to the set of target species or to flag the SOS and its upstream and downstream reactions as non-removable components during the reduction. Here we suppose that the dynamics of the total SOS protein bound to EGFR should also be preserved, thus extra data is added to the set of target species. The total SOS protein bound to EGFR is then also considered as another target species. It is given by

$$\text{SOS bound to EGFR} = [\text{R-Sh-G-S}] + [\text{R-G-S}]. \tag{3.21}$$

Applying the algorithm outlined above, we then arrive at the reduced network shown in Figure 3.6C with the new parameter values shown in Table 3.1 in the column of reduced model 2. Now, 27 parameters can be set to zero and hence are removed from the model. In addition, two additional parameters, K_8 and K_{16} , are also removed because they are half-life parameters in a Michaelis-Menten equation. Furthermore, one parameter, namely k_{14}, can be set to a very large value, which indicates that lumping is now possible. Therefore, we may lump [R-Sh] with [R-ShP] and consequently, the equation of [R-Sh] may be removed from the model. The new dynamics of [R-ShP] now reads as

$$\frac{d\,[\text{R-ShP}]}{dt} = v_{13} + v_{17} - v_{15} - v_{24}. \tag{3.22}$$

This concludes that the reduction in its number of parameters is now about 60%. The dynamics of the reduced model is shown in Figure 3.11.

The way we preserved (part of) the Ras cascade here is only one possibility. If we would have added to the set of target species the R-Sh-G-S and R-G-S signals separately, we would have ended up with a slightly different reduced model. This again shows that reduction is not an algorithm that can be applied as a black box, but that expert knowledge and the specific aim of the reduction should always be leading.

3.4 Discussion

Understanding the relation between the functional behavior of a network and its internal 'wiring' is not only valuable for its own sake, but also indispensable to answer questions like: Are all parts of the network required to perform specific tasks? If not, which part of the network is really needed? Are all parameters in the network identifiable? Which data could

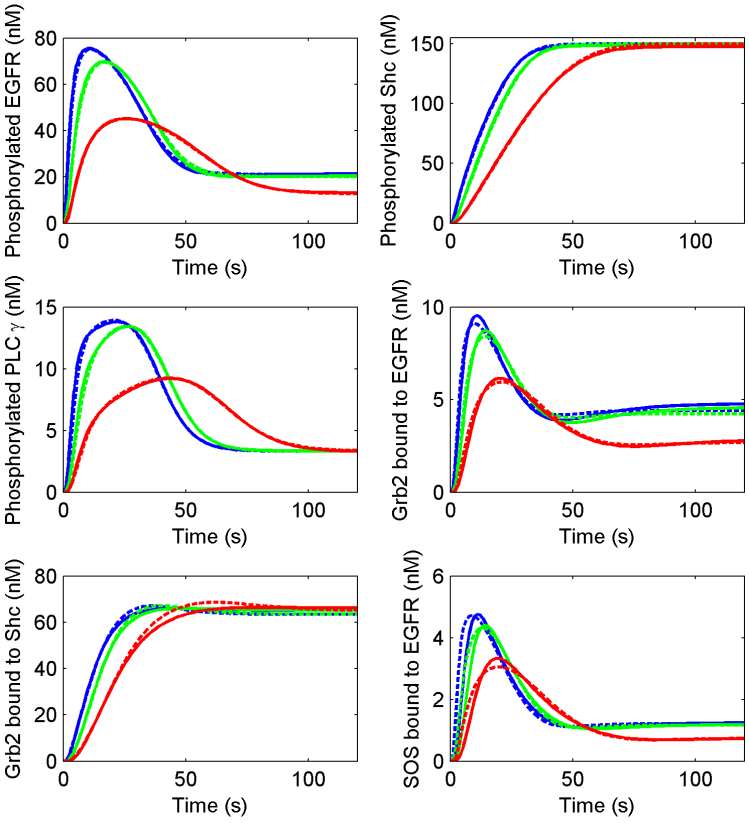

Figure 3.11: The dynamics of EGFR biochemical network where SOS bound to EGFR is now taken into account as target species. The solid lines represent the reference data for the target components; the dashed lines represent the output of the reduced system in Figure 3.6C. The blue line, green line, and red line are dynamics with EGF stimulation of 20, 5, and 2 nM, respectively. Note that only the reference data for 20 nM and 2 nM EGF are used in the reduction. The 5 nM EGF curves are plotted to show the predictive power of the reduced network.

yield the optimal information to estimate parameters? The first two questions are important to understand the principle design of biochemical systems, especially for applications in, e.g., medicine, pharmaceutical, and synthetic biology, whereas the latter questions stem from the modeling process.

In the present paper we work out on an efficient and easy to implement method to simplify a mathematical model from a given network. It leads to a reduced network with a number of nodes and parameters left out, that still is able to generate a prescribed output. Our proposed method is based on the insight that given the network and given some required behavior,

there exists a so-called admissible region in parameter space: if the network equations are evaluated with any parameter set in this region, the outcomes will fit the required network signals within some specified tolerance. The shape of the admissible region reveals a lot of information about the reducibility of the network. We explore these insights by proposing a systematic way of network reduction, in which first removal of nodes, then removal of parameters, and finally lumping of nodes, is investigated.

Since the proposed method is heuristic, sensitivity analysis around the nominal parameter set is used to guide the reduction. If the full model has not been established, then a nominal parameter vector can be obtained simply by fitting the parameters in the full model to the available dataset. Once the nominal vector is obtained, the parameter sensitivities can be calculated and the reduction procedure can be applied. Assuming that the model is sloppy, one may end up with several candidates for the nominal vector which may give different sensitivities and hence leads to different parameter ordering. Another option is to use a different rule of ordering other than sensitivity analysis, e.g., parameter ordering based on biological knowledge, and apply the reduction directly so that estimation to the full model can be skipped. In both choices, one could have different schemes for parameter ordering that may give different reduction result. This is the consequence of our heuristic approach. Nevertheless, they are mathematically equally acceptable since they lie in the admissible region.

Our findings also make clear that parameters with high sensitivity with respect to the target components are not always needed for a specified functioning of the network, whereas parameters with low sensitivity may be still important. This is typically a consequence of the nonlinearity of the model. Sensitivity is a local property which is only valid in a small neighborhood of some parameter vector, whereas setting one parameter to zero or to infinity is quite a radical perturbation. Thus, parameter sensitivity in itself is clearly not a reliable tool for reduction and should not be used to infer redundancy. Yet, in our technique it turns out to be a good choice to use sensitivity for ordering the parameters in the reduction procedure. In our method we use this information as a starting value and this heuristic strategy leads to detection of near-optimal redundancy rates.

It is important to realize that reduction is only allowed when we accept the possibility that some parts of the network do not play a role in the dynamics that we are interested in. We also notice that all parameters that can be removed are those that are strongly not identifiable based on the time-series that we want to reproduce. When some parameters in the full model have been removed, one should always check whether the reduced model is biologically plausible. Note that some details are always lost in a reduced model which eventually may affect its predictive power, regardless of the method that is used. Thus, it is a general property of any existing reduction method. In our method, however, expert knowledge can be easily incorporated to prevent a nonsensical reduced model and a proper procedure can be taken accordingly, as shown in the reduction of EGFR network above. In addition, to avoid unrealistic parameter values in the reduced model, variation of the parameters can always be limited by imposing their upper and/ or lower bounds in the optimization procedure. At this point, we argue that there is no guarantee that even the full model would yield a correct prediction when the system experiences a new perturbation, of which the model was not designed to account for it. Thus, the prediction from both the full and the reduced models should be equally appreciated. At the end, it is the biological knowledge and/ or a new experimental data that

can evaluate whether the reduced model is acceptable.

In the first reduced model of the EGFR network, in addition to the removal of SOS, there are other mechanisms that also fall out after the reduction. For example, [R-G], [R-G-S], [R-Sh-G-S], and [Sh-G-S] are eliminated so that the total Grb2 that bound to EGFR is exactly equal to the amount of [R-Sh-G]. There can be several hypotheses why these components can be omitted. First, it might be that they do not play a role in governing the dynamics of the target components which should be checked by experiment. Second, it might be that they are actually important, but the dataset is not enough to constrain the corresponding parameters. In both cases, our reduction method gives a clue to do a better experimental design. As we add more data, the rate of reduction is smaller, as shown in the result of reduction of the EGFR network. When we considered only the dynamics of five target species, we found that about 66% of the parameters in the original model is redundant. But when SOS bound to EGFR protein was included as additional target species, the redundancy of the parameters decreased to 60%.

It is also interesting to realize that the result of a lumping procedure can be easily interpreted from our method. When lumping of nodes is possible, it simply means that the reactions that occur between those nodes may assumed to be very fast. Once a reduced model is obtained, parameter estimation can be carried out more efficient and effectively as the number of parameters becomes smaller.

Acknowledgements

This work was carried out within the research programme of the Netherlands Consortium for Systems Biology (NCSB), which is part of the Netherlands Genomics Initiative/Netherlands Organization for Scientific Research.

Bibliography

[1] Ross J, Arkin AP (2009) Complex Systems: From chemistry to systems biology. Proceedings of the National Academy of Sciences 106: 6433-6434.

[2] Okino MS, Mavrovouniotis ML (1998) Simplification of mathematical models of chemical reaction systems. Chemical Reviews 98: 391–408.

[3] Klipp E, Liebermeister W, Wierling C, Kowald A, Lehrach H, et al. (2009) Systems Biology: A Textbook. Wiley-VCH.

[4] Hartwell LH, Hopfield JJ, Leibler S, Murray AW (1999) From molecular to modular cell biology. Nature 402: 47-52.

[5] Saez-Rodriguez J, Kremling A, Conzelmann H, Bettenbrock K, Gilles E (2004) Modular analysis of signal transduction networks. Control Systems Magazine, IEEE 24: 35 - 52.

[6] Conzelmann H, Saez-Rodriguez J, Sauter T, Bullinger E, Allg´ower F, et al. (2004) Reduction of mathematical models of signal transduction networks: simulation-based approach applied to egf receptor signalling. Systems Biology 1: 159 - 169.

[7] Saez-Rodriguez J, Kremling A, Gilles E (2005) Dissecting the puzzle of life: modularization of signal transduction networks. Computers & Chemical Engineering 29: 619 - 629.

[8] Saez-Rodriguez J, Gayer S, Ginkel M, Gilles ED (2008) Automatic decomposition of kinetic models of signaling networks minimizing the retroactivity among modules. Bioinformatics 24: i213-i219.

[9] Liebermeister W, Baur U, Klipp E (2005) Biochemical network models simplified by balanced truncation. FEBS Journal 272: 4034–4043.

[10] Danø S, Madsen MF, Schmidt H, Cedersund G (2006) Reduction of a biochemical model with preservation of its basic dynamic properties. FEBS Journal 273: 4862–4877.

[11] Dokoumetzidis A, Aarons L (2009) Proper lumping in systems biology models. IET Systems Biology 3: 40-51.

[12] Sunnaker M, Schmidt H, Jirstrand M, Cedersund G (2010) Zooming of states and parameters using a lumping approach including back-translation. BMC Systems Biology 4: 28.

[13] Sunnaker M, Cedersund G, Jirstrand M (2011) A method for zooming of nonlinear models of biochemical systems. BMC Systems Biology 5: 140.

[14] Alon U (2007) An introduction to systems biology: design principles of biological circuits. Chapman & Hall/CRC.

[15] Roussel MR, Fraser SJ (2001) Invariant manifold methods for metabolic model reduction. Chaos 11: 196–206.

[16] Kooi BW, Poggiale JC, Auger P, Kooijman SALM (2002) Aggregation methods in food chains with nutrient recycling. Ecological Modelling 157: 69 - 86.

[17] Radulescu O, Gorban A, Zinovyev A, Lilienbaum A (2008) Robust simplifications of multiscale biochemical networks. BMC Systems Biology 2: 86.

[18] Maas U, Pope S (1992) Simplifying chemical kinetics: Intrinsic low-dimensional manifolds in composition space. Combustion and Flame 88: 239 - 264.

[19] Zobeley J, Lebiedz D, Kammerer J, Ishmurzin A, Kummer U (2005) A new time-dependent complexity reduction method for biochemical systems. Transactions on Computational Systems Biology I : 90–110.

[20] Surovtsova I, Simus N, Lorenz T, Konig A, Sahle S, et al. (2009) Accessible methods for the dynamic time-scale decomposition of biochemical systems. Bioinformatics 25: 2816-2823.

[21] Petzold L, Zhu W (1999) Model reduction for chemical kinetics: An optimization approach. AIChE Journal 45: 869 - 886.

[22] Androulakis IP (2000) Kinetic mechanism reduction based on an integer programming approach. AIChE Journal 46: 361-371.

[23] Bhattacharjee B, Schwer DA, Barton PI, Green WH (2003) Optimally-reduced kinetic models: reaction elimination in large-scale kinetic mechanisms. Combustion and Flame 135: 191 - 208.

[24] Turányi T, Bérces T, Vajda S (1989) Reaction rate analysis of complex kinetic systems. International Journal of Chemical Kinetics 21: 83–99.

[25] Turányi T (1990) Sensitivity analysis of complex kinetic systems. tools and applications. Journal of Mathematical Chemistry 5: 203–248.

[26] Tomlin AS, Pilling MJ, Merkin JH, Brindley J (1995) Reduced mechanisms for propane pyrolysis. Ind Eng Chem Res 34: 3749 - 3760.

[27] Smets I, Bernaerts K, Sun J, Marchal K, Vanderleyden J, et al. (2002) Sensitivity function-based model reduction: A bacterial gene expression case study. Biotechnology and Bioengineering 80: 195–200.

[28] Liu G, Swihart MT, Neelamegham S (2005) Sensitivity, principal component and flux analysis applied to signal transduction: the case of epidermal growth factor mediated signaling. Bioinformatics 21: 1194-1202.

[29] Chassagnole C, Noisommit-Rizzi N, Schmid JW, Mauch K, Reuss M (2002) Dynamic modeling of the central carbon metabolism of escherichia coli. Biotechnology and Bioengineering 79: 53–73.

[30] Schmidt H, Madsen MF, Dano S, Cedersund G (2008) Complexity reduction of biochemical rate expressions. Bioinformatics 24: 848-854.

[31] Ropers D, Baldazzi V, de Jong H (2011) Model reduction using piecewise-linear approximations preserves dynamic properties of the carbon starvation response in escherichia coli. IEEE/ACM Transactions on Computational Biology and Bioinformatics 8: 166-181.

[32] Kholodenko BN, Demin OV, Moehren G, Hoek JB (1999) Quantification of Short Term Signaling by the Epidermal Growth Factor Receptor. Journal of Biological Chemistry 274: 30169-30181.

[33] Gutenkunst RN, Waterfall JJ, Casey FP, Brown KS, Myers CR, et al. (2007) Universally sloppy parameter sensitivities in systems biology models. PLoS Comput Biol 3: e189.

[34] Walter E, Pronzato L (1997) Identification of parametric models from experimental data. Springer.

[35] Applegate DL, Bixby RE, Chvátal V, Cook WJ (2006) The traveling salesman problem: a computational study. Princeton University Press.

[36] Olivier BG, Snoep JL (2004) Web-based kinetic modelling using JWS Online. Bioinformatics 20: 2143-2144.

[37] Keating SM, Bornstein BJ, Finney A, Hucka M (2006) SBMLToolbox: an SBML toolbox for MATLAB users. Bioinformatics 22: 1275-1277.

[38] Orton RJ, Sturm OE, Vyshemirsky V, Calder M, Gilbert DR, et al. (2005) Computational modelling of the receptor-tyrosine-kinase-activated MAPK pathway. Biochem J 392: 249-261.

Chapter 4

Identifying optimal models to represent biochemical systems[1]

Abstract

Biochemical systems involving a high number of components with intricate interactions often lead to complex models that consist of many equations with a large number of parameters. A large model could describe in detail the mechanisms that underlie the system, and hence might produce reliable predictions. Yet it could hinder us in understanding the behavior of the system. In terms of parameter identification, having a large model is also often problematic, especially in the view of limited data availability. Therefore, a reduced model may be preferred to represent the system. In order to efficaciously replace the large model, the reduced model should have the same ability as the large model to produce reliable predictions for any testable experimental conditions.

We present a novel method to extract an optimal model from a large model candidate to represent biochemical systems. The method combines a reduction method and a model discrimination method which are applied iteratively. The former assures that the reduced model contains only those components that are important to govern the dynamics obtained from experiments, whereas the latter ensures that the reduced model gives a good prediction for any experimental condition. Applying these two techniques iteratively, we end up with a simpler model with powerful prediction, and with a behavior that cannot be distinguished from that of the large model.

[1] Based on: M. Apri, M. de Gee, and J. Molenaar – *"Extracting optimal models to represent biochemical systems,"* to be submitted

4.1 Introduction

Biochemical networks are often very complex. The complexity may arise from the large number of components involved in the network and/or from their intricate interactions. When such systems are modeled by differential equations, we obtain a large non-linear differential equation system with many parameters. There are some advantages for having a large model, e.g., it may capture in detail the mechanisms of the system and, therefore, might give accurate predictions. On the other hand, model complexity also gives rise to severe problems, e.g., hard understanding of system behavior under varying conditions; long computing times, especially in case of stiff model; and parameter identification problems, especially in the view of limited data availability. To overcome these issues, reduced models that still capture the essential features of the system are highly desirable.

Several powerful methods for model reduction are already available, e.g., time-scale separation [1, 2, 3, 4], sensitivity analysis [5, 6, 7], and lumping [8, 9]. Of these methods, time-scale separation and sensitivity analysis typically require prior knowledge of the true parameter values of the model before they can be applied. Therefore, only the first two above-mentioned problems might be remedied in this way, whereas the problem of parameter identification, which is often the most problematic issue in systems biology, remains. On the other hand, lumping methods usually give reduced models that may be structurally different from the original one. This is because a component in the reduced model is a linear combination of several components in the original model and vice versa. This hinders us in the biological interpretation of the lumped model.

In previous work we successfully developed a reduction method to simplify biochemical models in systems biology, see the previous chapter which is based on [10]. This method is based on the so-called "admissible region" concept, that is the set of parameters for which the mathematical model yields some required output. This concept reflects the parameter sloppiness that commonly occurs in systems biology models [11]. In contrast to the methods mentioned above, our method does not require prior knowledge of the true parameter values. However, the procedure to yield a reliable reduced model was not yet complete. The method only makes use of data which were obtained from experiments under specific conditions. The behavior of the system under conditions that are different from these experiments, might not be well predicted.

In this paper we repair this shortcoming by presenting a novel approach to extract a reliable reduced model from a full model under all possible conditions. The proposed approach combines a reduction method and a model discrimination method. By combining these two methods, we arrive at a simpler model that still has powerful prediction capabilities. This in turn will help us in understanding the behavior of the complex system since such a reduced model apparently contains the core of the mechanisms underlying the system dynamics.

4.2 Method

Consider a biochemical network for which the dynamics of its n components is modeled by a system of ordinary differential equations (ODEs)

$$\begin{aligned} \frac{d\mathbf{x}}{dt} &= \mathbf{f}(\mathbf{x}, \mathbf{k}, \mathbf{e}) \\ \mathbf{y} &= \mathbf{g}(\mathbf{x}, \mathbf{k}, \mathbf{e}) \end{aligned} \tag{4.1}$$

with initial values

$$\mathbf{x}(t = 0) = \mathbf{x}_0. \tag{4.2}$$

Here, $\mathbf{x} \in \mathbb{R}^n$ represents the concentration of the species in the network, $\mathbf{k} \in \mathbb{R}^m$ is the parameter set in the model, $\mathbf{y} \in \mathbb{R}^q$ stands for the model output with $1 \leq q \leq n$, and $\mathbf{e} \in \mathbb{R}^p$ represents the experimental conditions under which the model output $\mathbf{y}$ is measured. Throughout this paper, the components of $\mathbf{y}$ are referred to as "the target components" of the system. The measured data for $\mathbf{y}$ are denoted by $\hat{\mathbf{y}}$.

In practice, a common approach is to estimate the parameter set $\mathbf{k} = (k_1, k_2, \ldots, k_m)$ by fitting the model in (4.1)-(4.2) to an initial dataset $\hat{\mathbf{y}}$. Next, a new experiment, based on optimal experimental design, is carried out to obtain a new dataset and the parameter estimation is repeated. These steps are applied iteratively until all parameters hopefully can be identified, as depicted in Figure 4.1A. Unfortunately, in most cases, it is very difficult to identify all of them. This especially happens if the number of parameter is large. The reason is that, in developing a huge model, one easily introduces reactions, and thus parameters, that in fact are redundant, since they are not necessary to secure the functioning of the system. In those cases, it is convenient to work with a simpler model with less parameters so that parameter identification can be carried out efficaciously.

Although any reduced model contains less components and/or parameters than the original model, it is important that it should still be able to reliably predict the behavior of the system for all possible experimental conditions. Only in this case, the reduced model can replace the full model and fully represent the system. Note that the experimental conditions can be varied in several ways. For example, if the initial condition of a particular biochemical species x_i in the experiment can be in the range of $a \leq x_i(0) \leq b$, then the behavior of the system should be well predicted by the reduced model for any initial condition $x_i(0) \in [a, b]$. Also, if a particular perturbation can be applied in an experiment, e.g., deletion of some genes, the behavior of the perturbed system should also be well predicted. The set of all possible experimental conditions is denoted by $\mathbb{E}$, and the reduced model that can reliably predict the dynamics of the target components for any $\mathbf{e} \in \mathbb{E}$ is referred to as "the optimal model".

Suppose that a measured dataset is obtained from an experiment. Then, the parameters $\mathbf{k}$ in the full model (4.1) can be estimated by fitting the model (4.1)-(4.2) to the data. Most likely, this parameter set is poorly identified, and correspondingly, there are many parameter sets that fit the data equally well. Alltogether, they establish the so-called "admissible region" in parameter space.

To extract an optimal model, we combine our reduction method with a model discrimination method. The procedure has been sketched in Figure 4.1B. The essence of this scheme is

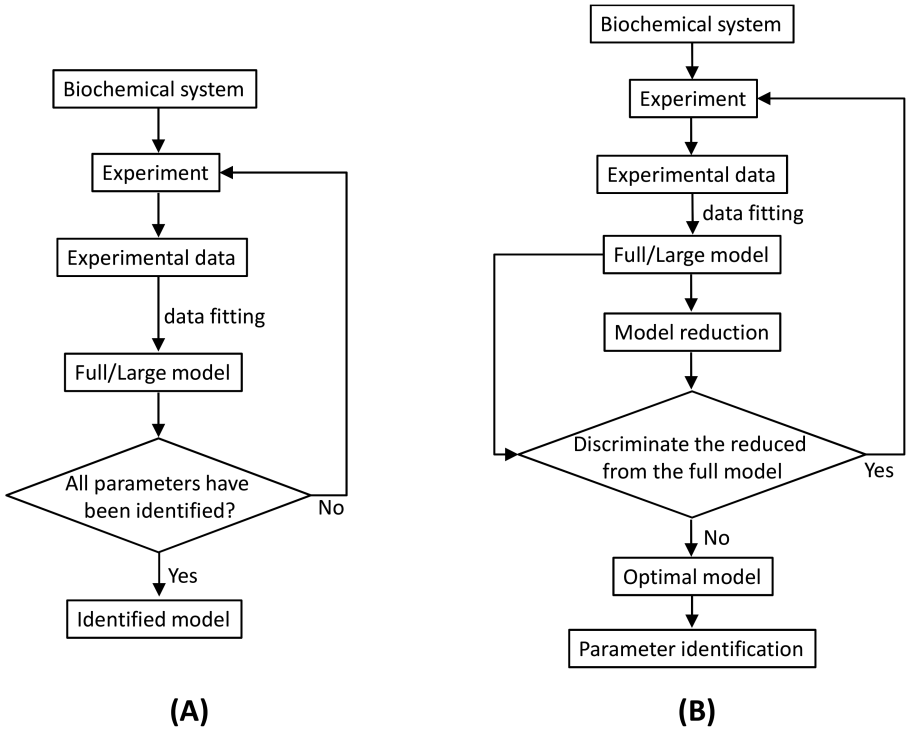

Figure 4.1: (A) Common approach to estimate parameter in systems biology, (B) Proposed approach to yield optimal model with fewer parameters.

that for the obtained reduced model, it is investigated whether an experimental condition can be found for which the reduced model yields an outcome that is significantly different from what the full model would predict. If this is the case, the reduced model is not accepted as being "optimal".

Notice that parameter estimation is frequently used in our procedure, for which a vast body of separate liturature exists, e.g., [12, 13, 14, 15, 16, 17]. In our calculation, we made use of the routine from MATLAB that are essentially based on [16].

4.2.1 Model reduction

After having obtained a parameter estimate $\mathbf{k}$ for the full model, the first step is to reduce the model complexity by removing redundant components and/or parameters that do not contribute to the dynamics of the target components. For this purpose, we have developed a reduction method in [10] that utilizes the concept of admissible region. To reduce a full model, the method does not necessarily require any prior biological knowledge. However, the method can easily be tuned to incorporate prior knowledge, if this is available. The main

features of our reduction method are summarized below.

Admissible region

Suppose that M time-series data of the target components $\hat{\mathbf{y}}^l(t_i, \mathbf{e}^l)$ are obtained from experiments, which were conducted under M different experimental conditions $\mathbf{e}^l$, with $i = 1, \ldots, N$, and $l = 1, \ldots, M$. We measure the distance of the model output (target components) to the time-series data in the usual way as the average of the squared relative residuals:

$$S(\mathbf{y}(t, \mathbf{k}, \mathbf{e}), \hat{\mathbf{y}}(t, \mathbf{e})) = \frac{1}{M \cdot q \cdot N} \sum_{l=1}^{M} \sum_{j=1}^{q} \sum_{i=1}^{N} \left(\frac{y_j^l(t_i, \mathbf{k}, \mathbf{e}^l) - \hat{y}_j^l(t_i, \mathbf{e}^l)}{\hat{y}_j^l(t_i, \mathbf{e}^l)} \right)^2 . \tag{4.3}$$

Let us introduce a tolerance ε^2 which indicates how much difference we accept the discrepancy between data and model prediction. Then, all parameter vectors $\mathbf{k}$ such that

$$S(\mathbf{y}(t, \mathbf{k}, \mathbf{e}), \hat{\mathbf{y}}(t, \mathbf{e})) < \varepsilon^2 \tag{4.4}$$

are acceptable to represent the parameters of the system, since they are capable of producing the dynamics within the required accuracy. We say that all parameter vectors $\mathbf{k}$ that satisfy (4.4) constitute the so-called "admissible region" (AR). Thus,

$$AR = \left\{ \mathbf{k} \in \mathbb{R}^m \mid S\left(\mathbf{y}(t, \mathbf{k}, \mathbf{e}), \hat{\mathbf{y}}(t, \mathbf{e})\right) < \varepsilon^2 \right\}. \tag{4.5}$$

In many cases, the measurement error in the experiments can be used as a guidance to choose a suitable value for ε. Notice that the region AR reflects the parameter sloppiness in the model. As long as AR consists of more than a single point, the parameters in the model are not identified given the tolerance ε [18].

Reduction method

Since all the parameter vectors in the admissible region yield an acceptable dynamical behavior of the system, it is easy to deduce if a reduction is possible from the shape of AR. For example, if the admissible region includes a part of a parameter axis, then this parameter can apparently be set equal to zero and could thus be excluded from the model. If the region extends to infinity in a certain parameter direction, then some terms or state-variables in the ODEs might be lumped. This analysis may thus lead to a simpler representation of the biochemical system.

Describing the admissible region and deducing the possible reductions is relatively easy for a small system. However, applying such analysis to a model with many parameters, which is typically the case in systems biology, can be very complicated. Fortunately, we notice that in practice it is not necessary to construct the admissible region completely. If one (or several) parameter(s) can be set to zero (or infinity) and the others can be re-optimized such that the resulting parameters $\mathbf{k}_r \in \mathbb{R}^m$ are still in the admissible region, then the model can be simplified. Thus,

$$\mathbf{k}_r = (k_{r1}, k_{r2}, \ldots, k_{rm}) \in AR, \quad \text{where } k_{rj} = 0 \text{ or } k_{rj} = \infty, \text{ for some } j. \tag{4.6}$$

The reduction procedure can be carried out in a systematic way by applying first node reduction, then parameter reduction, and finally node lumping.

Node reduction

First, we try to remove redundant nodes, one at a time. Here, e.g., node x_1 can be removed from the system if it can be eliminated in all equations and the parameters can be re-optimized such that (4.4) is satisfied. This procedure is repeated for $x_2, \ldots, x_n$. If one or more nodes have been removed, we cycle again through the remaining nodes and repeat the procedure until no further nodes can be removed.

Parameter reduction

To see whether parameter, say, k_1 can be removed, we simply set $k_1 = 0$ and re-estimate the other parameters to obtain

$$\mathbf{k}_r = \underset{k_{i\neq 1}}{\arg\min} \left[S(\mathbf{y}, \hat{\mathbf{y}}) \right], \quad \text{where } k_1 = 0. \tag{4.7}$$

If (4.4) is satisfied, then indeed k_1 can be removed from the model. Next, this procedure is repeated for $k_2, \ldots, k_m$. If one or more parameters have been removed, we cycle again through the remaining parameters and repeat the procedure until no further parameters can be removed.

Since the approach is heuristic, the result of the reduction might depend on the parameter ordering and might be not unique. In principle, all the the reduced models obtained this way are acceptable. However, for reasons of parsimony, the strongest reduction is preferable. For this purpose, we found in [10] that in general parameter ordering based on the sensitivities

$$C_j = \frac{k_j}{S} \frac{\partial S}{\partial k_j} \tag{4.8}$$

gives a very good reduction rate.

Lumping

If a parameter that represents the strength of a reaction can be set at a very large value and the others can be adjusted to satisfy (4.4), it indicates that the corresponding reaction can be considered as instantaneous. This implies that the two corresponding nodes that are connected by the reaction can be lumped, and hence may be replaced by one node. The procedure for lumping essentially follows the same steps as mentioned under parameter reduction.

4.2.2 Model discrimination

Suppose that from the model reduction procedure above, we obtain a reduced model

$$\begin{aligned} \frac{d\mathbf{x}_r}{dt} &= \mathbf{f}_r(\mathbf{x}_r, \mathbf{k}_r, \mathbf{e}) \\ \mathbf{y}_r &= \mathbf{g}(\mathbf{x}_r, \mathbf{k}_r, \mathbf{e}) \end{aligned} \tag{4.9}$$

where $\mathbf{x}_r, \mathbf{f}_r \in \mathbb{R}^R$ with $R < n$, and $\mathbf{y}_r \in \mathbb{R}^q$ denotes the dynamics of the target components of the reduced model. The next step is to investigate whether the reduced model will generate the same prediction as that of the full model for any possible experimental condition. If their predictions are indeed always the same, then we conclude that the full model can be replaced by the reduced model.

For this purpose, a model discrimination method is utilized. Model discrimination is commonly used to select the best suited model from different hypothetical models [19, 20, 21, 22]. In this work, we use it to search for an experimental condition $\mathbf{e}$ for which the reduced model can be distinguished from the full model. So, we look for an experimental condition $\mathbf{e} \in \mathbb{E}$ that maximizes the distance between the full and reduced models in terms of the distance function S in (4.3). Mathematically, this can be written as

$$\arg\max_{\mathbf{e}\in\mathbb{E}}[S(\mathbf{y}(t,\mathbf{k},\mathbf{e}),\mathbf{y}_r(t,\mathbf{k}_r,\mathbf{e}))]. \tag{4.10}$$

We say that a reduced model cannot be distinguished from the full model if their distance satisfies

$$S(\mathbf{y}(t,\mathbf{k},\mathbf{e}),\mathbf{y}_r(t,\mathbf{k}_r,\mathbf{e})) < \sigma^2, \quad \forall\, \mathbf{e} \in \mathbb{E}. \tag{4.11}$$

with σ a small number that denotes the tolerance criterion. Note that σ may have a different value from ε. Usually, σ will be larger than ε, because otherwise we might end up with modeling noise.

4.2.3 Model reduction and model discrimination applied iteratively

The hard task of model reduction is to find a simpler model that is still able to produce the same prediction for all possible experimental conditions as the original model. Only then we call such a reduced model "optimal". The admissible region, shown in Figure 4.2, contains an infinite number of parameter set candidates of the reduced model that, within measurement accuracy, exactly produce similar behavior as the full model as far as the measured target components are concerned. Note that the candidates for the parameter set of the reduced model are those that lie in the parameter axes within the admissible region.

To find the optimal model, we could in principle compare each parameter set candidate of the reduced model in AR to the full model under all possible conditions. In practice, this is completely impossible. That is why we propose an iterative algorithm that leads to at least one optimal model.

The idea is as follows. We first apply the reduction method in [10] and obtain a reduced model that at least for the measured target components shows the same behavior as the full model. Next, we compare this particular reduced model with the full model under all possible conditions and select experiment for which the difference is biggest. This is called "discrimination". Normally, this difference is still huge in this first step. Then, we add the data from this experiment to our dataset that consists of time-series for the target components. In the second step this extended dataset is used as starting point.

This second step starts with calculation of an updated AR for the full model. Then, the reduction method from [10] is applied leading to a new reduced model. If this second reduced

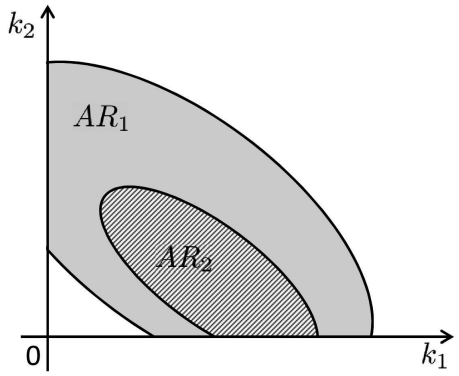

Figure 4.2: Illustration of the admissible region with respect to the available dataset. Initially, the admissible region of the system is AR_1. In this situation, a reduced model can be obtained either by setting $k_1 = 0$ or $k_2 = 0$. When a new dataset from a new experiment is incorporated, the admissible region shrinks to AR_2. Thus, $AR_2 \subset AR_1$. Now, a reduced model can only be obtained when $k_2 = 0$.

model is compared to the full model under all possible condition, one usually finds that the difference becomes smaller than found in the first step of the algorithm.

One again selects the experiment for which the difference is biggest. Most of the time this difference is bigger than a predefined threshold, so one has to start a third round, in which the last experimental dataset is added to the dataset of the target components and the experiment from the first round. The procedure is repeated until the difference for all possible experimental conditions between reduced model and full model is smaller than the threshold. The resulting model for which this holds is called “optimal”.

4.2.4 Algorithm

In a nutshell, the method that we propose consists of the following steps:

1) Obtain data from experiment.

2) Estimate the parameters in the full model.

3) Apply reduction to the full model.

4) Try to discriminate the reduced model from the full model.

5) If there indeed exists an experimental setting that can discriminate them, add the data from this experiment to the dataset and repeat step 2) - 4). Otherwise, the optimal model has been obtained.

4.3 Results

In this section, we show how the proposed approach works out in practice. The method is applied to two different examples. First we investigate a small artificial metabolic network, for demonstration purposes only. Next, we consider a big EGFR network model as a more realistic example.

4.3.1 Small network

Consider the metabolic system consisting of only three species as depicted in Figure 4.3A.

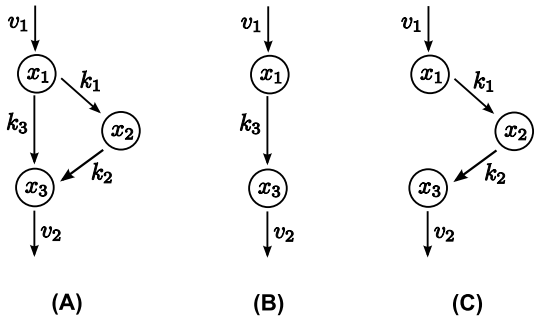

Figure 4.3: (A) Full model, (B) reduced model B with parameters k_1 and k_2 removed, (C) reduced model C with parameter k_3 removed.

The concentrations of $x_1(t)$, $x_2(t)$ and $x_3(t)$ are modeled with the system of ordinary differential equations

$$\begin{aligned} \frac{dx_1}{dt} &= v_1 - (k_1 + k_3)x_1 \\ \frac{dx_2}{dt} &= k_1 x_1 - k_2 x_2 \\ \frac{dx_3}{dt} &= k_3 x_1 + k_2 x_2 - v_2 x_3. \end{aligned} \tag{4.12}$$

The parameters v_1 and v_2 govern the input and output fluxes of the network, respectively. In this network, the chemical species x_1 can be converted to x_3 directly, but also by a detour through x_2. Thus, the concentration of x_1 is influenced by the input flux rate v_1 and the conversion reactions that contains parameters k_1 and k_3. Concentration x_3, on the other hand, is influenced by the conversion reactions which involve parameters k_2 and k_3 and the output flux v_2.

Suppose that we are interested in the dynamics of x_3 as a function of the input flux v_1 and the initial concentration $x_1(0)$. Thus, in the context of the framework above, feasible experiments are varying v_1 and $x_1(0)$, and we assume that in these experiments v_1 and $x_1(0)$ can only be varied in the ranges $0 \leq v_1 \leq 10$ and $0 \leq x_1(0) \leq 10$. Therefore,

$$\mathbb{E} = \{\{v_1, x_1(0)\} \,|\, 0 \leq v_1 \leq 10, 0 \leq x_1(0) \leq 10\}\,. \tag{4.13}$$

In this system, x_3 is the target component.

As seen from the network in Figure 4.3A, x_1 can be converted to x_3 through two separate pathways, and we are not sure a priori whether both pathways are necessary to describe the dynamics of x_3. Therefore, we set out to describe the dynamics of $x_3(t)$ by an optimal model. This optimal model should be able to correctly predict $x_3(t)$ for any plausible value of input v_1 and initial condition $x_1(0)$ and may not contain redundant reactions or parameters.

In our first experiment, we measure data for $x_3(t)$ with the input flux $v_1 = 1$ and the initial condition of the first component $x_1(0) = 0$. Thus,

$$\mathbf{e}^1 = \{v_1 = 1, x_1(0) = 0\}. \tag{4.14}$$

Instead of performing real experiments, we use the full model in (4.12) with $\mathbf{k} = (k_1, k_2, k_3) = (1, 1, 0.2), v_2 = 1, x_2(0) = x_3(0) = 0$ to obtain the data, with an added normally distributed random noise of 5% relative deviation. The measurement is carried out at every 2 time units, i.e., $t = 2, 4, \ldots, 14$. After adding noise, we obtain the measurement points that are denoted by '*' in Figure 4.4A.

Parameter estimation applied to the full model with a threshold value of $\varepsilon = 5\%$, yielded a large set of parameter vectors that fitted the data quite well. One of them is $\mathbf{k}_f^1 = (0.8125, 0.8002, 0.3244)$, which was chosen as reference parameter vector (note that in real situation, we would not know the true parameter values $\mathbf{k}$). Applying our reduction method described in Section 4.2.1, we found that the data can also be adequately represented by the reduced model in Figure 4.3B with $\mathbf{k}_{rB}^1 = (0, 0, 0.5208)$ and also by the reduced model in Figure 4.3C with $\mathbf{k}_{rC}^1 = (1.2288, 1.2128, 0)$. The results are shown in Figure 4.4A. Since we prefer a stronger reduction, the reduced model in Figure 4.3B with parameter set $\mathbf{k}_{rB}^1$ was chosen as our reduced model. Because in this case the number of parameters is small, it is easy to find the strongest reduction. In general this is not that easy.

Next, model discrimination with a threshold value of $\sigma = 10\%$ was carried out to search for an input flux rate v_1 and an initial condition $x_1(0)$ that can differentiate the reduced model from the full model. Mathematically speaking, we apply the following optimization:

$$\arg\max_{\mathbf{e}\in\mathbb{E}}[S(\mathbf{y}(t, \mathbf{k}_f^1, \mathbf{e}), \mathbf{y}_r(t, \mathbf{k}_{rB}^1, \mathbf{e}))]. \tag{4.15}$$

The resulting optimum is given by

$$\mathbf{e}^2 = \{v_1 = 0, x_1(0) = 10\} \tag{4.16}$$

It corresponds to a distance $S(\mathbf{y}, \mathbf{y}_r) = 0.0614$, which exceeds the threshold of $\sigma = 10\%$ considerably. This implies that the reduced model could be discriminated from the full model. The results of the full model (with the reference parameters) and the reduced model in Figure 4.3B for the values of v_1 and $x_1(0)$ in (4.16) are shown in Figure 4.4B. Note that these time series show a behavior that is distinctly different from the the original time series displayed in Figure 4.4A.

The next step in the discrimination procedure is to add the new data obtained from experiment with condition $\mathbf{e}^2$ to the old one and to proceed with the data from both conditions $\mathbf{e}^1$ and $\mathbf{e}^2$. The corresponding $x_3(t)$ data are denoted with '*' and '+' in Figure 4.4C.

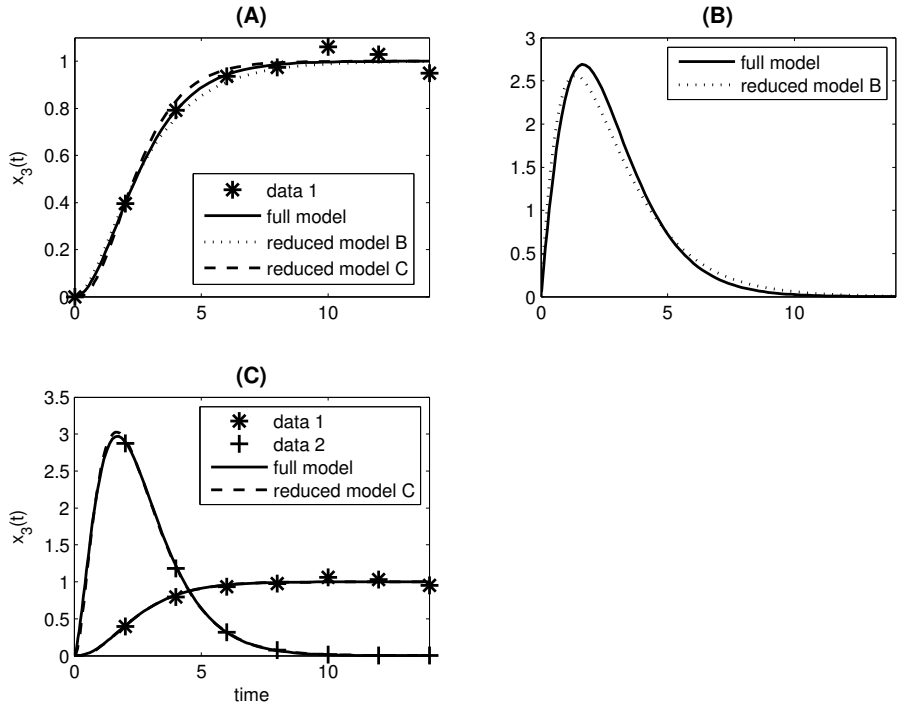

Figure 4.4: Dynamics of the target component $x_3(t)$. (A) Parameter fitting of the full model (solid line) and reduced models (dashed line and dotted line) to dataset 1, which was obtained by setting $\mathbf{e}^1 = \{v_1 = 1, x_1(0) = 0\}$. The full model has parameters $\mathbf{k}_f^1 = (0.8125, 0.8002, 0.3244)$, for the reduced model in Figure 4.3B we have $\mathbf{k}_{rB}^1 = (0, 0, 0.5208)$ and for reduced model C in Figure 4.3C $\mathbf{k}_{rC}^1 = (1.2288, 1.2128, 0)$. (B) Model discrimination with $\mathbf{e}^2 = \{v_1 = 0, x_1(0) = 10\}$ distinguishes the reduced model in Figure 4.3B with $\mathbf{k} = \mathbf{k}_{rB}^1$ from the full model with $\mathbf{k} = \mathbf{k}_f^1$. (C) Parameter fitting of the full model (solid line) and of the reduced model (dashed line) to dataset 1 and dataset 2. Dataset 2 was obtained by setting $\mathbf{e} = \mathbf{e}^2$. Parameter of the full model $\mathbf{k}_f^2 = (1.4795, 0.9, 0.1186)$ while that of the reduced model $\mathbf{k}_{rC}^2 = (2.1415, 0.8325, 0)$

Re-estimating the parameter vector of the full model using this extended dataset, we obtain the new parameter vector $\mathbf{k} = \mathbf{k}_f^2 = (1.4795, 0.9, 0.1186)$. We next apply the reduction procedure again and find that the full model can only be reduced to the model C with $\mathbf{k}_{rC}^2 = (2.1415, 0.8325, 0)$. In Figure 4.4C the dashed line stems from model C and it is clear that this reduced model is able to fit the extended data perfectly.

The question still remains whether another experiment exists that could discriminate between the full model and reduced model C. When the model discrimination is re-performed

similarly as we did for model B in (4.15), it turns out that there is no input flux v_1 and initial condition of $x_1(0)$ that can discriminate between the reduced model C with $\mathbf{k} = \mathbf{k}^2_{rC}$ and the full model with $\mathbf{k} = \mathbf{k}^2_f$.

Finally to validate our conclusion, we generated 12 datasets choosing random values of $\{v_1, x_1(0)\}$ and compared these to the prediction from the reduced model C. In Figure 4.5 both data points for $x_3(t_i)$ and the predicted curves from model C are given. We see that the predictions of the reduced model are in a very good agreement with all datasets. This demonstrates that the behavior of the network for any experimental condition in (4.13) can be very well described by the reduced model C with $\mathbf{k} = \mathbf{k}^2_{rC} = (2.1415, 0.8325, 0)$.

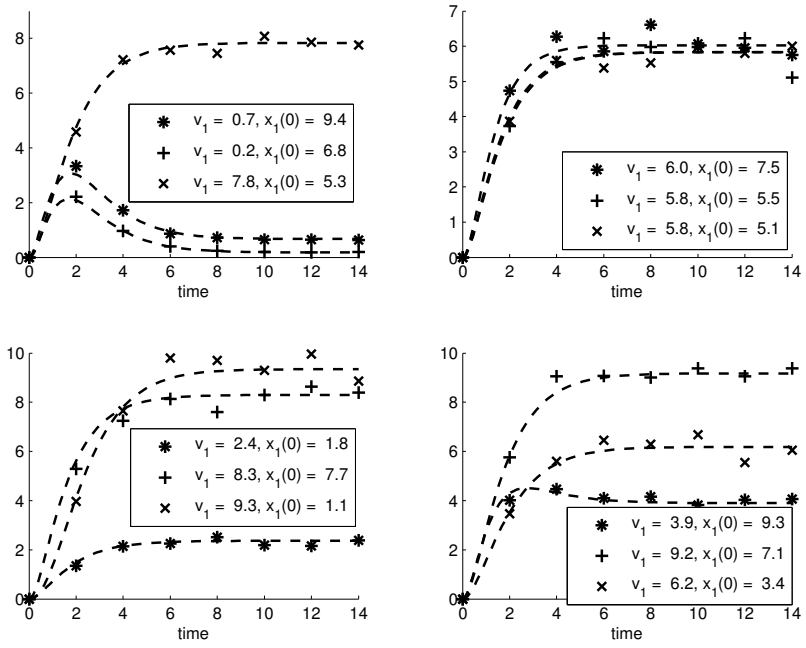

Figure 4.5: Validation of the reduced model C. The data are generated by choosing random values for v_1 and $x_1(0)$ and indicated by "*","+", and "x". The dashed lines are the predictions from reduced model C with $\mathbf{k} = \mathbf{k}^2_{rC} = (2.1415, 0.8325, 0)$.

.

4.3.2 EGFR Model

As a test, we apply our method also to the epidermal growth factor receptor (EGFR) model from [23], of which the network is shown in Figure 4.6A. This model describes the cellular response to an epidermal growth factor (EGF) stimulation. The model consists of 23 bio-

chemical components with 25 chemical reactions, described by ordinary differential equations (ODEs). This results in an ODE system with 23 state variables and 50 parameters. The parameter values of the full model are given in Table II in [23].

Since the kinetic scheme contains several cycles, the kinetic parameters involved in the cycles satisfy the so-called "detailed balance" relationships given by

$$\frac{k_9 \cdot k_{10} \cdot k_{11} \cdot k_{12}}{k_{-9} \cdot k_{-10} \cdot k_{-11} \cdot k_{-12}} = 1 \tag{4.17}$$

$$\frac{k_{15} \cdot k_{21} \cdot k_{-17} \cdot k_{-18}}{k_{-15} \cdot k_{-21} \cdot k_{17} \cdot k_{18}} = 1 \tag{4.18}$$

$$\frac{k_{18} \cdot k_{22} \cdot k_{-19} \cdot k_{-20}}{k_{-18} \cdot k_{-22} \cdot k_{19} \cdot k_{20}} = 1 \tag{4.19}$$

$$\frac{k_{12} \cdot k_{22} \cdot k_{21} \cdot k_{23}}{k_{-12} \cdot k_{-22} \cdot k_{-21} \cdot k_{-23}} = 1 \tag{4.20}$$

$$\frac{k_{15} \cdot k_{-20} \cdot k_{-23} \cdot k_{-24}}{k_{-15} \cdot k_{20} \cdot k_{23} \cdot k_{24}} = 1. \tag{4.21}$$

To validate their model, the system was stimulated with different EGF stimulations (20 nM, 2 nM, and 0.2 nM) and the resulted transient response of several proteins were measured. The measured responses are the concentrations of phosphorylated EGFR, phosphorylated Shc, phosphorylated PLCγ, Grb2 bound in Shc, and Grb2 bound in EGFR. These are composed of several species in the model:

$$\begin{aligned}
\text{Total phosphorylated EGFR} &= 2([\text{RP}] + [\text{R-PL}] + [\text{R-PLP}] + [\text{R-G}] + [\text{R-G-S}] + \\
&\quad [\text{R-Sh}] + [\text{R-ShP}] + [\text{R-Sh-G}] + [\text{R-Sh-G-S}]) && (4.22)\\
\text{Total phosphorylated PLC}\gamma &= [\text{R-PLP}] + [\text{R-PLC}\gamma\text{P}] && (4.23)\\
\text{Total phosphorylated Shc} &= [\text{R-ShP}] + [\text{R-Sh-G}] + [\text{R-Sh-G-S}] + [\text{ShP}] + \\
&\quad [\text{Sh-G}] + [\text{Sh-G-S}] && (4.24)\\
\text{Total Grb2 bound to EGFR} &= [\text{R-G}] + [\text{R-G-S}] + [\text{R-Sh-G}] + [\text{R-Sh-G-S}] && (4.25)\\
\text{Total Grb2 bound to Shc} &= [\text{R-Sh-G}] + [\text{Sh-G}] + [\text{R-Sh-G-S}] + [\text{Sh-G-S}]. && (4.26)
\end{aligned}$$

The model was used to predict the dependency of the transient responses on the relative abundance of some signaling proteins, that is when the initial concentration of Shc was decreased by a factor of 4, the initial concentration of Grb2 was increased by a factor of 4, and when the initial concentration of EGFR was increased by a factor of 4.

In this paper, we use this model to show how our proposed method can be applied to a real biological system. For this purpose, we assume that the parameters in the model are unknown and should be estimated from the experimental data. The measured responses are regarded as our target components in this example. Then we investigate whether the cellular response behavior can be described by a simpler model. Since the target components were measured and predicted for different EGF stimulations and different initial conditions of EGFR, Shc, and Grb2, we assume that the experimental setting can only account for variation of those

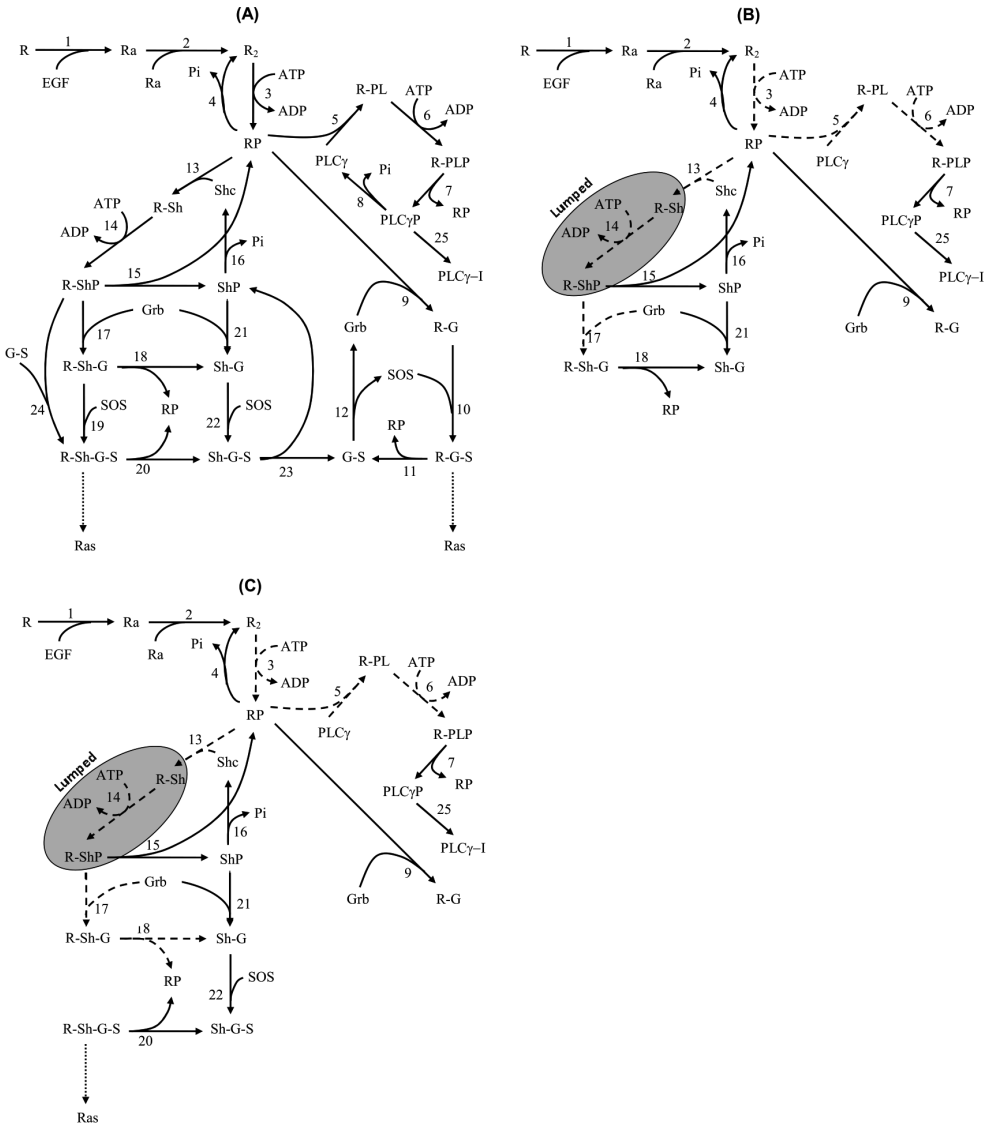

Figure 4.6: The EGFR biochemical network. A solid arrow represents a reaction with two kinetic parameters, and a dashed arrow represents a reaction with one kinetic parameter. (A) The full network from [23], (B) The optimal network to produce the dynamics of the five target components for any experimental condition $\mathbf{e} \in \mathbb{E}$ in (4.27), (C) The optimal network as in (B) but with an additional constraint to maintain the activation pathway to Ras protein.

species. Thus,

$$\begin{aligned}\mathbb{E} = \{(\text{EGF}_{\text{stimulation}}, \text{EGFR}_0, \text{Grb2}_0, \text{Shc}_0) \mid 0 \leq \text{EGF}_{\text{stimulation}} \leq 20 \text{ nM}, \\ 0 \leq \text{EGFR}_0 \leq 400 \text{ nM}, 0 \leq \text{Grb2}_0 \leq 340 \text{ nM}, 0 \leq \text{Shc}_0 \leq 150 \text{ nM}\},\end{aligned} \tag{4.27}$$

where $\text{EGFR}_0 = [\text{EGFR}](t=0), \text{Grb2}_0 = [\text{Grb2}](t=0), \text{Shc}_0 = [\text{Shc}](t=0)$. Notice that the space of possible experimental conditions is very broad.

Due to non-availability of the real experiment, we generate the data of the target components using the full model and the parameters in [23], adding a relative normal random noise of 5% deviation. The measurements are assumed to be performed at $t = 0, 15, 30, 45, 60, 120$ seconds.

For the initial dataset, we assume that it is obtained from experiments which are carried out at two different EGF stimulations, [EGF] = 20 nM and [EGF] = 2 nM. The other three initial conditions are set to $[\text{EGFR}]_0$ = 100 nM, $[\text{Grb2}]_0$ = 85 nM, $[\text{Shc}]_0$ = 150 nM. Thus, the initial dataset is obtained from experiments with conditions

$$\begin{aligned}\mathbf{e}^{1a} &= \{\text{EGF}_{\text{stimulation}} = 20 \text{ nM}, \text{EGFR}_0 = 100 \text{ nM}, \text{Shc}_0 = 150 \text{ nM}, \text{Grb2}_0 = 85 \text{ nM}\}, \\ \mathbf{e}^{1b} &= \{\text{EGF}_{\text{stimulation}} = 2 \text{ nM}, \text{EGFR}_0 = 100 \text{ nM}, \text{Shc}_0 = 150 \text{ nM}, \text{Grb2}_0 = 85 \text{ nM}\}.\end{aligned} \tag{4.28}$$

The dynamics of the target components are shown in Figure 4.7, denoted by '+' and 'x'. If ε in (4.4) is set to $\varepsilon = 5\%$ and parameter estimation is applied, we find that the dataset can be well represented by the model with many possible parameter sets; one of them is $\mathbf{k} = \mathbf{k}_f^1$. When reduction is applied, it turns out that 33 out of 50 parameters can be removed from the model. This parameter set is denoted by $\mathbf{k} = \mathbf{k}_r^1$. The reduced model can fit the dataset quite well, as shown in Figure 4.7.

Applying model discrimination, we find that by setting the experiment to

$$\mathbf{e}^2 = \{\text{EGF}_{\text{stimulation}} = 15.3824 \text{ nM}, \text{EGFR}_0 = 141 \text{ nM}, \text{Shc}_0 = 0 \text{ nM}, \text{Grb2}_0 = 340 \text{ nM}\}, \tag{4.29}$$

the reduced model can be clearly distinguished from the full model, as can be seen in Figure 4.8. Their distance in this case is $S(\mathbf{y}(t, \mathbf{k}_f^1, \mathbf{e}^2), \mathbf{y}_r(t, \mathbf{k}_r^1, \mathbf{e}^2)) \approx 3.1 \times 10^6$.

To obtain an optimal model, we follow the procedure outlined in Section 4.2.4. First, a new experiment is performed based on the experimental setting $\mathbf{e}^2$ to generate a new dataset. Thus, the new dataset now consists of the combined dataset obtained from experiments with conditions $\mathbf{e}^{1a}, \mathbf{e}^{1b}$ and $\mathbf{e}^2$. Parameter estimation, model reduction, and model discrimination are again carried out to the combined dataset. This procedure yields $\mathbf{k} = \mathbf{k}_f^2$ for the parameter set of the full model and $\mathbf{k} = \mathbf{k}_r^2$ for the parameter set of the reduced model. The number of parameters that can be reduced turns out to be 31. The experimental condition that can maximize the distance between the full model and the reduced model is $\mathbf{e} = \mathbf{e}^3$ with distance $S(\mathbf{y}(t, \mathbf{k}_f^2, \mathbf{e}^3), \mathbf{y}_r(t, \mathbf{k}_r^2, \mathbf{e}^3)) = 23.5362$. Suppose that for the EGFR network, the threshold value for model discrimination is set to $\sigma = 25\%$. Then repeating the procedure iteratively and performing the experiments accordingly we find that after performing four additional experiments, the reduced model with $\mathbf{k} = \mathbf{k}_r^6$ cannot be distinguished from the full model

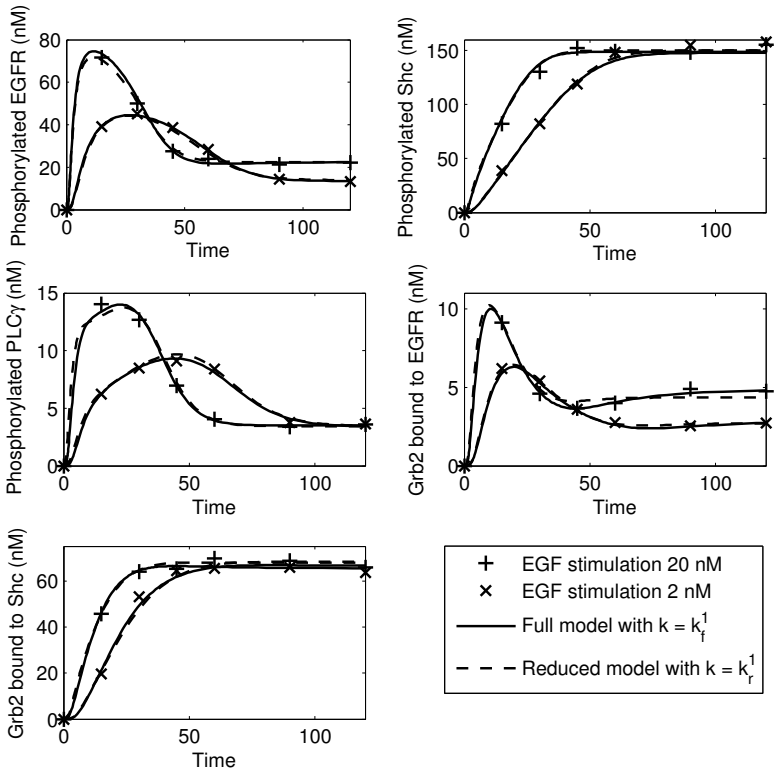

Figure 4.7: Dynamics of the target components for the start up dataset. The solid and dashed lines show that the dataset can be fitted by the full model with $\mathbf{k} = \mathbf{k}_f^1$ as well as by the reduced model with $\mathbf{k} = \mathbf{k}_r^1$.

with $\mathbf{k} = \mathbf{k}_f^6$. The iterative process to obtain the optimal model is shown in Figure 4.9 and the network of the optimal model is shown in Figure 4.6B.

In the optimal model in Figure 4.6B, 24 parameters can be set to zero while one parameter, namely k_{-14}, can be set to a very large value. The latter implies that the phosphorylation of [R-Sh] occurs very fast, and therefore, the components R-Sh and R-ShP can be lumped into one biochemical component in the optimal model. We now end up with a model that consists of 17 biochemical components with 25 kinetic parameters. This result shows that we may remove six redundant components and 25 redundant parameters from the original model. The prediction for the five target components from the reduced model would then deviate at most about 25% from that of the full model for *any* experimental condition in (4.27).

As a validation, a number of experiments are performed with different random experimental conditions and the dynamics of the target components are predicted by the reduced model,

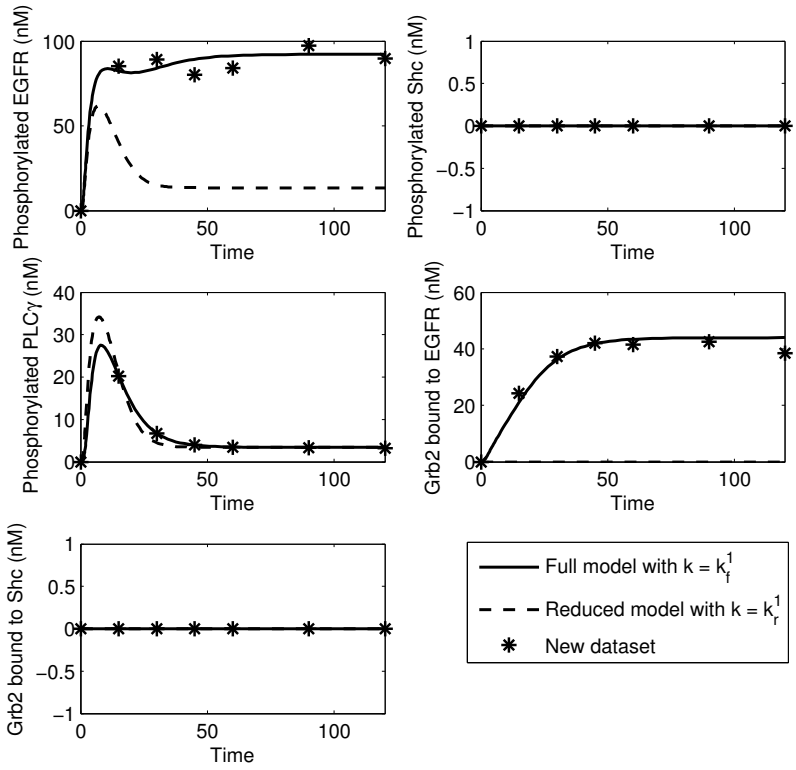

Figure 4.8: Model discrimination to distinguish the reduced model with $\mathbf{k} = \mathbf{k}_r^1$ from the full model with $\mathbf{k} = \mathbf{k}_f^1$. In this case, $\mathbf{e}^2 = \{\text{EGF}_{\text{stimulation}} = 15.3824\,\text{nM}, \text{EGFR}_0 = 141\,\text{nM}, \text{Shc}_0 = 0\,\text{nM}, \text{Grb2}_0 = 340\,\text{nM}\}$. The new dataset obtained from an experiment based on the setting $\mathbf{e} = \mathbf{e}^2$ is indicated by '*'. The dashed curve in the upper left corner shows that the reduced model cannot fit this dataset.

as shown in Figure 4.10. The result shows that the prediction of the reduced model are in a good agreement with the dynamics obtained from experiment. Only in the first experiment, the prediction for Grb2 bound to Shc slightly deviates from the measurement. However, the deviation is still acceptable. We, therefore, conclude that the reduced model in Figure 4.6B with parameter set $\mathbf{k} = \mathbf{k}_r^6$ is an optimal model to produce the dynamics of the five target components, given the threshold value of $\sigma = 25\%$.

The parameters of the full and optimal models and the list of experiments to obtain the optimal model are shown in Appendix in Table 4.1 and Table 4.2.

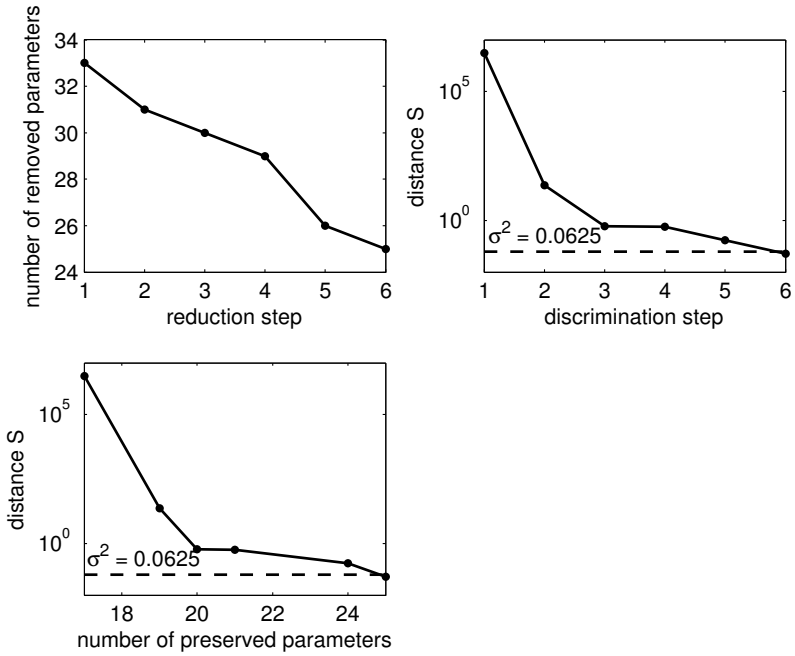

Figure 4.9: Result of iterative process to obtain the optimal model for EGFR model. The threshold value of $\sigma = 25\%$ is indicated by the dashed line. For the first dataset, the reduction procedure can remove 33 out of 50 parameters. However, the distance between the reduced and the full models in the first discrimination is still huge, namely $S(\mathbf{y}(t, \mathbf{k}_f^1, \mathbf{e}^2), \mathbf{y}_r(t, \mathbf{k}_r^1, \mathbf{e}^2)) \approx 3.1 \times 10^6$. When a new experiment based on experimental condition $\mathbf{e} = \mathbf{e}^2$ is carried out and the obtained dataset is combined with the first dataset, the number of reduced parameter in the second reduction decreases to 31. Finally, after performing five additional experiments, the distance $S < \sigma^2$, which means that there is no experimental condition that can distinguish the reduced model with $\mathbf{k} = \mathbf{k}_r^6$ from the full model with $\mathbf{k} = \mathbf{k}_f^6$. At this stage, the reduced model contains 25 parameters. Since the distance is already smaller than the tolerance, we conclude that the reduced model with $\mathbf{k} = \mathbf{k}_r^6$ is an optimal model.

Ras pathway

It is remarkable to notice that in the previous result, a number of chemical reactions that lead to the activation of Ras protein via SOS is no longer preserved in the optimal model. Mathematically speaking, this implies that the parameters that are related to these reactions cannot be identified only by measuring the five target components above. From a biological point of view, this is of course nonsensical since the activation of EGFR should lead to the activation of the Ras $\rightarrow$ Raf $\rightarrow$ Mek $\rightarrow$ ERK cascade [24]. Therefore, to preserve this chemical pathway

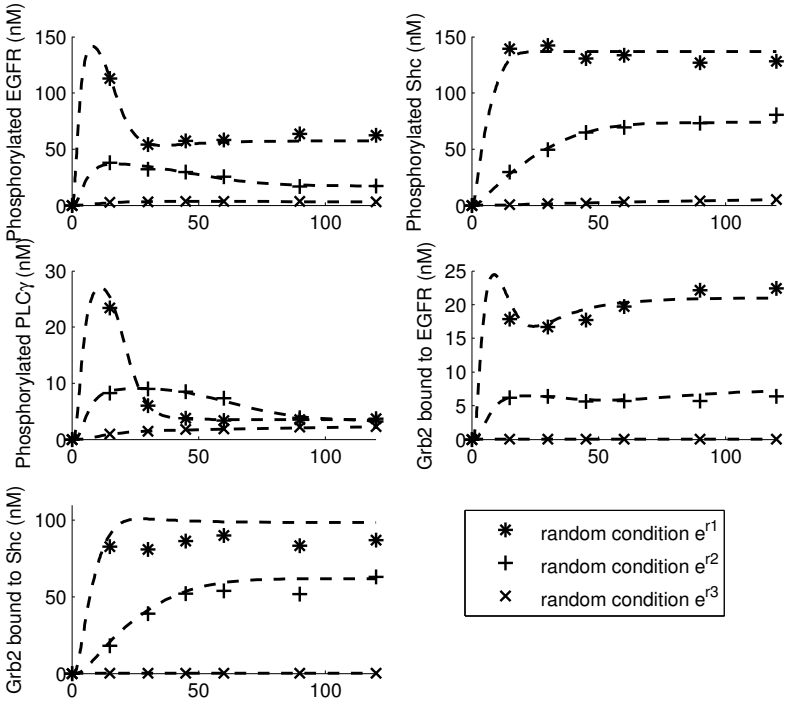

Figure 4.10: Validation of the optimal model with $\mathbf{k} = \mathbf{k}_r^6$. The data are obtained by setting the experimental conditions randomly to $\mathbf{e}^{r1} = \{538.48, 204.59, 143.78, 137.12\}, \mathbf{e}^{r2} = \{231.86, 55.45, 127.53, 74.43\}$, and $\mathbf{e}^{r3} = \{97.31, 8.1, 0.80, 13.28\}$. The dataset are indicated by "*", "+", and "x", respectively. Predictions from the optimal model are indicated by the dashed lines.

in the optimal model, one should think carefully which complex protein(s) should be treated as additional target component(s), or which constraint in the reduction should be taken into account. In other words, prior knowledge might help us to prevent such an undesired result. Fortunately, our method can easily be tuned to incorporate prior knowledge.

We observe from the network in Figure 4.6A that one possibility to maintain the pathway to the Ras protein is by preventing one of the incoming reactions to R-Sh-G-S or R-G-S from elimination. In practice, this can be done by preserving one of the following parameters from being zero, namely $k_{10}, k_{-11}, k_{19}, k_{-20}$ and k_{24}. If we use this condition as our constraint in the reduction and apply the proposed method, we obtained the optimal model that is depicted in Figure 4.6C. Here, the activation of Ras protein can be achieved via R-Sh-G-S. The iterative process to obtain this model is shown in Figure 4.11.

In this optimal model, again parameter k_{-14} can be set to a very large value and thus

R-ShP and R-Sh can be lumped into one biochemical component. The model contains 28 kinetic parameters, so about 44% of the kinetic parameters in the original model are redundant and not necessary to represent the dynamics of the five target components. As can be seen in Figure 4.11, the optimal model is now obtained after six new experiments have been performed.

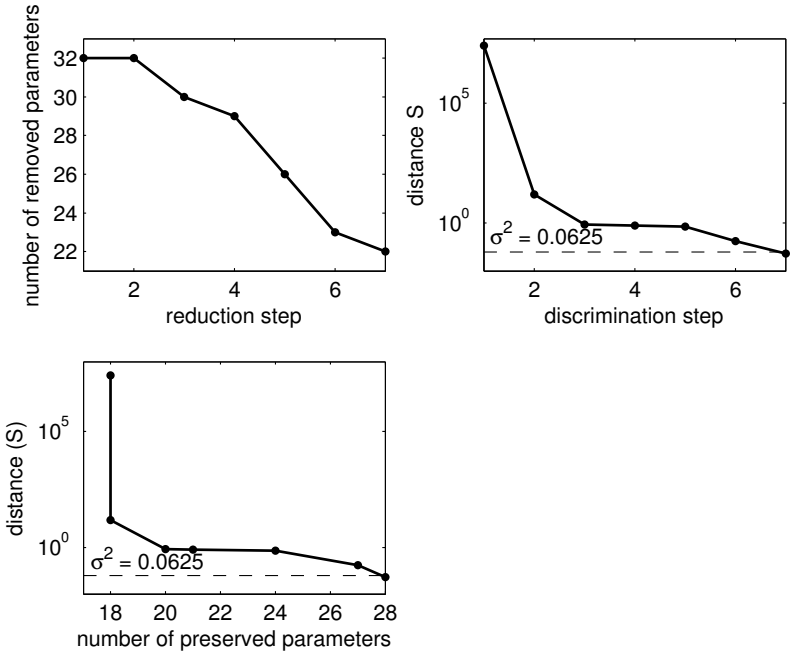

Figure 4.11: Result of iterative process to obtain the optimal model for EGFR model with a constraint to maintain the Ras pathway activation.

The parameters of the full and optimal models and the list of experiments to obtain the optimal model are shown in Appendix in Table 4.1 and Table 4.3.

4.4 Discussion

In systems biology, we often face the problem that several models can describe measured data equally well. In such situation one may sometimes choose between a complex model that includes a lot of the details of the underlying mechanisms but is complex, very time consuming, and its parameters are hard to identify, or a reduced version that is much more convenient to handle but might have less predictive power. For the sake of understanding the system, speeding up the computation, and parameter identification, a simpler model is usually more favorable. However, since a simpler model contain less detailed mechanisms,

its predictions might be less reliable. Therefore, model reduction requires a carefull approach.

In this paper, we propose a novel method to develop an optimal model to represent a biochemical system. The method combines a reduction method yielding the simplest model that can describe the measured data and model discrimination assuring that the reduced model has reliable prediction properties. The resulted model is a trade-off between reliability and simplicity. It does not contain redundant components but has enough predictive power to reliable predict the behavior of the system.

When we applied our method to the EGFR network in [23], we found that about 50% of the parameters in the original model can be reduced if one only takes into account the five concentrations that were measured in [23]. Apparently, the dynamical behavior of these five components can be described by a much smaller network. However, the function of the EGFR network is to trigger the activation of Ras protein rather than to maintain some specific behavior of intermediate products. So, from a biological point of view, this is nonsensical. However, from a mathematical point of view, the result indicates that the measured data of intermediate products are not enough to infer the parameters that are related to the Ras pathway. To preserve the Ras pathway in the optimal model, either another target component(s) should be measured or some constraints on the reduction procedure should be incorporated. In this example, we choose the latter one to show the flexibility of our method to incorporate available prior knowledge.

Acknowledgements

This work was carried out within the research programme of the Netherlands Consortium for Systems Biology (NCSB), which is part of the Netherlands Genomics Initiative/Netherlands Organization for Scientific Research.

Bibliography

[1] Roussel MR, Fraser SJ (2001) Invariant manifold methods for metabolic model reduction. Chaos 11: 196–206.

[2] Kooi BW, Poggiale JC, Auger P, Kooijman SALM (2002) Aggregation methods in food chains with nutrient recycling. Ecological Modelling 157: 69 - 86.

[3] Radulescu O, Gorban A, Zinovyev A, Lilienbaum A (2008) Robust simplifications of multiscale biochemical networks. BMC Systems Biology 2: 86.

[4] Surovtsova I, Simus N, Lorenz T, Konig A, Sahle S, et al. (2009) Accessible methods for the dynamic time-scale decomposition of biochemical systems. Bioinformatics 25: 2816-2823.

[5] Turányi T (1990) Sensitivity analysis of complex kinetic systems. tools and applications. Journal of Mathematical Chemistry 5: 203–248.

[6] Tomlin AS, Pilling MJ, Merkin JH, Brindley J (1995) Reduced mechanisms for propane pyrolysis. Ind Eng Chem Res 34: 3749 - 3760.

[7] Smets I, Bernaerts K, Sun J, Marchal K, Vanderleyden J, et al. (2002) Sensitivity function-based model reduction: A bacterial gene expression case study. Biotechnology and Bioengineering 80: 195–200.

[8] Danø S, Madsen MF, Schmidt H, Cedersund G (2006) Reduction of a biochemical model with preservation of its basic dynamic properties. FEBS Journal 273: 4862–4877.

[9] Dokoumetzidis A, Aarons L (2009) Proper lumping in systems biology models. IET Systems Biology 3: 40-51.

[10] Apri M, de Gee M, Molenaar J (2012) Complexity reduction preserving dynamical behavior of biochemical networks. Journal of Theoretical Biology 304: 16 - 26.

[11] Gutenkunst RN, Waterfall JJ, Casey FP, Brown KS, Myers CR, et al. (2007) Universally sloppy parameter sensitivities in systems biology models. PLoS Comput Biol 3: e189.

[12] Kirkpatrick S, Gelatt CD, Vecchi MP (1983) Optimization by simulated annealing. Science 220: 671 - 680.

[13] Srinivas M, Patnaik L (1994) Genetic algorithms: a survey. Computer 27: 17–26.

[14] Mendes P, Kell D (1998) Non-linear optimization of biochemical pathways: applications to metabolic engineering and parameter estimation. Bioinformatics 14: 869–883.

[15] Moles CG, Mendes P, Banga JR (2003) Parameter estimation in biochemical pathways: A comparison of global optimization methods. Genome Research 13: 2467–2474.

[16] Balsa-Canto E, Peifer M, Banga J, Timmer J, Fleck C (2008) Hybrid optimization method with general switching strategy for parameter estimation. BMC Systems Biology 2: 26.

[17] Lillacci G, Khammash M (2010) Parameter estimation and model selection in computational biology. PLoS Comput Biol 6: e1000696.

[18] Walter E, Pronzato L (1997) Identification of parametric models from experimental data. Springer.

[19] Atkinson A (1981) Likelihood ratios, posterior odds and information criteria. Journal of Econometrics 16: 15–20.

[20] Ghosh JK, Samanta T (2001) Model selection an overview. Current Science 80: 1135.

[21] Uciński D, Bogacka B (2005) T-optimum designs for discrimination between two multiresponse dynamic models. Journal of the Royal Statistical Society: Series B (Statistical Methodology) 67: 3–18.

[22] Skanda D, Lebiedz D (2010) An optimal experimental design approach to model discrimination in dynamic biochemical systems. Bioinformatics 26: 939-945.

[23] Kholodenko BN, Demin OV, Moehren G, Hoek JB (1999) Quantification of Short Term Signaling by the Epidermal Growth Factor Receptor. Journal of Biological Chemistry 274: 30169-30181.

[24] Orton RJ, Sturm OE, Vyshemirsky V, Calder M, Gilbert DR, et al. (2005) Computational modelling of the receptor-tyrosine-kinase-activated MAPK pathway. Biochem J 392: 249-261.

Appendix

Table 4.1: Parameter values of the full and optimal models in the last iteration. Here the average deviation at each point between the optimal and the full model is less than 25%. Model 1 refers to EGFR model without constraint to prevent the pathway to Ras protein whereas Model 2 refers to EGFR model with the constraint.

Parameter	Model 1		Model 2	
	$\mathbf{k}_f^6$	$\mathbf{k}_r^6$	$\mathbf{k}_f^7$	$\mathbf{k}_r^7$
k_1	3.1×10^{-3}	2.8×10^{-3}	3×10^{-3}	2.7×10^{-3}
k_{-1}	5.77×10^{-2}	5.31×10^{-2}	5.84×10^{-2}	5.09×10^{-2}
k_2	9.5×10^{-3}	9.9×10^{-3}	9.6×10^{-3}	9.8×10^{-3}
k_{-2}	0.1336	9.24×10^{-2}	8.22×10^{-2}	0.1087
k_3	1.0679	0.79	0.9481	1.0264
k_{-3}	0.0194	0	0.016	0
V_4	450.0001	477.8907	440.9235	437.1619
K_4	49.9990	48.2002	51.0252	46.1166
k_5	6.57×10^{-2}	5.95×10^{-2}	6.4×10^{-2}	5.1×10^{-2}
k_{-5}	0.1917	0	0.3116	0
k_6	0.9992	1.0237	0.9264	0.8975
k_{-6}	4.41×10^{-2}	0	4.04×10^{-2}	0
k_7	0.3079	0.2803	0.3053	0.2852
k_{-7}	4×10^{-3}	7.4×10^{-3}	5×10^{-3}	4.6×10^{-3}
V_8	0.9894	0	0.7757	0
K_8	100	112.7967	101.4729	97.2425
k_9	4.2×10^{-3}	4.4×10^{-3}	2.8×10^{-3}	2.7×10^{-3}
k_{-9}	7.95×10^{-2}	4.03×10^{-2}	4.45×10^{-2}	3.19×10^{-2}
k_{10}	5.8×10^{-3}	0	4.9×10^{-3}	0
k_{-10}	5.26×10^{-2}	0	4.05×10^{-2}	0
k_{11}	7.68×10^{-2}	0	9.18×10^{-2}	0
k_{-11}	1.66×10^{-2}	0	1.64×10^{-2}	0
k_{12}	1.73×10^{-2}	0	7.5×10^{-3}	0
k_{-12}	1.073×10^{-4}	0	5.07×10^{-5}	0
k_{13}	9.48×10^{-2}	0.1036	8.49×10^{-2}	8.39×10^{-2}
k_{-13}	0.6009	0	0.6059	0
k_{14}	5.9984	1×10^4	5.3676	1×10^4
k_{-14}	5.63×10^{-2}	0	9.71×10^{-2}	0
k_{15}	0.3346	0.2904	0.3024	0.2903
k_{-15}	1×10^{-3}	2.6×10^{-3}	1.6×10^{-3}	1.1×10^{-3}
K_{16}	1.6962	1.9833	1.7624	1.6462
V_{16}	340	330.3266	324.2768	327.9718
k_{17}	2.9×10^{-3}	2.8×10^{-3}	3.4×10^{-3}	2.7×10^{-3}
k_{-17}	0.1043	0	8.53×10^{-2}	0

Continued on next page

Table 4.1 – *Continued from previous page*

Parameter	Model 1		Model 2	
	$\mathbf{k}_f^6$	$\mathbf{k}_r^6$	$\mathbf{k}_f^7$	$\mathbf{k}_r^7$
k_{18}	0.2973	0.2272	0.2962	0.2016
k_{-18}	4×10^{-4}	1.6×10^{-3}	2.54×10^{-5}	0
k_{19}	1.83×10^{-2}	0	1.65×10^{-2}	0
k_{-19}	2.25×10^{-2}	0	0.1027	0
k_{20}	0.1235	0	0.1159	0.1928
k_{-20}	8.496×10^{-4}	0	2.596×10^{-4}	6.813×10^{-4}
k_{21}	2.7×10^{-3}	3.1×10^{-3}	2.8×10^{-3}	2.4×10^{-3}
k_{-21}	9.84×10^{-2}	3.54×10^{-2}	9.72×10^{-2}	7.51×10^{-2}
k_{22}	2.95×10^{-2}	0	7.48×10^{-2}	9.6×10^{-3}
k_{-22}	5.35×10^{-2}	0	1.38×10^{-2}	0.1298
k_{23}	9.66×10^{-2}	0	0.1307	0
k_{-23}	2.99×10^{-2}	0	4.13×10^{-2}	0
k_{24}	1.24×10^{-2}	0	1.41×10^{-2}	0
k_{-24}	4.86×10^{-2}	0	8.14×10^{-2}	0
k_{25}	1.0068	1.1123	0.9916	1.0597
k_{-25}	3.36×10^{-2}	3.41×10^{-2}	3.12×10^{-2}	3.43×10^{-2}

Table 4.2: List of experiments to obtain optimal model in Model 1.

Experiment index	Experimental condition ($\mathbf{e}$)			
	$EGF_{stimulation}$ (nM)	$EGFR_0$ (nM)	Shc_0 (nM)	$Grb2_0$ (nM)
1a	20	100	150	85
1b	2	100	150	85
2	15.3824	141	340	0
3	0.0746	2.5771	156.2478	10.4315
4	6.5245	26.4265	0.7839	0.5163
5	0.0118	400	6.2924	150
6	19.9934	399.9985	0.0506	150

Table 4.3: List of experiments to obtain optimal model in Model 2.

Experiment index	Experimental condition ($\mathbf{e}$)			
	$EGF_{stimulation}$ (nM)	$EGFR_0$ (nM)	Shc_0 (nM)	$Grb2_0$ (nM)
1a	20	100	150	85
1b	2	100	150	85
2	20	400	340	0
3	0.0653	2.1885	0	11.3049
4	0.0936	3.1826	340	150
5	20	0.4287	107.2116	149.9955
6	20	400	0.7385	0.8746
7	20	239.0186	0.1460	149.9980

Chapter 5

Modeling cell division and endoreplication in tomato fruit pericarp[1]

Abstract

In developing plant tissues and organs, cell growth sometimes shows a switch from the classical cell cycle into an alternative partial cycle. This partial cycle bypasses mitosis and allows for multiple rounds of genome duplication without cell division, giving rise to cells with high ploidy numbers. Several functional roles have been (putatively) assigned to this process of endoreduplication, as well as various mechanisms that could be responsible for the transition. However, it remains unclear to what extent the proposed roles and mechanisms of endoreduplication are universally applicable to different plant organs. Many studies and modelling efforts have focused on the development of polyploidy in trichomes or root meristems of the model organism Arabidopsis thaliana. However, due to the tight connection between endoreduplication and cell expansion and the prevalence of polyploidy in storage tissues, e.g., endosperm, a functional correlation with crop yield has regularly been implicated. In this paper, we assess the applicability of putative mechanisms for the onset of endoreduplication in tomato pericarp cells via development of a mathematical model for the cell cycle gene regulatory network. We focus on targets for regulation of the transition to endoreduplication by the phytohormone auxin, which is known to play a vital role in the onset of cell expansion in developing tomato fruit. We show that several putative mechanisms are capable of inducing the onset of endoreduplication. In nature, all these routes to endoreduplication are probably used in a combined fashion, which contributes to robustness of the regulation of the transition to endoreduplication.

[1] Based on: M. Apri, J. Kromdijk, P.H.B. de Visser, M. de Gee, J. Molenaar – *"Modeling cell division and endoreplication in tomato fruit pericarp,"* to be submitted

5.1 Introduction

Tomato (*Solanum lycopersicum*) is one of the most important vegetable crops worldwide and the recent publication of the tomato genomic sequence has enormously increased our knowledge at the genetic level [1]. To use this improved genetic understanding in explaining phenotypic behaviour, functional links need to be established between different knowledge fields. In this paper we provide a first step in order to better understand the processes and interactions that underlie the formation of tomato fruits. To that end we combine the findings of Arabidopsis and tomato research as for hormonal regulation of cell division and endoreduplication into a mechanistic model.

In most fleshly fruits, growth starts with intense cell division, which after the first weeks gradually declines and is replaced by cell enlargement [2]. During this period individual cells accumulate water and carbon resulting in spectacular increase in cell volume (more than 10,000-fold in tomato mesocarp cells) and fruit volume [3]. In many fleshly fruits, as in maize endosperm and Arabidopsis trichomes, this huge cell expansion is accompanied by an increase in ploidy through the process of endoreduplication, i.e., an incomplete cell cycle where cells continue to replicate their DNA without mitosis [4]. The endoreduplication cycle is a developmental, by default irreversible process, which in tomato pericarp tissue results in differentiating parenchyma cells.

Mechanistic models describing cell division have been available for some time, providing a relatively simple system of ordinary differential equations (ODEs) to describe the behaviour and interactions of a number of prominent cell cycle regulators, among which the so-called "Cyclin Dependent Kinase" (CDK) proteins play a leading part [5, 6]. Recently, these models have been extended to account for endoreduplication following proliferation in Arabidopsis trichomes [7]. This extended model adopts a valuable mechanism on SIM (a plant-specific class of CDK inhibitor) accumulation, that inhibits CDK activity to explain the transition to endoreduplication. However, recent findings on E2F transcription factors, the CDK inhibition by KIP-related proteins (KRP), and the involvement of auxin regulation in the cell cycle, should be evaluated to obtain a more universal model on division and endoreduplication.

In this work, we develop a mathematical model to describe the underlying mechanisms that govern the tomato growth. The model takes into account the role of auxin as hormonal regulation triggering endoreduplication. We show that, although several mechanisms can successfully block the mitosis and initiate the endoreduplication independently via auxin, the combined action of these mechanisms is necessary to induce the endoreduplication in a robust and efficacious manner.

5.2 Transition from mitotic cell cycles to endoreduplication

The most important events in the cell cycle are the duplication of DNA and the cell division. The duplication, which has to be done in a very precise way, occurs during the S-phase, whereas the cell division, which consists of nuclear division and cytoplasmic division (cytokinesis), occurs during the M-phase. In addition to these two events, two extra gap phases usually exist; the G1 phase in between the M and S phases, and the G2 phase in between

the S and M phases, as depicted in Figure 5.1A. In these gaps, the cell grows and carries out its normal metabolism. Furthermore, they act as check points to monitor the internal and external environments. If the conditions are favourable, the cell cycle progresses to the next phase. Otherwise, the progress is delayed [8].

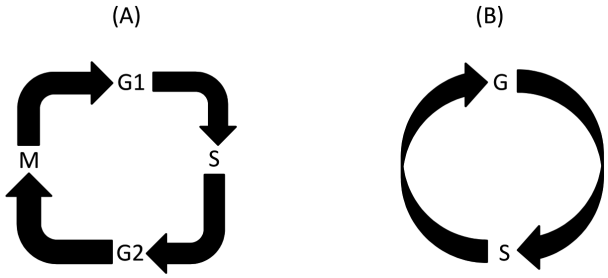

Figure 5.1: Cell cycle in plants. (A) Canonical cell division, consists of G1, S, G2, and M phases. In the S phase, the DNA is replicated whereas in the M phase, the nucleus and the cell divide. (B) Endoreduplication cycle. The phases are similar to that in the canonical cell cycle, except that the M phase is bypassed. Thus, the cell replicates its DNA, but it does not divide.

In some biochemical systems, such as in tomato pericarp and Arabidopsis trichome, the cell cycle may turn into endoreduplication [9]. Then, the cells continue to replicate their DNA, however, without entering mitosis, as depicted in Figure 5.1B. This leads to the increase of ploidy in the cells.

The state of the art of molecular control and functioning of endoreduplication has recently been reviewed in [10] and more specifically for tomato in [11]. In plants, normal G2-M progression is supposed to require significant activity of the 'mitosis promoting factor' (MPF). In plants the MPF is composed of the plant M-phase specific cyclin-dependent kinase CDKB1;1 which is activated by the A-type cyclin CYCA2;3. It controls whether the cell divides mitotically or undergoes repeated rounds of reduplication its DNA without mitosis [12]. Consequently, mechanisms that reduce the activity of the functional complex CDKB1;1/CYCA2;3 should inhibit cytokinesis and promote endoreduplication. Contrary to the M-phase specific CDKB1;1, A-type CDKs (referred to as CDKA) are needed both for G1-S and G2-M transitions. As a consequence, the transition from mitotic to endoreduplicating cycles also depends on factors influencing CDKA activity. In the following paragraphs, we summarise putative mechanisms involved in the onset of endoreduplication.

5.2.1 Proteolytic degradation of M-phase specific cyclins

Specific degradation of M-phase specific cyclins, such as the A-type cyclin CYCA2;3, may occur via the ubiquitin-mediated proteolysis pathway. In this pathway, the E3 ubiquitin ligase anaphase promoting complex / cyclosome (APC/C) selectively labels proteins for destruction (for reviews see [13] or [14]), based on the binding of the APC to the activating proteins CDH1 or CDC20 [15]. It is shown in [12] that CCS52A (the higher plant orthologue of

CDH1) affects the stability of CYCA2;3 in Arabidopsis. A further analysis on the APC activating subunits in tomato in [16] shows that SlCCS52A overexpression in young developing fruits led to significant alterations in cell division and DNA ploidy levels after eight days post-anthesis (dpa). In fruits younger than eight dpa cyclin transcription rates were suggested to be high enough to render the cell cycle progression insensitive to CCS52A expression [9]. It appears that the E2F transcription factor is the one that regulates the CCS52A [17, 18].

E2F is a group of genes that produce a family of transcription factors in higher plants. In Arabidopsis thaliana, the E2F family of transcription factors is composed of six transcription factors (E2F A-F) and two dimerization partners (DP-A and DP-B, [19]). The interplay between E2F transcriptional factor with Retinoblastoma-related protein 1 (RBR1) forms an important regulator of the expression of many prominent cell cycle control genes. Typical E2F factors A, B, and C dimerize with a DP to gain high DNA-binding specificity and can manipulate transcription via a transactivation domain. In contrast, atypical E2F factors D, E, and F (also called [DP-E2F-LIKE] DEL1-3, see [20]) have two DNA-binding domains, and as a result can bind DNA as monomers. Because E2FD-F/DEL1-3 lack the typical transactivation domain, they can inhibit (but not cause) transactivation of E2F responsive elements, by competing for DNA-binding with E2FA and E2FB [19]. In this case, E2FE/DEL1 regulates the CCS52A by repressing its expression [17, 18].

It is shown in [21] that E2FB and E2FC have an opposite regulatory effect on E2FE/DEL1, whereas E2FA (bound to RBR1) has multiple modes of action. The interplay of E2FA and RBR1 directly represses CCS52A and also promotes E2FE/DEL1 expression indirectly, perhaps via the balance of E2FB/E2FC [22].

5.2.2 CDK inhibition

Alternative to cyclin-specific degradation, CDKs can also be subject to inhibition. By blocking the activity of specific CDKs needed for G2-M transition, CDK inhibitors can promote the transition from mitotic to endoreduplicating cycles.

KIP-related proteins (KRP)

The Kip-related proteins (KRP), also called Interactors of CDC2-kinases (ICK) [23], consist of a family of highly redundant CDK-inhibitors [24, 20]. Whereas many studies showed KRPs to generally inhibit CDKA;1 activity, e.g., [24, 25], some family members might also target CDKB [26, 27]. An interesting feature of KRPs is the apparent dose-dependency of their inhibitory action. At low concentrations KRPs inhibit G2-M transition, whereas high concentrations also block G1-S [28, 29]. Consistent with these results, specific overexpression of SlKRP1 during the expansion phase in tomato pericarp (when mitotic activity has already ceased) led to decreased polyploidy [30].

To explain the KRP dose-dependency, in [28] a mechanism is proposed, whereby the inhibitory target of KRP is CDKA;1. At low levels of inhibition, only mitotic CDKA;1 activity would be blocked, whereas more complete inhibition would also prevent CDKA;1 activity in endoreduplicating cycles. Rather than needing two forms of CDKA;1, it is explained in [10] that CDKA;1 could simply be needed at lower concentration for endocycle progression,

being enough for G1-S transition, but not for G2-M to occur. The link between the previously mentioned MPF complex (CDKB1;1/CYCA2;3) and CDKA;1 remains unclear. The interdependency between CDKA;1 and CDKB1;1 was proposed in [28] to occur via phosphorylation of KRPs by CDKB1;1. However, the antagonistic regulation of expression between CDKB (1 and 2) and CDKA1 in tomato pericarp was also shown in [31].

SIAMESE (SIM)/SMR

Another CDK-inhibitor in plants is the SIAMESE (SIM) gene, which was first identified in [32] in Arabidopsis trichomes. SIM and other members of the SIAMESE-related (SMR) family, were subsequently found to target CDKA;1 as well as D-type cyclins [33]. As a result, increased expression of an SMR homolog was postulated to be a central factor controlling endoreplication onset in trichomes, leaves and petals in Arabidopsis [34, 35, 7].

WEE1 kinase

The final CDK inhibitor that we mention in this paper is involved in the commitment to mitosis during the G2 phase. The CDK inhibitor WEE1 kinase mediates the specific inhibition of CDKA via reversible phosphorylation. This inhibition is proposed to govern CDK activity during G2 to ensure that DNA replication and DNA repair have finished before mitosis is entered. Subsequent de-phosphorylation occurs at G2/M progression to allow significant CDK activity during M-phase progression (for a review see [36]). It is shown in [37] that WEE1 kinase activity was not required for normal growth and cell cycle progression in Arabidopsis, but instead regulates cell cycle arrest in response to DNA integrity checkpoints signalling cascades. This seemed to contradict the fact that WEE1 had been shown to be highly expressed in tissues with very high nuclear DNA content like maize endosperm [38] and tomato pericarp [39]. Additionally, it is shown in [11] that downregulating WEE1 in tomato, resulted in increased levels of CDKA and short-cell phenotypes in all examined tissues. It has therefore been proposed that, contrary to the findings for Arabidopsis, in some plant species WEE1 may have a more important role in governing the length of the G2 phase [40, 11].

5.3 Auxin involvement in endoreduplication onset

The regulatory effects of auxin during development of tomato fruit have been known for a long time [41, 42, 43]. In this section, we will briefly summarise involvement of auxin in the control of cell cycle regulators (for reviews see [44, 45, 46]), which provides the rationale behind the selection of candidate parameters in the model analysis of the progression from mitotic to endoreduplication cycles in tomato pericarp cells. In this paper we are specifically focusing on the onset of endo-reduplication. We therefore decided to neglect the role of WEE1 kinase, which has a putative role in sustaining endocycles to obtain high ploidy levels [40], found in tomato pericarp or maize endosperm.

5.3.1 Auxin interactions with E2F

Auxin has many modes of interaction with the expression of E2F transcription factors. Because of the E2F network cross-talk, it is hard to discriminate between direct and indirect influences of the auxin to the E2F transcription factor as the promoter sequences of all E2F members, except E2FA, contain E2F-responsive elements. Here we summarise some of the most prevalent interactions.

It was shown in [47] that the presence of auxin greatly enhances E2FB stability, which promotes G1-S and G2-M transitions. E2FC bound to DP-B is involved in the transition from mitotic cell cycles to endoreduplication cycles, by arresting G1-S transition [48]. E2FC/DP-B appears to be regulated post-transcriptionally by ubiquitin-mediated degradation [49], in which the stability of the targeting complex SCFSKP2A is negatively regulated by auxin [50, 51]. The presence of atypical E2FD/DEL2 also enhances the expression of several genes involved in cell proliferation. The promoter domain of E2FD/DEL2 in Arabidopsis thaliana contains two putative auxin response factors and E2FD/DEL2 was shown to be subject to negative post-transcriptional modification by auxin [52]. These auxin effects on E2FD could also influence expression of other E2F family members as E2FD overexpression lines appeared to have higher expression of E2FA, E2FB, RBR1, and E2FE/DEL1, which was strongly upregulated [52]. However, compared to wild-type, E2FD mutants did not have altered levels of E2FE/DEL1.

To summarise, auxin effects via the E2F family and interaction with RBR1 are integrated in the expression of CCS52A. Interactive effects are difficult to generalize, but by influencing the expression of CCS52A, auxin generally promotes cell proliferation and represses endocycles.

5.3.2 Transcriptional regulation of KRP by auxin

The existence of PROPORZ1 (PRZ1) in *Arabidopsis thaliana* as a mediator of auxin and cytokinin signals in the control of cell proliferation was reported in [53]. It was shown in [54] that PRZ1 in Arabidopsis is needed to modulate histone acetylation in response to auxin by exposing the effects of PRZ1 on transcription on the family of KIP Related Proteins (KRP), thus providing a functional link between auxin and KRP expression. PRZ1 appeared to antagonize the repressive auxin signals in the regulation of KRP expression. In the PRZ1-1 mutant, several KRP genes (as well as E2FC) are misexpressed [53, 54]. Overexpression of KRP genes could in part rescue the PRZ1-1 phenotype and silencing of multiple KRP genes led to hyperproliferation.

5.3.3 Auxin involvement in expression of cyclins or cyclin-dependent kinases

Finally, there is plenty of circumstantial evidence implicating auxin involvement in the expression of cyclins or cyclin-dependent kinases. For example, in [55] a severely reduced expression of CYCA2;1, CYCA2;2, CYCB2;1 and CYCB2;2 was shown in suspensions of A. thaliana cells grown in medium lacking the synthetic auxin α-naphtaleneacetic acid (NAA).

CYCB1;1 expression was induced in Arabidopsis thaliana root cells incubated in indole-3-acetic acid (IAA) [55] and incubation in either IAA or NAA also stimulated expression of CDKA;1 [56]. Furthermore, in [57] reductions in SlCDKB2.1 and SlCyclinB1;1 in transgenic tomato lines with reduced SlARF7 (Auxin Response Factor 7) mRNA content were reported. However, SlARF7 is also implicated in regulatory pathway of gibberellic acid, which makes these results difficult to interpret. It also seems that transcription of several SlCycA genes increases in leaves of tomato seedlings grown on 10 μM IAA [58].

It was also shown in [59] that depletion of auxin (via inhibition by an auxin antagonist) does result in reduction of CYCB1;1 and CYCA2;3 expression as well as increased ploidy levels in nuclei from Arabidopsis thaliana cotyledons and leaves. However, in the context of the previously mentioned alternative influences of auxin on endoreduplication onset, the mechanistic nature of this correlation remains undecided.

5.4 Mathematical Model

In this section, we present a mathematical model to describe the mechanisms underlying the cell cycle in tomato fruit. The model is obtained by adjusting the cell cycle model for Arabidopsis [7], taking into account the auxin hormonal regulation role. Since the link between auxin and SIM in tomato is not yet unraveled, the role of SIM is taken over by KRP in our model, in view of the fact that both SIM and KRP regulate the cell cycle in the same way by inhibiting the CDKs. We assume that KRP inhibits both CDKA and CDKB. Furthermore, we assume that the CDKs are abundantly available and immediately bind to available cyclins. Therefore, auxin is considered to be involved in cyclin expression rather than in CDK expression. Consequently, the dynamics of complex CDK/Cyclin solely depends on the dynamics of the cyclins.

Cyclins are produced by ribosomes in the cytoplasm. In line with the work from [5, 60], we assume that their production rates increase as the cell grows. Once cyclins have been produced, they move into the nucleus which is assumed to have a fix size. The effective activity of cyclins, therefore, increases as the cell grows since their concentration in the nucleus increases. We assume that the production rate of cyclins is proportional to the ratio of cell mass/DNA, whereas the effective concentrations of the other proteins are not influenced by the cell mass. Note that the influence of cell growth is not incorporated in the Arabidopsis model in [7].

5.4.1 Continuous dynamics

As mentioned earlier, cell division in plants is triggered by the activity of MPF, i.e., the dimer CDKB1;1/ CYCA2;3 [12]. In eukaryotic and arabidopsis cells, the transcription factor of CYCA2;3 is activated through MPF [6, 7]. Inspired by the known mechanisms in Arabidopsis, we assume the dynamics of this transcription factor to be governed by the ODE

$$\frac{dTFA_{23}}{dt} = (k_{21p} + k_{21} \cdot MPF) \cdot \frac{(1 - TFA_{23})}{(J_{afb} + 1 - TFA_{23})} - k_{22} \cdot \frac{TFA_{23}}{(J_{ifb} + TFA_{23})}, \quad (5.1)$$

where TFA_{23} and $(1 - TFA_{23})$ are the active and inactive forms of the transcription factor of CYCA2;3 respectively, of which the total amount is assumed to be constant.

The production of cyclins CYCA2;3 is influenced by the auxin level. Cyclin is then degraded by APC/C, which is activated by CCS52A (the ortholog of CDH1) and CDC20. Therefore,

$$\frac{d\,CYCA2;3}{dt} = (k_{1p} + f_{cyca23}(aux) \cdot k_1 \cdot TFA_{23}) \cdot mass - Vdcyca_{23} \cdot CYCA2;3 \quad (5.2)$$

where $f_{cyca23}(aux)$ is a function representing the interaction between auxin and CYCA2;3 production and $Vdcyca_{23}$ is given by

$$Vdcyca_{23} = k_{2p} + k_{2pp} \cdot CCS52A + k_{2ppp} \cdot CDC20_A. \quad (5.3)$$

Here $CDC20_A$ denotes the active form of CDC20.

The molecular mechanisms of Ste9 and Slp1, the orthologs of CDH1 and CDC20 in fission yeast [61], are used to describe the dynamics of CCS52A and CDC20. In this work, the dynamics of Ste9 is slightly modified to account the influence of auxin on the CCS52A via E2F. Thus,

$$\frac{d\,IE}{dt} = k_9 \cdot MPF \cdot \frac{(1 - IE)}{(J_9 + 1 - IE)} - k_{10} \cdot \frac{IE}{(J_{10} + IE)} \quad (5.4)$$

$$\frac{d\,CDC20_A}{dt} = k_7 \cdot IE \cdot \frac{(1 - CDC20_A)}{(J_7 + 1 - CDC20_A)} - k_8 \cdot \frac{CDC20_A}{(J_8 + CDC20_A)} \quad (5.5)$$

$$\frac{d\,CCS52A}{dt} = (f_{E2F}(aux) \cdot k_{3p} + k_{3pp} \cdot CDC20_A) \cdot \frac{(1 - CCS52A)}{(J_3 + 1 - CCS52A)} \quad (5.6)$$

$$-(k_{4p} \cdot SPF + k_4 \cdot MPF) \cdot \frac{CCS52A}{(J_4 + CCS52A)}. \quad (5.7)$$

where IE and $(1 - IE)$ are the active and inactive forms of a hypothetical intermediary enzyme that is included in the model to create a delay between the rise of MPF and CDC20, and $f_{E2F}(aux)$ is a function that models the interaction between auxin and CCS52A via E2F activity.

Once CYCA2;3 is produced, it immediately binds to CDKB1;1 to form MPF. Since CDKs (and hence also CDKB1;1) are assumed to be abundantly available, the dynamics of MPF depends on the dynamics of CYCA2;3 and the inhibition activity due to KRP. The latter leads to the formation of trimer TrimMPF which is the inactive form of the MPF. Thus,

$$\frac{d\,MPF}{dt} = (k_{1p} + f_{cyca23}(aux) \cdot k_1 \cdot TFA_{23}) \cdot mass + (lm + Vdkrp) \cdot Trim_{MPF}$$
$$-(lp \cdot freeKRP + Vdcyca_{23}) \cdot MPF \quad (5.8)$$

$$\frac{d\,Trim_{MPF}}{dt} = lp \cdot freeKRP \cdot MPF - (lm + Vdcyca_{23} + Vdkrp) \cdot Trim_{MPF} \quad (5.9)$$

where

$$freeKRP = KRP - Trim_{MPF} - Trim_{SPF} \quad (5.10)$$

denotes the KRPs that neither inhibit MPF nor SPF (the complex protein that governs G1/S phases).

The dynamics of KRP is described by

$$\frac{dKRP}{dt} = f_{PRZ1}(aux) \cdot k_{11} - Vdkrp \cdot KRP, \tag{5.11}$$

$$Vdkrp = k_{12} + k_{12p} \cdot SPF + k_{12pp} \cdot MPF, \tag{5.12}$$

where $f_{PRZ1}(aux)$ denotes a function representing the interaction between auxin and KRP mediated by PRZ1.

In addition to MPF, there is also another complex that plays an important role for the progression through the S-phase, which is governed by the A-type CDKs. We refer to such a complex as the "S-phase Promoting Factor" (SPF).

$$\frac{dTF}{dt} = k_{15p} \cdot \frac{(1-TF)}{(J_{15}+1-TF)} - (k_{16p} + k_{16pp} \cdot MPF) \cdot \frac{TF}{(J_{16}+TF)} \tag{5.13}$$

$$\frac{dSPF}{dt} = (k_{13p} + k_{13pp} \cdot TF) \cdot mass + (lcm + Vdkrp) \cdot Trim_{SPF} - (lcp \cdot freeKRP + k_{14p} + k_{14} \cdot CDC20_A) \cdot SPF \tag{5.14}$$

$$\frac{dTrim_{SPF}}{dt} = lcp \cdot freeKRP \cdot SPF - (lcm + Vdkrp + k_{14p} + k_{14} \cdot CDC20_A) \cdot Trim_{SPF} \tag{5.15}$$

where TF and $(1-TF)$ are the active and inactive forms of the transcription factor of SPF, respectively, of which the total amount is assumed to be constant. $Trim_{SPF}$ denotes the concentration of SPF that is inhibited by KRP. To complete the model, the mass/DNA is modeled by the linear ODE

$$\frac{dmass}{dt} = \mu \cdot mass \tag{5.16}$$

with $mass(t=0) = mass_0$.

To incorporate the relative effect of the auxin decrease, the functions $f_{cyca23}(aux)$, $f_{E2F}(aux)$ and $f_{PRZ1}(aux)$ representing the interactions between auxin and the cell cycle regulators are described as step functions, with value 1 at the normal (high) auxin level. Thus

$$f_{cyca23}(aux) = \begin{cases} 1 & \text{if auxin is high,} \\ a & \text{if auxin is low,} \end{cases} \tag{5.17}$$

and similarly for f_{E2F} and f_{PRZ1}.

5.4.2 Discrete events

DNA is duplicated when the cell has completed the S-phase. In our model we set this occurrence when the SPF passes a threshold value of 0.25 from above. At that moment the DNA is duplicated, and consequently, the cell mass/DNA is halved. Subsequently, the mass/DNA starts building up again according to (5.16).

A second event is the cell division (cytokinesis) at the end of the M phase. In our model, this event is triggered when MPF passes the threshold value 0.25 from above. At this moment the cell mass itself is halved, but the mass/DNA is continuous, and it keeps growing according to (5.16). Thus, we have two discrete events with two corresponding threshold values; the first is to indicate the DNA duplication which leads to halving of the cell mass/DNA, and the second is to indicate the cytokinesis event.

5.5 Results

The mathematical model described above is simulated for two different conditions: 1) the normal condition where the cell division takes place, and 2) the onset of endoreduplication where the cell skips the mitosis and undergoes polyploidization. For both conditions, all parameter values are the same and given by:

$$k_1 = 0.01, \quad k_{1p} = 0.1, \quad k_{2p} = 0.05, \quad k_{2pp} = 11, \quad k_{2ppp} = 1, \quad k_{3p} = 1, k_{3pp} = 10, \\ k_{4p} = 5, \quad k_4 = 1, \quad J_3 = 0.01, \quad J_4 = 0.01, \quad k_7 = 5, k_8 = 0.32, \; J_7 = 0.01, J_8 = 0.01, \\ k_9 = 0.24, \quad k_{10} = 0.046, \quad J_9 = 0.01, \quad J_{10} = 0.01, \quad k_{11} = 0.1, \; k_{12} = 0.12, k_{12p} = 1, \\ k_{12pp} = 1, \quad lp = 1000, \quad lm = 1, \quad k_{13p} = 0, \quad k_{13pp} = 0.01, \quad k_{14p} = 0.02, \quad k_{14} = 50, \\ k_{15p} = 0.25, \quad k_{15pp} = 0, \quad k_{16p} = 0.01, \quad k_{16pp} = 2, \quad J_{15} = 0.1, \; J_{16} = 0.1, \; k_{21p} = 0, \\ k_{21} = 10, \quad k_{22} = 0.5, \quad J_{afb} = J_{ifb} = 1, \quad lcp = 400, \quad lcm = 1, \mu = 0.01. \tag{5.18}$$

5.5.1 High auxin levels and mitotic cell division

When the auxin level is sufficiently high, the canonical cell cycle with cell division takes place. In our model, this corresponds to

$$f_{cyca23} = f_{E2F} = f_{PRZ1} = 1. \tag{5.19}$$

If the model is simulated with these values, we obtain the dynamics of the components shown in Figure 5.2. Here, the G1 phase is the interval in which CC52A and KRP are very high whereas MPF and SPF are very low. The CCS52A and KRP are then switched off by SPF and MPF so that SPF and MPF start to rise and the cell enters the S phase.

When the cell has completed the S phase, specified when the SPF passes 0.25 from above, the DNA is duplicated. Thus, the mass/DNA which initially increases exponentially becomes halved when the DNA is duplicated, as shown in Figure 5.2C. The cell then enters the G2 phase and not long after that the cytokinesis event takes place. This occurs during the M phase which is indicated when the MPF passes 0.25 from above. At that moment, the cell mass itself is halved. Thereafter, the cell restarts the cycle from G1 phase again.

5.5.2 Low auxin levels and possible routes to endoreduplication

As discussed in Section 5.3, auxin can trigger endoreduplication in the tomato pericarp by influencing the production of CYCA2;3, the activity of CCS52A via E2F, and the dynamics

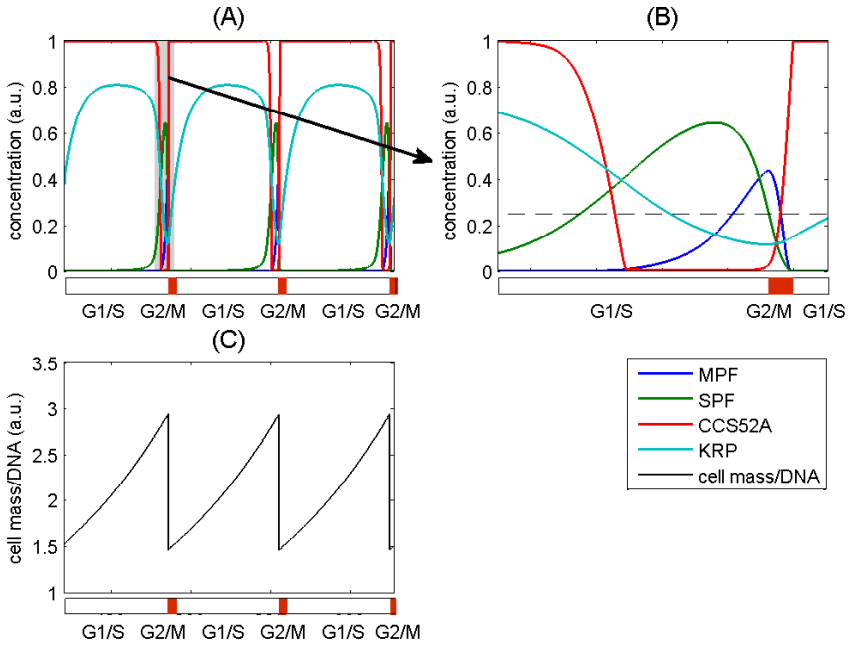

Figure 5.2: The dynamics of the cell cycle. The DNA is duplicated when the SPF passes 0.25 from above, and hence, the cell mass/DNA is halved. The cell undergoes division when the MPF passes 0.25 from above. (A) The overall dynamics, (B) Zoom-in of a part of one cycle of the dynamics, (C) The cell mass/DNA behaviour. The cell mass and the concentration of the components MPF, SPF and KRP are in arbitrary units (a.u.), CCS52A is expressed as an activated fraction.

of KRP via PRZ1. In this work, we focus on the first two mechanisms. Therefore, we set $f_{PRZ1}(aux) = 1$ for any auxin level.

Interaction of Auxin with E2F

As previously discussed, E2FE/DEL1 regulates the cell cycle via CCS52A by repressing the CCS52A expression. The concentration of E2FE/DEL1 is influenced by the auxin activity. When the auxin concentration is low, the repression of CCS52A by E2FE/DEL1 also becomes low. Consequently, the activity of CCS52A increases. Thus, the activity of CCS52A is inhibited by auxin via E2FE/DEL1. This effect is incorporated in $f_{E2F}(aux)$ in our model, for which we take

$$f_{E2F}(aux) = \begin{cases} 1 & \text{if auxin is high,} \\ 2.7 & \text{if auxin is low.} \end{cases} \tag{5.20}$$

If the cell cycle model is simulated with these values, we obtain the results shown in Figure 5.3.

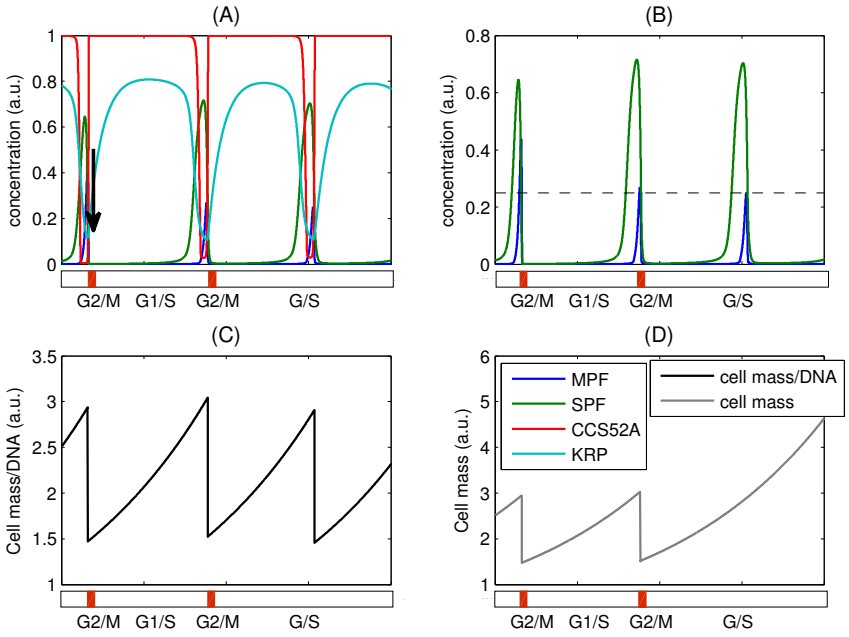

Figure 5.3: The dynamics of the cell cycle and the onset of endoreduplication triggered by the interaction between auxin and the E2F transcription factor. In the tomato pericarp, the endoreduplication occurs after 8 dpa (days post anthesis). In our simulations the decrease of auxin occurs after the first G2/M phase is completed, indicated by the arrow in (A). The effect of this decrease on CCS52A is modeled by increasing $f_{E2F}(aux)$ from 1 to 2.7. Note that the DNA is duplicated when the S phase is completed, which is triggered when the SPF (the green line) passes 0.25 from above. The cell divides when the MPF (the blue line) passes 0.25 from above. Notice in (A) that, when auxin decreases, the minimum level of CCS5A (red line) is slightly higher than in the canonical cycle, indicating the increase of CCS52A activity. This has the effect that in each cycle the concentration of MPF is decreased a bit so that it eventually becomes lower than the threshold value and then the mitosis is skipped. Yet, the cell keeps duplicating the DNA. Since it does not undergo mitosis, the cell mass grows, as can be seen in (D).

In Figure 5.3, initially the auxin level is high. Therefore, the cell undergoes mitosis whenever MPF passes 0.25 from above. After several cell cycles, we let the auxin concentration drop suddenly. This moment is indicated by the arrow in Figure 5.3A. Then the repression of E2FE/DEL1 to CCS52A becomes low, so that more active CCS52A becomes available in the cell. This condition is described in Figure 5.3A, where the minimum level of the active

CCS52A (red line) is higher compared to the situation with a high auxin level. As a result, the cyclin CYCA2;3 degradation by APC/C becomes more pronounced, even when active CCS52A is at minimum. Hence, the concentration of MPF decreases, as shown in Figure 5.3B.

As can be seen in Figure 5.3B, MPF eventually becomes lower than the threshold value, with as consequence the arrest of mitosis. However, the G/S cycle is preserved, which means that the cell undergoes endoreduplication. In this process, the cell keeps duplicating its DNA without cell division. Since the cell does not divide anymore, the cell mass increases as shown in Figure 5.3D. However, the cell mass/DNA is still halving as shown in Figure 5.3C. The time scale in these plots is in arbitrary unit (a.u.). In the tomato pericarp, endoreduplication occurs after 8 dpa.

Influence of auxin on CYCA23

Cyclins are assumed to be positively regulated by auxin. Therefore, in our model the function $f_{cyca23}(aux)$ becomes smaller when the auxin drops. We represent this via

$$f_{cyca23}(aux) = \begin{cases} 1 & \text{if auxin is high,} \\ 0.3 & \text{if auxin is low.} \end{cases} \tag{5.21}$$

When these values are plugged into the model, we obtain the results shown in Figure 5.4.

We start at a high auxin level so that the cell undergoes mitosis. If at the moment indicated by the black arrow in Figure 5.4A, the auxin level is lowered, the production of cyclins decreases. Consequently, there is less CYCA2;3 available in the nucleus to bind to CDKB1;1, which causes a decreasing concentration of MPF. Its concentration eventually becomes lower than the threshold value for the mitosis, as shown in Figure 5.4B. The dynamics of the components then jumps from the canonical cell cycle to endoreduplication.

The combined effect of auxin on CCS52A and CYCA2;3

In the previous sections we have simulated the separate effects of auxin on the cell cycle via its interactions with CCS52A and cyclin CYCA2;3 production. Each mechanism can lead to a shift from mitotic cytokinesis to endoreduplication.

Here we investigate the combined effect of auxin decrease to CCS52A activity and CYCA2;3 expression on the cell cycle. This is carried out by searching function values for f_{E2F} and f_{cyca23} at low auxin levels that can trigger the shift to endoreduplication. The result is shown in Figure 5.5. The region of function values that can trigger endoreduplication is indicated in gray. This region is obtained by searching for f_{E2F} and f_{cyca23} values for low auxin levels that produce endoreduplication. Referring to the previous chapters, in this context this region is called the "admissible region" or "robustness region". Thus, any function value combination that lies within this region can lead the system to endoreduplication.

As can be noticed from Figure 5.5, the admissible/robustness region is quite large. This allows for more flexibility in the values of $f_{E2F}(aux)$ and $f_{cyca23}(aux)$ at low auxin level that can trigger the system to endoreduplication. For example, we do not need to increase $f_{E2F}(aux)$ exactly to $f_{E2F}(aux) = 2.7$ or to decrease $f_{cyca23}(aux)$ strictly to $f_{cyca23}(aux) =$

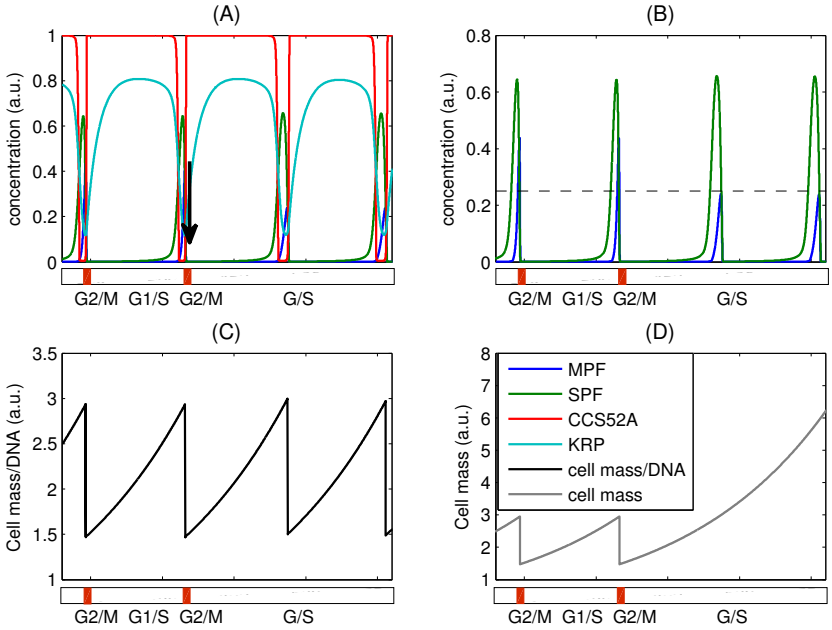

Figure 5.4: The dynamics of the cell cycle and the onset of endoreduplication triggered by the interaction between auxin and CYCA2;3 expression. The timing when auxin decreases is indicated by black arrow. If the effect of the auxin decrease on CYC2;3 is modelled by changing $f_{cyca23}(aux)$ from 1 to 0.3, the MPF becomes lower than the threshold value, consequently the cell skips the mitosis. Thus, it never divides but keeps duplicating the DNA. Since it does not undergo mitosis, the cell mass grows, as can be seen in (D).

0.3 to have endoreduplication. Instead, their values can be more relaxed, e.g., by choosing $f_{cyca23}(aux) = 2.4$ and $f_{cyca23}(aux) = 0.7$. This implies that endoreduplication can occur as a combined effect of a decreased auxin level on the cyclin CYCA2;3, by both decreasing its production rate and by increasing its degradation rate via CCS52A. Indeed, for the values above the MPF decreases after a few cycles below its threshold value, as shown in 5.6. From that moment on, the cell then undergoes endoreduplication.

5.6 Discussion

We have developed a mathematical model to describe the mechanisms that underlie the cell cycle and its transition to endoreduplication in tomato pericarp. The model is an extension and adjustment of an existing model for Arabidopsis. In contrast to the model from [7], the trigger that leads to endoreduplication in our model comes from auxin activity. The effect of auxin is represented in terms of step functions that influence the production, the degradation,

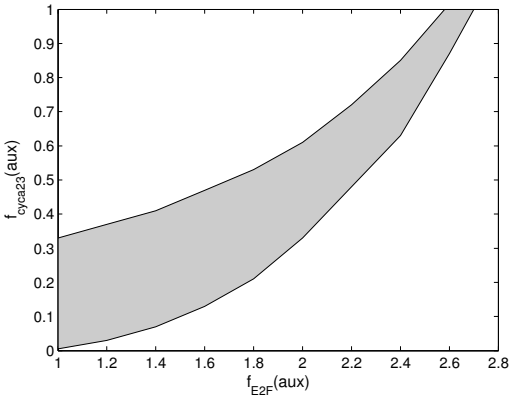

Figure 5.5: Region of the values of f_{E2F} and f_{cyca23} at low auxin levels. These values represent the auxin interaction with the cell cycle regulators. Any point in the gray region leads to endoreduplication when the auxin level in the cell is lowered.

and the inhibition of the cell cycle regulators.

Auxin may trigger both the reduced production of CYCA2;3 and an increased activity of CCS52A. Our results show that each of these mechanisms may cause endoreduplication separately. Further analysis from the region in Figure 5.5 shows that combination of both mechanisms could yield the same effect. This suggests that the mechanisms that may trigger endoreduplication are not necessarily independent. The existence of different routes to endoreduplication assures that the transition is rather robust. If the auxin fails to activate one of the mechanisms, the other mechanism can take over so that the cell cycle can still evolve to endoreduplication.

As has been reported in [28, 29], KRP influences the cell cycle in a manner that is dose-dependent. If it is weakly overexpressed, only the G2/M phases are blocked and hence the cell undergoes endoreduplication. However, if it is strongly overexpressed, the G1/S phases are also blocked. In our model, this dose-dependency is not incorporated. So, there is still room for improvement in the future.

The model that we described above yields the expected dynamical behaviour. However, it is still a qualitative model, in which the parameter values are adjusted from the theoretical knowledge of the Arabidopsis cell cycle. It would, of course, gives us more insight into the underlying mechanisms, when the modelling work would be combined with experimental work so that the parameters could be estimated from tomato data.

It would also be interesting to describe the auxin interaction with the cell cycle regulators dynamically rather than only by step functions. This would give us more insight on the role of auxin in regulating the cell cycle.

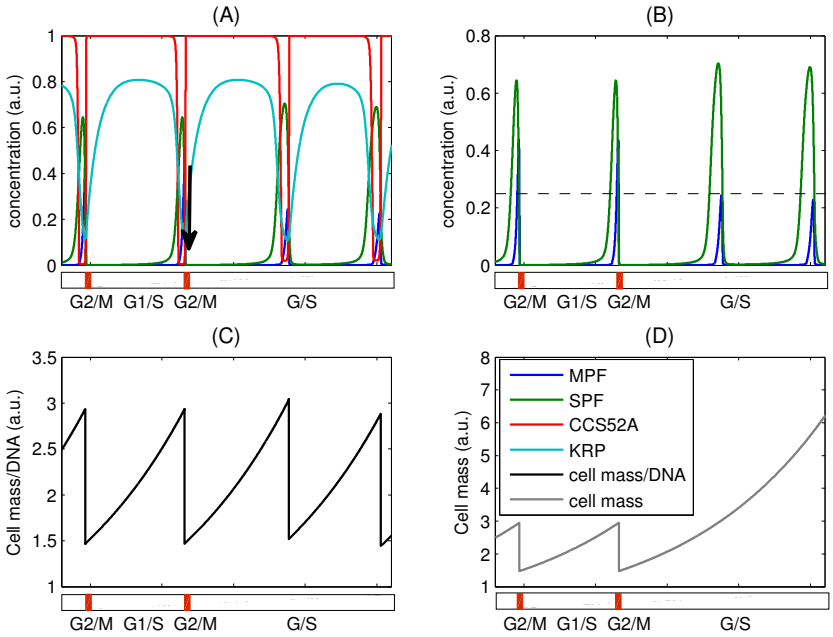

Figure 5.6: Dynamics of the cell cycle and the onset of endoreduplication triggered by auxin interactions with CCS52A via E2F, and CYCA2;3 production. The sudden decrease of auxin at the moment indicated by the black arrow in (A), is modeled by step changes from $f_{E2F}(aux) = 1$ and $f_{cyca23}(aux) = 0.1$ to $f_{E2F}(aux) = 2.4$ and $f_{cyca23}(aux) = 0.7$. Eventually, the MPF becomes lower than the threshold value. Consequently, the cell skips the mitosis and hence no longer divides, but keeps duplicating the DNA. As seen in (C), the halving of the cell mass/DNA continues to happen. Since the cell does not undergo mitosis, the cell mass remains growing, as can be seen in (D).

Acknowledgements

This work was carried out within the research programme of the Netherlands Consortium for Systems Biology (NCSB), which is part of the Netherlands Genomics Initiative/Netherlands Organization for Scientific Research.

Glossary

General abbreviations

CDK	Cyclin dependent kinase
CKI	Cyclin dependent kinase inhibitor
APC/C	Anaphase promoting complex
KRP/ICK	Kip-related protein/Interactor of CDKs, family of CKIs
E2F	Family of transcription factors
DP	Dimerization partner
DEL	Dimerization partner - E2F - like protein, alternative name for a-typical E2F factors
CCS52A	Cell cycle switch protein 52A
RBR1	Rhetinoblastoma-related protein
SIM/SMR	SIAMESE/SIAMESE-related plant-specific family of CKIs
CYC	cyclin, controls the cell cycle progression
SKP	S-phase kinase-associated protein
SCFSKP2A	SKP, Cullin, F-box, SKP2
PROPORZ1	Putative Arabidopsis Transcriptional Adaptor Protein, an Arabidopsis gene, important for the switch from cell proliferation to differentiation in response to the changes of phyto auxin and cytokinin concentrations

Bibliography

[1] Consortium TTG (2012) The tomato genome sequence provides insights into fleshy fruit evolution. Nature 485: 635641.

[2] Gillaspy G, Ben-David H, Gruissem W (1993) Fruits: A developmental perspective. The Plant Cell Online 5: 1439-1451.

[3] Cheniclet C, Rong WY, Causse M, Frangne N, Bolling L, et al. (2005) Cell expansion and endoreduplication show a large genetic variability in pericarp and contribute strongly to tomato fruit growth. Plant Physiology 139: 1984-1994.

[4] Bourdon M, Frangne N, Mathieu-Rivet E, Nafati M, Cheniclet C, et al. (2010) Endoreduplication and growth of fleshy fruits. In: Progress in Botany 71, Springer Berlin Heidelberg, volume 71. pp. 101-132.

[5] Tyson JJ, Novak B (2001) Regulation of the eukaryotic cell cycle: Molecular antagonism, hysteresis, and irreversible transitions. Journal of Theoretical Biology 210: 249 - 263.

[6] Csiksz-Nagy A, Battogtokh D, Chen KC, Novk B, Tyson JJ (2006) Analysis of a generic model of eukaryotic cell-cycle regulation. Biophys J 90: 4361–4379.

[7] Roodbarkelari F, Bramsiepe J, Weinl C, Marquardt S, Novak B, et al. (2010) Cullin 4-ring finger-ligase plays a key role in the control of endoreplication cycles in arabidopsis trichomes. Proceedings of the National Academy of Sciences .

[8] Alberts B, Johnson A, Lewis J, Raff M, Roberts K, et al. (2008) Molecular Biology of The Cell. Garland Science, 5th edition.

[9] Joubès J, Chevalier C (2000) Endoreduplication in higher plants. Plant Molecular Biology 43: 735-745.

[10] De Veylder L, Larkin JC, Schnittger A (2011) Molecular control and function of endoreplication in development and physiology. Trends in Plant Science 16: 624–634.

[11] Chevalier C, Nafati M, Mathieu-Rivet E, Bourdon M, Frangne N, et al. (2011) Elucidating the functional role of endoreduplication in tomato fruit development. Annals of Botany 107: 1159–1169.

[12] Boudolf V, Lammens T, Boruc J, Van Leene J, Van Den Daele H, et al. (2009) CDKB1;1 forms a functional complex with CYCA2;3 to suppress endocycle onset. Plant Physiology 150: 1482–1493.

[13] Capron A, Serralbo O, Flp K, Frugier F, Parmentier Y, et al. (2003) The arabidopsis anaphase-promoting complex or cyclosome: Molecular and genetic characterization of the APC2 subunit. The Plant Cell Online 15: 2370-2382.

[14] Peters JM (2006) The anaphase promoting complex/cyclosome: a machine designed to destroy. Nat Rev Mol Cell Biol 7: 644–656.

[15] Vodermaier HC (2001) Cell cycle: Waiters serving the destruction machinery. Current Biology 11: R834 - R837.

[16] Mathieu-Rivet E, Gévaudant F, Sicard A, Salar S, Do PT, et al. (2010) Functional analysis of the anaphase promoting complex activator CCS52A highlights the crucial role of endo-reduplication for fruit growth in tomato. The Plant Journal 62: 727–741.

[17] Vlieghe K, Boudolf V, Beemster GT, Maes S, Magyar Z, et al. (2005) The DP-E2F-like gene DEL1 controls the endocycle in arabidopsis thaliana. Current Biology 15: 59–63.

[18] Lammens T, Boudolf V, Kheibarshekan L, Panagiotis Zalmas L, Gaamouche T, et al. (2008) Atypical E2F activity restrains APC/CCCS52A2 function obligatory for endocycle onset. Proceedings of the National Academy of Sciences 105: 14721–14726.

[19] Mariconti L, Pellegrini B, Cantoni R, Stevens R, Bergounioux C, et al. (2002) The E2F family of transcription factors from Arabidopsis thaliana. Journal of Biological Chemistry 277: 9911–9919.

[20] Vandepoele K, Raes J, De Veylder L, Rouz P, Rombauts S, et al. (2002) Genome-wide analysis of core cell cycle genes in arabidopsis. The Plant Cell Online 14: 903-916.

[21] Berckmans B, Lammens T, Van Den Daele H, Magyar Z, Bgre L, et al. (2011) Light-dependent regulation of DEL1 is determined by the antagonistic action of E2Fb and E2Fc. Plant Physiology 157: 1440–1451.

[22] Magyar Z, Horvath B, Khan S, Mohammed B, Henriques R, et al. (2012) Arabidopsis E2FA stimulates proliferation and endocycle separately through RBR-bound and RBR-free complexes. EMBO J 31: 1480–1493.

[23] Wang H, Fowke LC, Crosby WL (1997) A plant cyclin-dependent kinase inhibitor gene. Nature 386: 451–452.

[24] De Veylder L, Beeckman T, Beemster GT, Krols L, Terras F, et al. (2001) Functional analysis of cyclin-dependent kinase inhibitors of arabidopsis. The Plant Cell Online 13: 1653–1668.

[25] Zhou Y, Li G, Brandizzi F, Fowke LC, Wang H (2003) The plant cyclin-dependent kinase inhibitor ICK1 has distinct functional domains for *in vivo* kinase inhibition, protein instability and nuclear localization. The Plant Journal 35: 476–489.

[26] Nakai T, Kato K, Shinmyo A, Sekine M (2006) Arabidopsis KRPs have distinct inhibitory activity toward cyclin D2-associated kinases, including plant-specific B-type cyclin-dependent kinase. FEBS Letters 580: 336–340.

[27] Pettkó-Szandtner A, Mészáros T, Horváth GV, Bakó L, Csordás-Tóth E, et al. (2006) Activation of an alfalfa cyclin-dependent kinase inhibitor by calmodulin-like domain protein kinase. The Plant Journal 46: 111–123.

[28] Verkest A, Manes CLdO, Vercruysse S, Maes S, Van Der Schueren E, et al. (2005) The cyclin-dependent kinase inhibitor KRP2 controls the onset of the endoreduplication cycle during arabidopsis leaf development through inhibition of mitotic CDKA;1 kinase complexes. The Plant Cell Online 17: 1723–1736.

[29] Weinl C, Marquardt S, Kuijt SJ, Nowack MK, Jakoby MJ, et al. (2005) Novel functions of plant cyclin-dependent kinase inhibitors, ICK1/KRP1, can act non-cell-autonomously and inhibit entry into mitosis. The Plant Cell Online 17: 1704-1722.

[30] Nafati M, Cheniclet C, Hernould M, Do PT, Fernie AR, et al. (2011) The specific over-expression of a cyclin-dependent kinase inhibitor in tomato fruit mesocarp cells uncouples endoreduplication and cell growth. The Plant Journal 65: 543–556.

[31] Czerednik A, Busscher M, Bielen BA, Wolters-Arts M, de Maagd RA, et al. (2012) Regulation of tomato fruit pericarp development by an interplay between CDKB and CDKA1 cell cycle genes. Journal of Experimental Botany 63: 2605–2617.

[32] Walker J, Oppenheimer D, Concienne J, Larkin J (2000) SIAMESE, a gene controlling the endoreduplication cell cycle in *Arabidopsis thaliana* trichomes. Development 127: 3931–3940.

[33] Churchman ML, Brown ML, Kato N, Kirik V, Hlskamp M, et al. (November 2006) SIAMESE, a plant-specific cell cycle regulator, controls endoreplication onset in arabidopsis thaliana. The Plant Cell Online 18: 3145–3157.

[34] Roeder AHK, Chickarmane V, Cunha A, Obara B, Manjunath BS, et al. (2010) Variability in the control of cell division underlies sepal epidermal patterning in *Arabidopsis thaliana*. PLoS Biol 8: e1000367–.

[35] Kasili R, Walker JD, Simmons LA, Zhou J, De Veylder L, et al. (May 2010) Siamese cooperates with the CDH1-like protein CCS52A1 to establish endoreplication in Arabidopsis thaliana trichomes. Genetics 185: 257–268.

[36] O'Farrell PH (2001) Triggering the all-or-nothing switch into mitosis. Trends in Cell Biology 11: 512–519.

[37] De Schutter K, Joubés J, Cools T, Verkest A, Corellou F, et al. (January 2007) Arabidopsis wee1 kinase controls cell cycle arrest in response to activation of the dna integrity checkpoint. The Plant Cell Online 19: 211–225.

[38] Sun Y, Dilkes BP, Zhang C, Dante RA, Carneiro NP, et al. (1999) Characterization of maize (Zea mays L.) Wee1 and its activity in developing endosperm. Proceedings of the National Academy of Sciences 96: 4180–4185.

[39] Gonzalez N, Hernould M, Delmas F, Gévaudant F, Duffe P, et al. (2004) Molecular characterization of a WEE1 gene homologue in tomato (*Lycopersicon esculentum* mill.). Plant Molecular Biology 56: 849–861.

[40] Gonzalez N, Gévaudant F, Hernould M, Chevalier C, Mouras A (2007) The cell cycle-associated protein kinase WEE1 regulates cell size in relation to endoreduplication in developing tomato fruit. The Plant Journal 51: 642–655.

[41] Crane JC (1964) Growth substances in fruit setting and development. Annual Review Of Plant Physiology 15: 303–&.

[42] Crane JC (1969) The role of hormones in fruit set and development. HortScience 4: 108 - 111.

[43] Nitsch JP (1970) Hormonal factors in growth and development. In: Hulme AC, editor, The biochemistry of fruits and their products, London, UK: Academic Press. p. 427472.

[44] Stals H, Inzé D (2001) When plant cells decide to divide. Trends in Plant Science 6: 359 - 364.

[45] Richard C, Lescot M, Inzé D, De Veylder L (2002-05-01) Effect of auxin, cytokinin, and sucrose on cell cycle gene expression in *Arabidopsis thaliana* cell suspension cultures. Plant Cell, Tissue and Organ Culture 69: 167–176.

[46] Teale WD, Paponov IA, Ditengou F, Palme K (2005) Auxin and the developing root of arabidopsis thaliana. Physiologia Plantarum 123: 130–138.

[47] Magyar Z, De Veylder L, Atanassova A, Bakó L, Inzé D, et al. (September 2005) The role of the arabidopsis E2FB transcription factor in regulating auxin-dependent cell division. The Plant Cell Online 17: 2527–2541.

[48] del Pozo JC, Diaz-Trivino S, Cisneros N, Gutierrez C (September 2006) The balance between cell division and endoreplication depends on E2FC-DPB, transcription factors regulated by the ubiquitin-SCFSKP2A pathway in arabidopsis. The Plant Cell Online 18: 2224–2235.

[49] del Pozo JC, Boniotti MB, Gutierrez C (2002) Arabidopsis E2Fc functions in cell division and is degraded by the ubiquitin-SCFAtSKP2 pathway in response to light. The Plant Cell Online 14: 3057–3071.

[50] Jurado S, Díaz-Triviño S, Abraham Z, Manzano C, Gutierrez C, et al. (2008) SKP2A, an F-box protein that regulates cell division, is degraded via the ubiquitin pathway. The Plant Journal 53: 828–841.

[51] Jurado S, Abraham Z, Manzano C, López-Torrejón G, Pacios LF, et al. (2010) The arabidopsis cell cycle F-Box protein SKP2A binds to auxin. The Plant Cell Online 22: 3891–3904.

[52] Sozzani R, Maggio C, Giordo R, Umana E, Ascencio-Ibaez J, et al. (2010-03-01) The E2FD/DEL2 factor is a component of a regulatory network controlling cell proliferation and development in arabidopsis. Plant Molecular Biology 72: 381–395.

[53] Sieberer T, Hauser MT, Seifert GJ, Luschnig C (2003) PROPORZ1, a putative arabidopsis transcriptional adaptor protein, mediates auxin and cytokinin signals in the control of cell proliferation. Current Biology 13: 837–842.

[54] Anzola JM, Sieberer T, Ortbauer M, Butt H, Korbei B, et al. (2010) Putative arabidopsis transcriptional adaptor protein (PROPORZ1) is required to modulate histone acetylation in response to auxin. Proceedings of the National Academy of Sciences 107: 10308–10313.

[55] Ferreira P, Hemerly A, de Almeida Engler J, Bergounioux C, Burssens S, et al. (1994) Three discrete classes of arabidopsis cyclins are expressed during different intervals of the cell cycle. Proceedings of the National Academy of Sciences 91: 11313–11317.

[56] Hemerly AS, Ferreira P, de Almeida Engler J, Van Montagu M, Engler G, et al. (1993) CDC2A expression in arabidopsis is linked with competence for cell division. The Plant Cell Online 5: 1711-23.

[57] de Jong M, Wolters-Arts M, Garca-Martnez JL, Mariani C, Vriezen WH (2011) The Solanum lycopersicum AUXIN RESPONSE FACTOR 7 (SlARF7) mediates cross-talk between auxin and gibberellin signalling during tomato fruit set and development. Journal of Experimental Botany 62: 617–626.

[58] Guo J, Kwon HK, Wang MH (2010) Characterization of three A-type cyclin genes in tomato (Solanum lycopersicum) treated with auxins. Journal of the Korean Society for Applied Biological Chemistry 53: 266-274–.

[59] Ishida T, Adachi S, Yoshimura M, Shimizu K, Umeda M, et al. (2010) Auxin modulates the transition from the mitotic cycle to the endocycle in arabidopsis. Development 137: 63-71.

[60] Chen K, Calzone L, Csikasz-Nagy A, Cross F, Novak B, et al. (2004) Integrative analysis of cell cycle control in budding yeast. Mol Biol Cell 15: 3841-3862.

[61] Novak B, Pataki Z, Ciliberto A, Tyson JJ (2001) Mathematical model of the cell division cycle of fission yeast. Chaos 11: 277–286.

Chapter 6

General discussion

6.1 Scope of this thesis

Biological functions that appear to be fundamental in nature nearly always come into existence as emergent properties, i.e., they are only present when the components are in full interaction and disappear if one decouples the different modules. The study of biological systems, therefore, will only be really successful if it is carried out at the systems level. This insight has led to the introduction of the term systems biology. Understanding biological systems at the systems level, however, turn out to be very difficult due to the complex interactions between the components in time and space. This complexity stems both from the large number of components involved and from the intricate interactions between these components. When the system is described by a mathematical model, we frequently end up with a large nonlinear set of mathematical equations that contains many parameters. Such a large model usually has a number of undesirable properties, e.g., its dynamical behavior is hard to understand, its parameters are difficult to identify, and its simulation requires very long computing times. In this thesis, we present several strategies that may help to overcome these problems. On the level of method development, we focus on two issues: a) method development to analyze robustness, b) method development to reduce model complexity. On the level of practical systems biology, we develop and analyse a model for the cell cycle in tomato fruit pericarp.

A fundamental issue in modeling biological processes is robustness. Robustness is the ability of a system to preserve biological functionality in spite of internal and external perturbations. It is an essential feature of biological systems and any mathematical model that describes such a system should reflect this property. This implies the needs of a mathematical method to evaluate the robustness of mathematical models for biological processes. Unfortunately, assessing robustness of a complex non-linear model that contains many parameters is not straightforward. In this thesis, we have presented a method to evaluate the robustness of mathematical models efficiently. It enables us to find which parameter combinations in a model are responsible for its robustness. In this way, we get more insight into the underlying mechanisms that govern the dynamics of the biological system. The advantage of our

method is that the effort to apply the method scales linearly with the number of parameters. It is therefore very efficient when it is applied to mathematical models that contain a large number of parameters.

The complexity of a model can be brought down by simplifying the model. In this thesis, we have developed a novel reduction method to simplify mathematical representations of biological models. In this method, biological components and parameters that do not contribute to the observed dynamics are considered redundant and hence are removed. This results in a simpler model with less components and parameters, without losing predictive capabilities for any testable experimental condition. Since the reduced model contains less parameters, parameter identification can be carried out more efficaciously.

In the last part of this thesis we showed how modeling can help us in understanding the cell cycle in tomato fruit pericarp. The cell cycle in this system is quite special since it starts as a classical cell cycle, in which cell division takes place, but after some periods it turns into a partial cycle where the cell keeps replicating its DNA but skips the division. Several mechanisms that are putatively responsible for this transition have been proposed. With modeling, we show that although each of these putative mechanisms on its own can lead the cell cycle to this transition, also their combination could lead to the same result. We also found that this transition occurs in a robust manner.

In the rest of this chapter, the results of the previous chapters are discussed and elaborated further.

6.2 Reflection on the thesis results

6.2.1 Robustness analysis

As robustness is one of the essential features of biological systems, it has attracted much attention in systems biology, see, e.g., [1, 2]. Robustness is defined as a property that allows a system to preserve its functions against internal and external perturbations [3]. This definition implies that robustness concerns the conservation of system functionality rather than of system states, and therefore it is different from stability. For example, if it is necessary that the state of a system switches from a steady state into oscillating behavior in order to survive a change in the external temperature, then the biological system is called robust to the change of temperature. However, robustness and stability can be identical, namely when the function of the system is to maintain the stability of system states.

In Chapter 2, we presented a method to estimate the robustness of biological systems. Here, we focus on the capability of the system to produce stable oscillatory behavior under parametric perturbations. The robustness of a model is then determined by answering the question how far the parameters of the model could be perturbed so that the qualitative behavior of the system does not change. An example of such a change is, e.g., the transition from oscillatory behavior to a steady state equilibrium. Therefore, robustness in this chapter is highly connected to the concept of bifurcation in mathematics. Instead of using the classical eigenvalue approach to determine the behavioral changes, in this method we utilize Floquet theory to detect the bifurcations. One of the central issues here is handling the multi-

parameters difficulty. In most of the work that is available in the literature, the robustness of the model is quantified by perturbing all parameters with the same percentage, tacitly assuming that all parameters have the same robustness sensitivity. This leads to a symmetric robustness region, which is not very useful when in reality the model is more sensitive to some parameters than to the others. Instead of presenting the robustness of the model by one value, here we aim at estimating the whole robustness region, taking into account the parameter-dependent sensitivity. Starting from a nominal parameter set, we construct an estimate for the robustness region by scanning the parameter space in orthogonal directions. If necessary, the obtained estimate is refined by shifting the nominal point to a carefully chosen new position. This gives a robustness region that in general is far from symmetric. We note that the computing time necessary to find this estimated robustness region scales linearly with the number of parameters involved. In this respect our method compares favorably with, e.g., Monte-Carlo simulations, for which the computing time scales exponentially with the dimension, and hence faces the so-called "dimensional curse" problem. Therefore our method is really efficient to investigate robustness of a model that has a high number of parameters.

Oscillation is a ubiquitous phenomenon in biological systems. For example, consider the bovine estrous cycle that controls the cow's fertility. This cycle was modeled in [4] with a system of 15 differential equations containing 60 parameters. It simulates the follicle and corpus luteum development and the periodic changes in hormone level. In this system, however, robustness is defined differently. The functioning of this system is not to maintain the stability of periodic oscillations, but rather to preserve the characteristics of the oscillations of some biological components. In this system, a cycle is considered normal when the luteal phase length ranges from 9 to 19 days and the inter-luteal phase length is less than 12 days. Luteal phase is a term that is used to describe the time period calculated from the day after ovulation until the remainder of the cycle. If the luteal phase length is more than 19 days, the cycle experiences the so-called 'delayed luteolysis', whereas if the inter-luteal phase lengthe more than 12 days, the cycle experiences 'delayed ovulation'. Both conditions may indicate infertility. Robustness in the estrous cycle is thus violated whenever the cycle shows either delayed luteolysis or delayed ovulation. Although the definition of robustness in this system is different from the one that we discussed in Chapter 2, the general idea to investigate the multi-parameter robustness region is the same. Therefore, the method that is presented in Chapter 2 was adjusted to estimate the robustness region in this model. In this way we were able to find parameter configurations that can lead to infertility in cows. This work is not included in the thesis but published in [5].

6.2.2 Complexity reduction

One way out to overcome the complexity of a mathematical model for a large biological system is by simplifying it through model reduction. Model reduction can be carried out in several ways, and the choice for the most appropriate approach depends on the purpose that one has in mind. For example, one could dissect a biological network into several sub-networks or modules that are independent from each other. In this way, the biological network is more manageable, easier to analyze, and the sub-networks can be studied independently. Or, one could choose to restrict the system to components and reactions that are relevant

for the functions of interest. This can be achieved through time-scale separation, sensitivity analysis, or a lumping approach. Despite their power, these methods suffer from some weaknesses. Time-scale separation and lumping, for example, typically require transformation of the original system of equations into another system before the reduction can take place. This transformation hinders us in understanding the reduced model. Furthermore, these methods, including sensitivity analysis, require prior knowledge on the true parameter values of the model before they can be applied; otherwise, the reduction results are not reliable. Therefore, parameter identification, which is often the most problematic issue in systems biology, remains the bottle neck.

The reduction method that we presented in Chapter 3 utilizes the concept of the so-called "admissible region", that is a region in parameter space where the model outcomes match the observed data within some given tolerance. Here, a parameter is considered redundant when it can be set to zero or to infinity whereas the others can be re-optimized such that the model outcomes are still in a good agreement with the dataset. In contrast to the methods that we mentioned above, our method does not require a transformation, thus the biological interpretation on the reduction result is straightforward. Furthermore, it does not need prior knowledge on the true parameter values; yet, the model becomes smaller and has less parameters. From an identification point of view, the parameters that can be removed are those that are badly identified, since the available data can still be fitted without their presence in the model. Indeed, it is the power of our method that it can be applied to a model for which its parameters have not yet been identified. In this way, our approach results in a model in which the parameters are more identifiable. Conversely, our method is not applicable if all the parameters in the model are well-identified.

When we have reduced a model, we could consider the question, whether the remaining model can replace the full/complex model. To answer this question, we must first define what requirements a reduced model has to fulfil in order to replace the full model. In my opinion, there are at least two conditions that have to be satisfied. First, the reduced model should be able to fit the observed data quite well; and second, the reduced model should have the same ability as the full model to reliably predict the behavior of the system for any testable experimental condition. The method that we presented in Chapter 3 only assures the first requirement. To satisfy the last requirement, in Chapter 4 the reduction method is extended by combining it with a model discrimination method. The discrimination method is commonly used to choose the most appropriate model among many alternatives to represent biological systems. Here it is used to find whether there exists an experimental condition that can distinguish the reduced model from the full model. The most significant experimental condition is the one that maximizes the distance between the output of the reduced model and that of the full model. If there is such kind of condition, a new experiment based on the setting that is found by model discrimination is carried out, and the new observed data is combined with the previous data and the reduction is re-performed. Otherwise, we may be confident that the reduced model has powerful prediction capabilities. The model discrimination in our method can also be viewed as a way to verify or falsify whether the omitted components, reactions, and/or parameters in the reduced model give a meaningful contribution to the model prediction. If they do, the dataset from the new experiment will confirm this so that in the next reduction, the method cannot remove the corresponding components and/or parameters.

As already mentioned above, identifying parameters in systems biology models with a high accuracy is often very difficult. As a result, most parameters will have large uncertainties, which is related to " parameter sloppiness" [6]. In spite of this, surprisingly, Gutenkunst et.al. find that the large uncertainty in the parameters does not always correlate to a large discrepancy in the model prediction. In contrast, the uncertainty in model predictions could be already tight and this occurs for all the models they examined. Therefore, to obtain a useful model, they suggest to focus on model prediction rather than on parameter identification. The method that we presented in Chapter 4 shares the same spirit. Our approach is based on minimizing the discrepancy between the model prediction from the reduced model and that of the full model. The remaining parameters in the reduced model might still have large uncertainties, but the correspondence between the model prediction from the reduced model and that of the full model is very good. If required, additional parameter identification could be carried out on the remaining parameters in the reduced model. Since the reduced model contains less parameters, parameter identification can be carried out more efficaciously.

The more informative the dataset incorporated in the reduction is, the more reliable the prediction of the reduced model is. By applying reduction, we arrive at a simple but powerful model. It is important to realize, however, that typically only a limited number of components can be observed in experiments and only several factors in experiments can be changed. At the end, it is always crucial to keep in mind which functionality we want to preserve in the reduced model. Otherwise, we will arrive at a reduced model that does not serve our purposes.

6.2.3 Understanding of the cell cycle in tomato fruit pericarp

In the last part of this thesis, i.e., Chapter 5, we have developed a mathematical model to describe the cell cycle process in tomato fruit pericarp. In this system, the cell undergoes a complete cell cycle for several rounds including cell division, and then it jumps to a partial cell cycle where the division no longer occurs. This partial cycle is known as *endoreduplication*. Several putative mechanisms that might trigger endoreduplication have been proposed. To understand better the underlying mechanisms, we develop and analyze a mechanistic model in which the interactions between the cell cycle regulators, such as 'Cyclin Dependent Kinase (CDK)', SIM (a plant-specific class of CDK inhibitor), and the CDK inhibitor KRP, are described using differential equations. The model is based on the cell cycle model of Arabidopsis trichomes [7], however, it is adapted for tomato. For example, in the Arabidopsis model, the cyclin production does not depend on cell mass whereas in our model it does. This is necessary to ensure that the cyclin production increases as the cell grows. Furthermore, in our model, the auxin hormonal regulation is taken into account acting as a trigger for endoreduplication. Since the connection between auxin and SIM in tomato is not yet unraveled, the role of SIM in inhibiting the CDK is taken over by KRP in our model.

The involvement of cell mass in cyclin production makes our model similar to the models from Novak and Tyson, see e.g., [8, 9, 10]. However, they propose that the cell mass influences the cyclin production rather than the ratio of cell mass and DNA denoted as cell mass/DNA. As our model is designed to represent both the regular mitotic cycle and the endoreduplication cycle, we make use of two discrete events; the first is halving of the cell mass/DNA, which occurs when the cell has accomplished the S phase, and the second is halv-

ing of the cell mass, which corresponds to cell division. Therefore, we employ two threshold values. The first is for SPF (S-phase Promoting Factor) to trigger the duplication of DNA and the second one is for MPF (M-phase Promoting Factor) to trigger cell division. In contrast, the models from Novak and Tyson have only one discrete event, namely halving of the cell mass. Accordingly, they only have one threshold value, which is assigned to MPF to specify cell division.

The role of putative mechanisms due to the interaction between auxin and cyclin production, and auxin and CCS52A actvitivy were investigated. We found that each of them could on its own lead to the transition from classical cell cycle to endoreduplication. However, their combinations could also lead to the same result. When we investigated the function values that represent the interaction between auxin and cyclin production, and auxin and CCS52A, we found that in parameter space these values may vary over quite a large region. In terms of robustness that we discussed above, this large region reflects the insensitivity of the transition to endoreduplication with respect to the variation of auxin effects on cyclin production and CCS52A activity. We conclude that cell cycle in tomato undergoes the transition to endoreduplication in a robust manner. This conclusion, however, need confirmation from experimental work.

The model that we developed is a qualitative model. Our main concern was to build in the transition from the classical cell cycle to endoreduplication. Therefore, the role of other proteins that do not play a role in that transition, e.g., Wee1 that governs the length of the G2 phase, is not incorporated. By not incorporating the non-essential components for the functioning that we are interested in, we consciously applied model simplification.

6.3 Future research

In this thesis, we have developed methodologies that are expected to overcome some difficulties arising from complexity in systems biology. We realize that there is still a huge number of problems that have to be solved to obtain a better understanding of biological systems. Here we discuss several possibilities how our work could be extended to solve some of these.

When we model biological processes, we might have incomplete information about the system and this leads to an incomplete model [11]. The incompleteness of the model can lie for example in still unknown reactions in a biochemical network. The method that we presented in Chapter 4, might be extended to solve the problem of incompleteness. This can be done, e.g., by re-describing the model so that each node in the network influences all nodes. The new model obtained in this way is called the full model: it contains all possible reactions between all the nodes. A model reduction and model discrimination are then carried out to the full model to find out which reactions should be preserved to represent the dataset. However, this technique is certainly not efficient since the number of reactions and parameters in the full model will increase dramatically. Moreover, each reaction can regulate the node in positive or negative ways. Finding an efficient extension to handle this problem, could therefore, be a future research topic.

The multi-parameter method to estimate robustness regions in Chapter 2 could also be extended to systems that have biological functions other than maintaining stable oscillation.

In this case, it is important to realize that robustness is not always related to bifurcations in the classical sense. Examples of this extension are found in the bovine estrous cycle and in the endoreduplication transition in tomato fruit that we discussed above. In the near future, the robustness of the endoreduplication transition will be investigated further by taking into account other putative mechanisms.

For tomato cell cycle, the role of KRP in triggering endoreduplication still has to be investigated. KRP is a protein that inhibits CDK and hence, MPF. KRP is negatively regulated by auxin, so when the auxin level drops, more KRPs become available in the cell. The more KRPs are available in the nucleus, the lower the MPF concentration will be. When the MPF concentration is not high enough, the mitosis will be blocked and hence the cell will go into endoreduplication. Most likely, this mechanism also contributes to the robustness transition to endoreduplication. Interestingly, however, when there are too much KRPs in the cell, not only the mitosis will be blocked, but also the DNA replication. This KRP dose-dependent mechanisms should be incorporated to improve the current model in Chapter 5.

The current tomato cell cycle model in Chapter 5 is still a qualitative model. The parameters are adjusted from the model in Arabidopsis. To really reflect the behavior of the system, more quantitative data should be obtained from experimental work and parameter estimation should be carried out accordingly. Furthermore, in this model the effects of a sudden drop in auxin concentration are described as step functions in the various putative mechanisms. It will be interesting, of course, to describe this effect dynamically. To make it even more interesting, Wee1 can be incorporated in the future model so that the length of G2 phase will be closer to reality. Finally, the current model contains not less than 42 parameters. It would also be interesting to check whether some of the parameters are redundant in governing the cell cycle so that we could arrive at a reduced cell cycle model for tomato.

Bibliography

[1] Alon U, Surette MG, Barkai N, Leibler S (1999) Robustness in bacterial chemotaxis. Nature 397: 168–171.

[2] Ingolia NT (2004) Topology and robustness in the *Drosophila* segment polarity network. PLoS Biol 2: e123.

[3] Kitano H (2004) Biological robustness. Nat Rev Genet 5: 826–837.

[4] Boer H, Stötzel C, Röblitz S, Deuflhard P, Veerkamp R, et al. (2011) A simple mathematical model of the bovine estrous cycle: Follicle development and endocrine interactions. Journal of Theoretical Biology 278: 20–31.

[5] Boer H, Apri M, Molenaar J, Stötzel C, Veerkamp R, et al. (2012) Candidate mechanisms underlying atypical progesterone profiles as deduced from parameter perturbations in a mathematical model of the bovine estrous cycle. Journal of Dairy Science 95: 3837–3851.

[6] Gutenkunst RN, Waterfall JJ, Casey FP, Brown KS, Myers CR, et al. (2007) Universally sloppy parameter sensitivities in systems biology models. PLoS Comput Biol 3: e189.

[7] Roodbarkelari F, Bramsiepe J, Weinl C, Marquardt S, Novak B, et al. (2010) Cullin 4-ring finger-ligase plays a key role in the control of endoreplication cycles in arabidopsis trichomes. Proceedings of the National Academy of Sciences .

[8] Tyson JJ, Novak B (2001) Regulation of the eukaryotic cell cycle: Molecular antagonism, hysteresis, and irreversible transitions. Journal of Theoretical Biology 210: 249 - 263.

[9] Novak B, Pataki Z, Ciliberto A, Tyson JJ (2001) Mathematical model of the cell division cycle of fission yeast. Chaos 11: 277–286.

[10] Csiksz-Nagy A, Battogtokh D, Chen KC, Novk B, Tyson JJ (2006) Analysis of a generic model of eukaryotic cell-cycle regulation. Biophys J 90: 4361–4379.

[11] Guimerà R, Sales-Pardo M (2009) Missing and spurious interactions and the reconstruction of complex networks. Proceedings of the National Academy of Sciences 106: 22073–22078.

Summary

Most biological processes are very complex as they results from a highly intricate interplay between many biological components and environmental conditions. This interplay is essential as nearly all biological functions that appear to be fundamental in nature come into existence as emergent properties, i.e., they are only present when the components are in full interaction and disappear if one decouples the different modules. The study of biological systems, therefore, will only be really successful if it is carried out at the systems level. This insight has led to the introduction of the term systems biology. Understanding biological systems at the systems level, however, turns out to be difficult due to the intricate interactions between the components of the systems in time and space. So, to gain information on the underlying biological processes from data, one needs to integrate them with a modeling approach. Of course, the complexity in biological systems translates itself into the complexity of biological models. This complexity, which is indicated by large number of involved components and parameters in the model, together with the nonlinear interactions give rise to several critical issues, e.g., hard understanding of the dynamical behavior, difficulty in parameter identification, and very long computing times. Therefore, mathematical methods that can efficaciously tackle the complexity are required. In this thesis, we develop methods to handle complexity. We focus on three topics: a) method development to analyze robustness of biological models, b) method development to reduce model complexity, and c) model development to elucidate the cell cycle process in tomato fruit pericarp.

One of the crucial features of biological systems that need to be understood is robustness. Robustness is the ability of a system to maintain its functioning although it undergoes strong internal or external perturbations. Since robustness is an essential feature of any biological system, any mathematical model describing a living system should reflect this property. Robustness of a model is determined by answering the question how strong the parameters of the model could be perturbed so that the qualitative behavior of the system does not change. An example of such a qualitative change is the transition from oscillatory behavior to a steady state equilibrium. It is by no means simple to understand the robustness of complex models. For example, if there are many parameters in the model, it is very hard to find which parameter combinations are responsible for the robustness of the system. Many methods to evaluate robustness of biological models suffer from the so-called ”dimensional curse”, i.e., the computing time scales exponentially with dimension. For example, if we would use a Monte-Carlo approach for estimating the shape of a robustness region in parameter space,

we would certainly be confronted with this limiting factor. In Chapter 2, we developed an efficient method to estimate the robustness region of biological models that contain large numbers of parameters. We focus on parametric robustness of the models that show stable oscillatory dynamical behavior. In this case, robustness is violated whenever the system fails to preserve its stable oscillatory behavior. Therefore, robustness in this context is highly connected to the bifurcation concept in mathematics. In our approach, the robustness region is constructed by scanning the parameter space in orthogonal directions. Starting in a so-called nominal point in parameter space for which a stable periodic behavior exists, the parameter space is scanned along orthogonal directions to detect where along these lines bifurcations occur. This yields an initial estimate of the robustness region that is gradually improved by shifting the nominal point and varying the directions. Our method scales linearly with the number of parameters and is therefore highly efficient for models that have large numbers of parameters.

One way to overcome problems that arise from the complexity of a model is by simplifying it, also referred to as *reduction*. A suitable reduction method may lead to a reduced model that is still reliable for a given purpose, but much easier to manage. In Chapter 3, we developed a novel reduction method, in which components and/or reactions that do not contribute to the dynamics of the system are removed from the model. This yields a reduced model with fewer parameters that can still represent observed data. Our method is based on the so-called 'admissible region' concept, that is a region in parameter space where the model outcomes match the observed data within some given tolerance. From the shape of this region, important conclusions can be drawn. For example, if this region includes a part of one of the parameter axes, this parameter can apparently be set to zero. If, on the other hand, this region extends to infinity in some direction, this indicates that lumping of nodes might be allowed. Therefore, a parameter in the model can be removed whenever it can be set to zero or to a large value while the others can be re-optimized such that the model outcomes still fit the dataset. The reduction can be carried out systematically by first applying the node reduction, then parameter reduction, and finally lumping some nodes. In contrast to available methods in the literature, to apply our reduction, the original model does not need to be transformed. This has the advantage that the results of the reduction can be easily biologically interpreted. In addition, our method does not require prior knowledge on the true parameter values as is the case in, e.g., time-scale separation or sensitivity analysis. Yet, the redundant components and parameters are removed so that we end up with a smaller model with fewer parameters. In this way, our method may help parameter identification more efficaciously.

A reduced model obtained with the method described in Chapter 3 will be a satisfactory representation of the system for the conditions under which the data used are obtained. However, if one requires more and wants the reduced system to represent the original model for any possible experimental condition, the reduction method in Chapter 3 is not suitable. Therefore, in Chapter 4, the method is extended by combining the reduction method in Chapter 3 with a model discrimination method. Model discrimination method is commonly used to select the most suitable model among available alternatives to represent a biological system. Here we use it to find whether there exists an experimental condition that can discriminate between the reduced model and the original full model. If yes, then a new experiment based

on that condition is performed to obtain a new dataset. The dataset is combined with the previous dataset and the reduction is repeated. This procedure leads to reduced models that can in the experimental practice not be discriminated from their original full models and thus form real substitutes. When applied to a particular model for a phenomenon, our extended reduction procedure leads to the insight which parts of the original model are redundant and which parts belong to the core of the model.

In Chapter 5 we presented research results that are of a slightly different character compared to the methodological approaches in the preceding chapters. Here, we developed a mathematical model to describe the cell cycle in tomato fruit pericarp. Special attention is paid to the transition into a partial cycle, also referred to as 'endoreduplication'. An exhaustive literature research on the putative mechanisms that may trigger this transition is discussed. The knowledge is then put in the form of a mathematical model. We discovered that although each putative mechanism can on its own lead to this transition, it is more likely that nature combines them since this improves the robustness of the transition.

Finally, in Chapter 6, the results of our work are summarized and elaborated further. Also some future work is suggested.

Samenvatting

De meeste biologische processen zijn zeer complex, omdat zij voortkomen uit een uiterst ingewikkeld samenspel van verschillende biologische componenten en omgevingscondities. De interacties tussen de verschillende componenten zijn essentiee,l omdat die bepalen welke biologische functies van een systeem tot uiting komen. Deze functies worden 'emergent' genoemd omdat ze het resultaat vormen van het samenspel van de componenten. Ze kunnen verdwijnen als n van de componenten wordt verwijderd of als n van de interacties wordt geblokkeerd. Het bestuderen van biologische systems zal alleen dan succesvol zijn als daarbij holistische gedacht wordt: het systeem is intrinsiek een samenstelling van diverse componenten. Dit inzicht heeft geleid tot de introductie van de term 'systeembiologie'. Het op deze manier bestuderen van een biologisch systeem blijkt moeilijk te zijn vanwege de ingewikkelde interacties van de componenten die plaats vinden zowel in tijd en als in plaats. Om uit data informatie te verkrijgen over de onderliggende biologische processen is het daarom nodig dat de data gecombineerd worden met een modelmatige aanpak. De complexiteit van biologische systemen vertaalt zich uiteraard naar de complexiteit van de bijbehorende biologische modellen. Deze complexiteit komt vooral tot uiting in het feit dat de modellen veel variabelen en veel parameters hebben. In combinatie met sterk niet-lineaire interacties leidt dit tot moeizaam begrijpen van het dynamisch gedrag, problemen met parameter identificatie en zeer lange rekentijden. Daarom zijn er wiskundige methoden nodig die op een effectieve manier de modelcomplexiteit kunnen reduceren. In dit proefschrift ontwikkelen we dergelijke methoden om in de praktijk goed om te kunnen gaan met complexe modellen, waarbij we ons richten op a) methoden voor het analyseren van de robuustheid van biologische modellen, b) methoden om de modelcomplexiteit te reduceren, en c) het opstellen van een model voor de celcyclus in tomaat.

En van de cruciale eigenschappen van biologische systemen is 'robuustheid'. Robuustheid is het vermogen van een systeem om te kunnen blijven functioneren ook als er sterke interne of externe verstoringen optreden. Omdat robuustheid een essentile eigenschap is van iedere biologisch systeem moeten ook biologische modellen deze eigenschap bezitten. De mate van robuustheid van een model kan bepaald worden door de vraag te beantwoorden hoe sterk de modelparameters verstoord kunnen worden zonder dat het kwalitatieve gedrag van het model verandert. Een voorbeeld waarbij het gedrag wel kwalitatief verandert, is de overgang van oscillerend gedrag naar een toestand waarin het gedrag constant is. Het is zeker niet eenvoudig om de robuustheid van complexe modellen te begrijpen. Zeker als er veel parameters zijn is het moeilijk na te gaan welke parameters verantwoordelijk zijn voor robuustheid

en welke niet. Vele methoden om modelrobuustheid te bepalen lijden aan de zogeheten 'dimensievloek', dat wil zeggen dat de rekentijd exponentieel schaalt met het aantal parameters, oftewel met de dimensie van de parameterruimte. Bijvoorbeeld, als we een Mont-Carlo aanpak zouden volgen om de vorm van de robuustheidsregio in de parameterruimte te bepalen, dan zouden we zeker met deze beperkende factor te maken krijgen. In Hoofdstuk 2 hebben we een methode ontworpen om de robuustheidsregio te schatten, die ook efficint is indien er heel veel parameters zijn. We richtten ons daarbij op modellen die stabiel oscillerend gedrag vertonen. In dit geval is de robuustheid verbroken wanneer het systeem niet meer op een stabiele manier oscilleert. In deze context is robuustheid dus nauw verbonden aan het concept 'bifurcatie' in de wiskunde. In onze aanpak wordt een schatting van de robuustheidsregio gevonden door de parameterruimte te scannen langs onderling orthogonale richtingen, waarbij er gestart wordt in een 'nominaal' punt waarvan het bekend is dat het in de robuustheidsregio ligt. De schatting van de vorm van de robuustheidsregio wordt verfijnd door het nominale punt te verschuiven en de orthogonale richtingen opnieuw te kiezen. De methode is bijzonder efficint omdat de rekentijd lineair schaalt met het aantal parameters, zodat ook zeer grote aantallen parameters geen beletsel vormen.

Een manier om de problemen ten gevolge van de complexiteit van een model terug te brengen is om de modelcomplexiteit te reduceren. Een geschikte reductiemethode leidt tot een model dat nog steeds de gewenste eigenschappen heeft maar veel eenvoudiger is om te hanteren, In Hoofdstuk 3 presenteren we een nieuwe methode, waarbij componenten en/of interacties die niet wezenlijk bijdragen aan het functioneren van het model eenvoudig worden verwijderd. Dit leidt dan tot een eenvoudiger model met minder parameters, dat toch nog steeds de data kan beschrijven. De methode is gebaseerd op het concept van 'toegestane regio', dat is een gebied in de parameterruimte waarbinnen het model de data binnen zekere nauwkeurigheid kan reproduceren. De vorm van deze regio geeft belangrijke informatie voor mogelijke reductie. Bijvoorbeeld, als deze regio n van de parameterassen snijdt, dan kan deze parameter kennelijk op nul gezet worden. Als aan de andere kant deze regio zich uitstrekt tot oneindig, dan is dit een indicatie dat componenten van het model samengenomen kunnen worden. Er zijn dus twee redenen waarom een parameter verwijderd kan worden. In het eerste geval wordt de betreffende parameter op nul gezet en er wordt nagegaan of, door het opnieuw fitten van de andere parameters, het model de data kan blijven genereren. Indien dit het geval is kan de betreffende term in de vergelijkingen verwijderd worden uit het model. In het tweede geval wordt de parameter een zeer grote waarde gegeven en wordt weer nagegaan of, door het opnieuw fitten van de andere parameters, het model de data kan blijven genereren. Indien dit het geval is geeft dit aan dat er twee variabelen in het model samengenomen kunnen worden, wat in termen van modelvergelijkingen inhoudt dat het model toe kan met n vergelijking minder. In tegenstelling tot bestaande reductiemethoden, behoeft in onze aanpak het model niet te worden getransformeerd. Dit heeft het voordeel dat het gereduceerde model eenvoudig te interpreteren blijft. Een bijkomend voordeel is dat onze methode niet vereist dat er voorkennis beschikbaar is over de parameterwaarden, zoals het geval is bij methoden zoals 'tijdschaalseparatie' en 'gevoeligheidsanalyse'. Omdat onze aanpak leidt tot sterk gereduceerde modellen met een sterk gereduceerd aantal parameters, wordt het schatten van de overblijvende parameters simpeler.

Een model dat is gereduceerd met behulp van de methode in Hoofdstuk 3 vormt een

goede representatie van het oorspronkelijke model zolang men zich beperkt tot de data die gebruikt werden in de reductie. Echter, indien men meer wil en ook eist dat het gereduceerde model het oorspronkelijke model kan vervangen onder alle mogelijke condities, dan is de methode in Hoofdstuk 3 niet geschikt. Daarom hebben we in Hoofdstuk 4 deze methode uitgebreid met behulp van de techniek van 'modeldiscriminatie'. Bij modeldiscriminatie gaat het erom het meest geschikte model te kiezen uit een groot aantal beschikbare modellen zodanig dat een gegeven biologisch systeem zo goed mogelijk wordt gerepresenteerd. Hier gebruiken we deze methode om na te gaan of er een experimentele conditie bestaat waarin het gereduceerde model en het oorspronkelijke model zich duidelijk verschillend (binnen de aangenomen marges) gedragen. Als het laatste het geval is dan wordt de dataset behorend bij deze conditie toegevoegd aan de oorspronkelijke data en de reductiemethode wordt toegepast op beide datasets tegelijk. In het algemeen zal dit een minder gereduceerd model opleveren. Ook van dit model wordt weer getest of er een experimentele conditie bestaat waarin het gereduceerde model en het oorspronkelijke model zich duidelijk verschillend (binnen de aangenomen marges) gedragen. Indien dit het geval is, dan wordt de betreffende dataset weer toegevoegd aan de reeds gebruikte twee datasets. Enzovoorts. Het blijkt dat het veel modellen te reduceren zijn, ondanks dat deze methode zeer strenge eisen stelt. Het uiteindelijke gereduceerde model is in geen enkel opzicht (binnen zekere toegestane onnauwkeurigheid) te onderscheiden van het oorspronkelijke model en is toch (meestal) veel simpeler. Deze aanpak leidt tot goed inzicht welke onderdelen van een model echt essentieel zijn en welke redundant.

In Hoofdstuk 5 presenteren we onderzoeksresultaten die een enigszins ander karakter hebben vergeleken met de voorgaande hoofdstukken. In dit hoofdstuk ontwikkelen we een model voor de celcyclus van de tomaat. Speciale aandacht wordt besteed aan de overgang van de gewone cyclus naar een partile cyclus, ook wel aangeduid als 'endoreduplication'. In dit hoofdstuk hebben we een uitputtende literatuurstudie over dit onderwerp opgenomen, waarin de mogelijke mechanismen die deze overgang kunnen veroorzaken worden samengevat. Deze kennis is gebruikt om voor dit fenomeen een wiskundig model op te stellen. Wij ontdekten dat elk van de verschillende mechanismen separaat de overgang kunnen bewerkstelligen, maar dat in de natuur waarschijnlijk een combinatie wordt gebruikt omdat dat leidt tot een veel robuuster systeem.

Tenslotte, in Hoofdstuk 6 worden de resultaten van dit werk samengevat en verder bediscussieerd. Ook worden er suggesties gedaan hoe dit onderzoek voorgezet kan worden.

Acknowledgments

After completing my Post-Master's program in Mathematics for Industry at TU Eindhoven in 2008, I decided to take a PhD research position in Systems Biology at Biometris, Wageningen University to prepare myself for my dream career as a researcher and a university lecturer. It turns out that the four years PhD period became one of the most exciting moments in my life with all the challenges, collaborations, and friendships that I had during the journey.

The completion of this PhD thesis was made possible by the great working atmosphere at Biometris, Wageningen University. Many people directly or indirectly contributed in making the completion of this thesis possible. Therefore, I would like to express my gratitude to all those who made it possible.

First of all, I would like to sincerely thank my promoter, Pak Jaap, and co-promoter Maarten for all the guidance and unlimited support I got during the last four years. It was really a privilege for me to work under their supervision. The fruitful discussions, stimulating support, patient guidance, and positive encouragement have groomed me into a mature scientist and for this I am highly indebted to them. They always left their doors open for me to discuss any idea that I had in my mind, which made them as my truly daily supervisors. I also highly appreciate their assistance and supports in non-academic matters especially on my first year when I encountered difficulty to find housing. In my view, Pak Jaap and Maarten are really an excellent supervision team.

Secondly, I wish to thank George van Voorn for helping me with work on AUTO and bifurcation and led to my first paper. Many people said that publishing the first paper is always difficult, but with his expertise I managed to overcome the obstacle. I also would like to thank Wanne and Pieter de Visser for the fruitful discussions on the tomato project. They showed and guided me to the light when I was in the darkness in the pile of tomato papers. My appreciation also goes to Marike Boer, for which my collaboration with her turned out to be one of the most efficient cooperation which resulted in a paper published in the Journal of Dairy Science. The paper even became a highlighted article of the month in July 2012.

I would also like to extend my gratitude to Hans Stigter for all the invaluable discussions on model reduction and experimental design, which gave inspiration for my research. Also, for the DREAM competition which was really an amazing experience. Although we did not make the DREAM came true, I learnt a lot from Hans about experimental design and parameter estimation. In the same spirit, I should not forget to thank Laura, Simon, Joost, Aalt-Jan, and Johannes for being great team members.

I also want to thank Joost van Opheusden for supporting me with the fast computer facil-

ity, Onno for offering me an opportunity to give tutorial in the practical class which helped me to develop my teaching skill. I am also very grateful to Thomas Odong for the warm friendship he offered me since the first day I started my work at Biometris. Thanks also go to Santosh, Marian, Sabine, Martin, Willem, Maggie, Rianne, Nurudeen, Nadya, George, Robert, Jeroen, Cassandra, and other Biometris colleagues for all the supports they provided me. Special thanks also go to the two secretaries of Biometris, Dinie and Hanneke, for helping me with the administrational stuff. I would certainly miss Biometris with all its friendly and helpful people.

My appreciations also go to Indonesian community in Wageningen, especially Hadiyanto family who helped us a lot at the beginning of my PhD. Also to Teh Aisyah and Kang Asep, Kang Maman's family, Mbak Atin, Teh Ria, Mbak Yessie, for being our close friends, and to Awang, Firdaus, Bu Rina's family, Teh Novi, Indra, Pak Yongky, Mbak Nurmi, Pak Hidayat, and other Indonesian students, for all their kindness so that we never feel alone in this city. I would also not forget the warm friendship and true kindness of Gusti Andi's family in Utrecht, Indra Tosri's family in Nijmegen, the Sundanese community and other Indonesian friends in Netherlands. It is really a gift to have friends like them.

Special thank goes to my wife, Yayu Rismawati, who has sacrificed a lot to be with me. She had to keep her homesickness away, which was definitely not easy, to give me a full support to finish this PhD project. Without her, certainly it would have not been possible. I would like to say this to her: *Hatur nuhun geulis kana sadaya pengorbanan sareng pengertianna. Insya Allah saatos ieu, urang tiasa riung mungpulung deui sareng Apa, Mamah, Teteh, Aa, Nissa, keponakan, & keluarga besar sadayana*. In a special way I would like to thank my mother for all her support: *Hatur nuhun pisan kana sagala usaha Mamah supados barudak Mamah sadayana tiasa sakola dugi ka rengse. Sanaos Bapak ngantunkeun pas barudak mamah sadaya peryogi biayaeun, sumanget sareng usaha mamah kanggo nyakolakeun barudak Mamah teu pernah pareum. Insya Allah sumanget mamah ieu bakal teras ngagedur dina dada barudak mamah sadayana.* They (mother and wife) are the most influencing women in my life! I also wish to extend my gratitude to Apa and Mamah, and to all my brothers and sisters for their understanding and their never ending prayers. This success is for all of you!

Last but not least, I would like to thank Allah Subhanahu Wata'alaa! *Alhamdu-lillaahi-rabbil-'aalamiin* (All praise and thanks is for God, The Creator, Owner, Sustainer of the Worlds).

About the author

Mochamad Apri was born on 9 April 1980 in Bandung, Indonesia. He obtained his bachelor degree in Applied Mathematics from Institut Teknologi Bandung (ITB), Indonesia, in 2002. In the last year of his bachelor education, he took part in the "Mathematical Contest in Modeling" held by the Consortium for Mathematics and its Applications (COMAP), USA, and obtained an honorable mentioned participant award. After obtaining his bachelor, he joined the oil and gas research consortium (OPPINET) at ITB as a research assistant, and conducted research on oil and gas flow optimization. His main tasks were to estimate and simulate the gas well deliverability.

In 2003, he continued his study at the Kaiserslautern University of Technology, Germany, with a scholarship from Institut für Techno und Wirtschaftsmathematik (ITWM) Fraunhofer Institute and received MSc degree in Industrial Mathematics and Scientific Computing. Since Apri wanted to get experienced in working on industrial problems, after completing his Master education, he took the Post Master programme of Mathematics for Industry at Eindhoven University of Technology for two years. There he carried out several modeling projects from, among others, Phillips Medical System, Oce Technology, Teijin Aramid, and Dow Europe.

As he wanted to pursue an academic career for his future, in 2008 he decided to take a PhD research position in Systems Biology at Biometris group, Wageningen University and Research Centre, The Netherlands, under supervision of Prof. Dr. Jaap Molenaar and Dr. Maarten de Gee. In the middle of his PhD, he accepted an offer to become a lecturer at the Mathematics Department of his former campus, ITB, which will start in 2013.

List of publications

1. Arsegianto, Soewono E, Apri M (2002), Non-Linear Optimization Model for Gas Transmission System: A Case of Grissik Duri Pipeline, SPE Asia Pacific Oil and Gas Conference, pp. 367-375

2. Apri M, Molenaar J, de Gee M, van Voorn G (2010) Efficient Estimation of the Robustness Region of Biological Models with Oscillatory Behavior, PLoS ONE 5(4):e9865

3. Apri M, de Gee M, Molenaar J (2012) Complexity reduction preserving dynamical behavior of biochemical networks, Journal of Theoretical Biology, Vol. 304, pp. 16-26

4. Boer HMT, Apri M, Molenaar J, Stötzel C, Veerkamp R, Woelders H (2012) Candidate mechanisms underlying atypical progesterone profiles as deduced from parameter perturbations in a mathematical model of the bovine estrous cycle, Journal of Dairy Science, Vol. 95, Issue 7, pp.3837-3851

5. Apri M, de Gee M, Molenaar J (2012) Extracting optimal models to represent biochemical systems (to be submitted)

6. Apri M, Kromdijk J, de Visser PHB, de Gee M, Molenaar J (2012) Modelling cell cycle and endoreduplication of tomato (to be submitted)

PE&RC PhD Education Certificate

With the educational activities listed below the PhD candidate has complied with the educational requirements set by the C.T. de Wit Graduate School for Production Ecology and Resource Conservation (PE&RC) which comprises of a minimum total of 32 ECTS (= 22 weeks of activities)

Review of literature (6 ECTS)

- Robustness of oscillation of biological systems
- Complexity reduction in biological systems
- Cell cycle in tomato fruit pericarp

Writing of project proposal (4 ECTS)

- Developing methods to analyse the dynamics of biological networks

Post-graduate courses (4.5 ECTS)

- Summer school on cell and systems; DISC (2008)
- Summer school: Mathematical modelling in cell biology; DFKZ (2009)
- Winter school: model reduction ; DISC (2010)

Competence strengthening / skills courses (3.3 ECTS)

- Techniques for writing and presenting a scientific paper; WGS (2009)
- Reviewing scientific paper; WGS (2011)
- Writing grant proposal; WGS (2012)

PE&RC Annual meetings, seminars and the PE&RC weekend (2.1 ECTS)

- PE&RC Day (2009)
- PE&RC Weekend (2009)
- PE&RC Weekend (2012)

Discussion groups / local seminars / other scientific meetings (5.8 ECTS)

- Systems Biology Meeting; CWI, Amsterdam (2008/2009)
- Systems Biology Study Group (2008/2009)
- Systems Biology Study Group (2009/2010)
- Systems Biology Study Group (2010/2011)
- Systems Biology Study Group (2011/2012)

International symposia, workshops and conferences (9 ECTS)

- RECOMB; USA (2009)
- CHSL Meeting on Systems Biology: Networks; Hinxton, UK (2010)

- International Conference on Systems Biology; Edinburgh, UK (2010)
- European Conference for Mathematical and Theoretical Biology, Poland (2011)
- Systems Biology Europe; Madrid, Spain (2012)

Lecturing / supervision of practical's / tutorials (3 ECTS)

- Mathematical methods and application; 6 days (2009)
- Mathematical methods and application; 6 days (2011)
- Introduction to Systems Biology; 3 days (2011)

The research described in this thesis was financially supported by IP/OP Systems Biology program of Wageningen University.

The cover of this thesis was designed by Asep Bayu Ekawijaya and Mochamad Apri